J. Mech. Phys. Solids 216 (2026) 106772

Contents lists available at ScienceDirect

Journal of the Mechanics and Physics of Solids

journal homepage: www.elsevier.com/locate/jmps

Fracture and crack-face stability of pre-deformed soft electroactive solids

Lizichen Chen [a], Yangkun Du [a,*], Rongqiao Xu [b], Michel Destrade [a,e], C.W. Lim [a], Weiqiu Chen [a,c,d,e,*]

[a] Key Laboratory of Soft Machines and Smart Devices of Zhejiang Province, Department of Engineering Mechanics, Soft Matter Research Center, Zhejiang University, Hangzhou, 310027, PR China
[b] Department of Civil Engineering, Zhejiang University, Hangzhou, 310051, PR China
[c] Intelligent Structures and Advanced Equipments Technology Center, Huanjiang Laboratory, Zhuji, 311800, PR China
[d] Faculty of Mechanical Engineering and Mechanics, Ningbo University, Ningbo, 315211, PR China
[e] School of Mathematical and Statistical Sciences, University of Galway, University Road, Galway, Ireland

A R T I C L E I N F O

Keywords:
Fracture analysis
Incremental theory
Potential method
Soft electroactive material
Crack-face stability
Topological number

A B S T R A C T

Fracture and crack-face instability may occur separately or concurrently, severely impairing the reliability of flexible electroactive devices. Based on the nonlinear theory of electroelasticity and incremental field theory, this work establishes general solutions to the governing equations for a soft electroelastic body subjected to particular yet common biasing fields. We use potential theory method to obtain and validate explicit analytical solutions of the resulting integro-differential equations for both crack and anti-crack problems under various elementary loading conditions. We examine two types of surface instabilities in pre-deformed cracked electroactive bodies for perturbations in the x–z and ρ–z planes. To quantitatively describe the fracture and stability behavior, we further introduce incremental intensity factors and incremental energy release rates to assess crack propagation, together with a buckling topological number to classify crack-face buckling and persistent stability. The derived bifurcation equations further reveal re-entrant phenomena as pre-stretch and initial electrical displacement vary. Overall, the proposed framework provides a unified, quantitative analysis for electromechanically coupled fracture and instability in soft electroelastic materials.

1. Introduction

Dielectric elastomers (DEs) are typical soft electroactive materials capable of achieving more than 100% reversible large strains under an electric field. Their high energy density, fast response, and low cost make DEs suitable for fabricating lots of functional devices such as actuators, energy harvesters, and flexible sensors (Bar-Cohen, 2002; Koh et al., 2011; Kornbluh et al., 2012a; 2012b; Maas and Graf, 2012; Sharma et al., 2022; Sun et al., 2023; Zhou et al., 2024). These devices further endow DEs with significant application potential in soft robotics, aerospace, and intelligent bionics (Shian et al., 2015; Gu et al., 2017; Branz and Francesconi, 2017; Cao et al., 2019; Ji et al., 2019; Huang et al., 2025). Nevertheless, the failure of DE-based devices considerably limits their

* Corresponding authors at: Key Laboratory of Soft Machines and Smart Devices of Zhejiang Province, Department of Engineering Mechanics, Soft Matter Research Center, Zhejiang University, Hangzhou, 310027, PR China.
E-mail addresses: yangkundu@zju.edu.cn (Y. Du), chenwq@zju.edu.cn (W. Chen).

https://doi.org/10.1016/j.jmps.2026.106772
Received 10 February 2026; Received in revised form 24 June 2026; Accepted 12 July 2026
Available online 15 July 2026

performance in those scenarios. Specifically, electromechanical coupling failure in DEs involves multiple factors, including material fracture and electromechanical instability. Accurately characterizing their electromechanical failure behavior and quantitatively analyzing such failures are essential for engineering applications of DEs (Ahmad et al., 2019; Manikkavel et al., 2020; Moreno-Mateos et al., 2024). Thus, effectively suppressing or strategically utilizing electromechanical failure represents a key challenge in enhancing the functional performance of DE-based devices, and there is an acute need to develop rigorous theoretical models to understand the underlying mechanisms.

The operating principle of DE-based devices hinges on Coulomb forces between compliant electrodes and material polarization, which transduce an applied electric field into mechanical deformations (Kornbluh et al., 1999; O'Halloran et al., 2008; Suo, 2010). Though large actuation strain enables their functionality, it also renders DEs highly susceptible to various failure modes, especially the onset and formation of cracks under high electric fields and excessive deformations (Pelrine et al., 2000; Chen et al., 2017). To this end, plenty of practical strategies in modifying the material properties have been adopted to enhance fracture resistance (Long and Hui, 2016), such as tuning the polymer chain network to improve intrinsic toughness (Hua et al., 2021; Kim et al., 2021; Liu et al., 2023) and incorporating fiber reinforcements to enhance matrix toughness (Li et al., 2020; Khatami et al., 2024) or microstructural features to arrest crack propagation (Gent et al., 2003; Lee and Pharr, 2019). Although those strategies (e.g., microstructure-induced crack path alteration and energy dissipation) work in certain scenarios, the fracture process is complicated by its intrinsic coupling with electromechanical instabilities and electric breakdown. This interplay makes the failure modes even more complex (Leng et al., 2009; Park and Nguyen, 2012; Yamada et al., 2014; Zhou et al., 2020) (Fig. 1).

Research efforts increasingly combine experimental characterization with advanced numerical simulations. Foundational works have examined fracture under purely mechanical loading experimentally (Pharr et al., 2012; Ahmad et al., 2019). Phase-field modeling is also involved to study crack evolution in these electroactive soft materials (Kaliske et al., 2022). While existing studies have explored the computational and experimental aspects of fracture problems, achieving a unified theoretical framework that accurately describes the complex interplay between mechanical stress, electric field, and material damage remains an ongoing and central challenge. In this regard, there have been limited attempts to establish theoretical models for the description of electromechanical fracture. For example, a simple fracture model for an electrode and interfacial crack in a DE under tensile loading was developed by Manikkavel et al. (2020). Although quantitatively analyzing techniques have been integrated into the development of fracture models, only few explicit analytical solutions exist.

As a potent analytical approach (originally proposed by Fabrikant (1989)), the potential theory method has made essential contributions to transversely isotropic elasticity, piezoelectricity, and magnetoelectric thermoelasticity (Chen, 2000; Chen and Ding, 2004). A series of exact solutions was derived and extended by Chen and his collaborators (Chen, 2015). Building upon the incremental field theory established by Dorfmann and Ogden (2010; 2014), Zhang et al. (2012) first applied the potential theory method to contact analysis. They analyzed compressible isotropic soft electroactive half-spaces under uniform finite deformation, demonstrating the applicability of this method to problems involving finite pre-deformation and electromechanical coupling. However, to the best of our knowledge, no studies have yet been conducted on fracture analysis of finite deformed solids from the perspective of potential theory, nor has an analytical model for coupled cracking and instability been developed. Hence, the present work seeks to utilize and extend the potential theory method to not only analytically solve fracture problems in soft electroactive materials but also conduct effective stability analysis.

This article is structured as follows. Section 2 presents the nonlinear theory of electroelasticity and the corresponding incremental field theory. We describe the configurations of a soft electroactive continuum containing an internal crack under a general pre-deformation. In Section 3, we specialize the governing equations derived in the previous section to the case of equi-biaxial stretch and establish a general solution to the equations. In Section 4, we develop complete solutions via the potential theory method and provide analytical treatments for problems with penny-shaped cracks and flat cracks of general shape. Besides, we derive explicit analytical solutions for crack and anti-crack problems under various loading conditions, and we verify the solutions via finite element simulations. In Section 5, we investigate two types of surface instability of the cracked electroactive body. A buckling topological number is introduced to assess persistent stability. Finally, the article is summarized in Section 6, with perspectives proposed for future

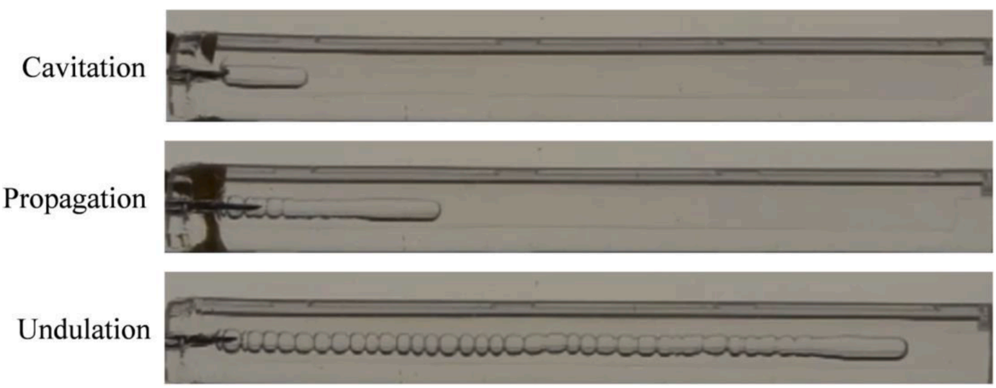

Fig. 1. Crack cavitation, propagation, and surface undulation in soft materials (Wang et al., 2023).

investigation. Note that Appendix B provides a detailed exposition of the potential theory method. Furthermore, it incorporates a singular term that was previously omitted in the literature, which enhances the completeness of the theory.

2. Nonlinear theory of electroelasticity and incremental field theory

Consider a compressible electroactive body that occupies a region $\overline{\mathbb{B}}_r$ with boundary $\partial\overline{\mathbb{B}}_r$ (outward unit normal of $\partial\overline{\mathbb{B}}_r$ is $\mathbf{N}$) in the reference configuration. A material frame is established in $\overline{\mathbb{B}}_r$ by identifying a material point via its position vector $\mathbf{X}$. Upon the application of specified elastic and electric loads or displacements, the body deforms into a novel configuration (i.e., the initial configuration) $\overline{\mathbb{B}}$ with boundary $\partial\overline{\mathbb{B}}$ (outward unit normal of $\partial\overline{\mathbb{B}}$ is $\mathbf{n}$), and the position vector of the material point becomes $\mathbf{x}$ in a space-fixed frame. The mapping $\boldsymbol{\chi}:\mathbf{X}\mapsto\mathbf{x}$ between the vectors in $\overline{\mathbb{B}}_r$ and $\overline{\mathbb{B}}$ is assumed to be a twice-differentiable tensor function. The deformation gradient is defined as $\mathbf{F} = \mathrm{Grad}\boldsymbol{\chi}$, where Grad denotes the gradient operator in $\overline{\mathbb{B}}_r$. The left and right Cauchy-Green deformation tensors are $\mathbf{b} = \mathbf{F}\mathbf{F}^{\mathrm{T}}$ and $\mathbf{C} = \mathbf{F}^{\mathrm{T}}\mathbf{F}$, respectively, with the superscript T indicating tensor transpose. The surface and volume elements in the initial ($\mathrm{d}\widehat{\boldsymbol{a}}$ and $\mathrm{d}v$) and reference ($\mathrm{d}\widehat{\boldsymbol{A}}$ and $\mathrm{d}V$) configurations are related by $\mathrm{d}\widehat{\boldsymbol{a}} = \mathbf{n}\mathrm{d}\widehat{a} = J\mathbf{F}^{-\mathrm{T}}\mathbf{N}\mathrm{d}\widehat{A}$ (Nanson formula) and $\mathrm{d}v = J\mathrm{d}V$, respectively, where $J = \det\mathbf{F}$ is the volume ratio. Definitions of symbolic notations and connections among the three configurations are summarized in Fig. 2 below.

Under the quasi-electrostatic approximation and in the absence of free charges, electric currents, and body forces, the equilibrium equations can be expressed as

$$\mathrm{Div}\mathbf{T} = \mathbf{0}, \quad \mathrm{Div}\mathscr{D} = 0, \quad \mathrm{Curl}\mathscr{E} = \mathbf{0}, \tag{1}$$

where $\mathbf{T} = J\mathbf{F}^{-1}\boldsymbol{\tau}$ is the nominal stress tensor; while $\mathscr{D} = J\mathbf{F}^{-1}\mathbf{D}$ and $\mathscr{E} = \mathbf{F}^{\mathrm{T}}\mathbf{E}$ represent the Lagrangian electric displacement and electric field vectors, respectively. Note that the operators Div and Curl are both defined in $\overline{\mathbb{B}}_r$. If fixed charges are compactly distributed on a plane to generate an electric field (specifically, the plane in the infinite medium discussed later refers to the $z = 0$ plane, which is a plane of symmetry within the electroactive body), the boundary conditions on $\partial\overline{\mathbb{B}}$ read

$$\boldsymbol{\tau}\mathbf{n} = \mathbf{t}_{\hat{a}}, \quad \mathbf{n}\cdot\mathbf{D} = q_{\hat{a}}, \quad \mathbf{n}\times\mathbf{E} = \mathbf{0}, \tag{2}$$

where $\mathbf{t}_{\hat{a}}$ and $q_{\hat{a}}$ are the surface traction and charge density (per unit area) on $\partial\overline{\mathbb{B}}$, respectively. The material behavior is characterized by an energy density (per unit reference volume) function $\Omega = \Omega(\mathbf{F},\mathscr{D})$, such that $\Omega(\mathbf{I},\mathbf{0}) = 0$ in $\overline{\mathbb{B}}_r$, with $\mathbf{I}$ being a two-point identity tensor. The nonlinear constitutive relations (Dorfmann and Ogden, 2006) are established as

$$\mathbf{T} = \frac{\partial\Omega}{\partial\mathbf{F}}, \quad \mathscr{E} = \frac{\partial\Omega}{\partial\mathscr{D}}. \tag{3}$$

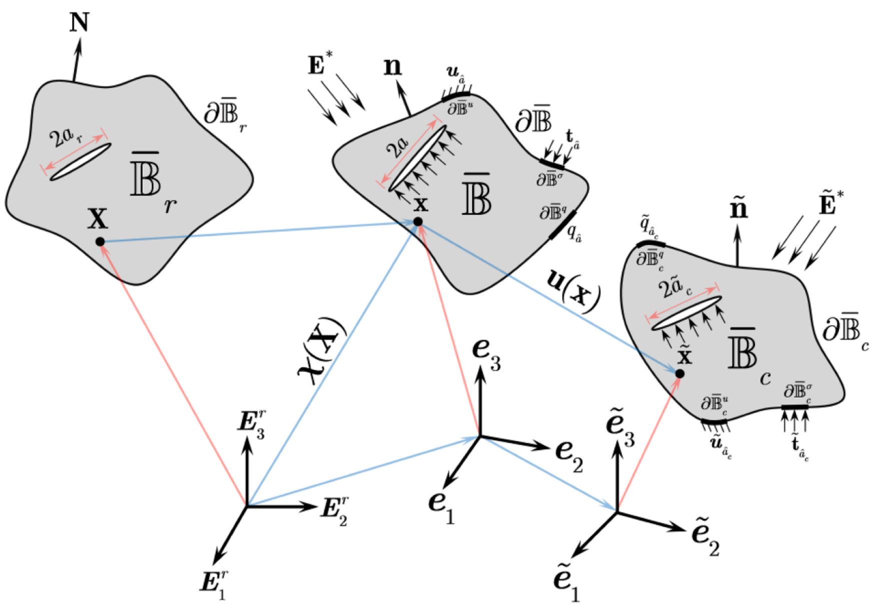

Fig. 2. The reference ($\overline{\mathbb{B}}_r$), initial ($\overline{\mathbb{B}}$), and current ($\overline{\mathbb{B}}_c$) configurations of a soft electroactive continuum with an internal crack. $\{\boldsymbol{E}_\alpha^r\}$, $\{\boldsymbol{e}_i\}$, and $\{\tilde{\boldsymbol{e}}_a\}$ are configuration bases. $\mathbf{N}$, $\mathbf{n}$, and $\tilde{\mathbf{n}}$ are outward unit normal vectors. $\mathbf{X}$, $\mathbf{x}$, and $\tilde{\mathbf{x}}$ are material point position vectors. a_r, a, and $\tilde{a}_c$ are the radius of crack surface in $\overline{\mathbb{B}}_r$, $\overline{\mathbb{B}}$, and $\overline{\mathbb{B}}_c$, respectively. $\mathbf{E}^*$ and $\tilde{\mathbf{E}}^*$ are exterior electric field vectors in $\overline{\mathbb{B}}$ and $\overline{\mathbb{B}}_c$, respectively. The mechanical and electrical boundary conditions are marked on the corresponding configurations. Compatible mechanical loads are applied on the crack surfaces.

Assuming that the energy density is a scalar-valued isotropic tensor function, then it can be represented in terms of six invariants (Zheng, 1994) as $\Omega(\mathbf{F}, \mathscr{D}) = \Omega(\mathscr{I}_1, \mathscr{I}_2, \mathscr{I}_3, \mathscr{I}_4, \mathscr{I}_5, \mathscr{I}_6)$, where

$$\begin{aligned} &\mathscr{I}_1 = \mathrm{tr}\mathbf{C}, \quad \mathscr{I}_2 = \frac{1}{2}\left[(\mathrm{tr}\mathbf{C})^2 - \mathrm{tr}\left(\mathbf{C}^2\right)\right], \quad \mathscr{I}_3 = \det\mathbf{C}, \\ &\mathscr{I}_4 = \mathscr{D}\cdot\mathscr{D}, \quad \mathscr{I}_5 = \mathscr{D}\cdot(\mathbf{C}\mathscr{D}), \quad \mathscr{I}_6 = \mathscr{D}\cdot\left(\mathbf{C}^2\mathscr{D}\right). \end{aligned} \tag{4}$$

Applying the chain rule, Eq. (3) leads to

$$\mathbf{T} = \sum_{m=1, m\neq 4}^{6} \Omega_m \frac{\partial \mathscr{I}_m}{\partial \mathbf{F}}, \quad \mathscr{E} = \sum_{m=4}^{6} \Omega_m \frac{\partial \mathscr{I}_m}{\partial \mathscr{D}}, \tag{5}$$

with $\Omega_m \equiv \partial\Omega / \partial\mathscr{I}_m$ for $m = 1, 2, \cdots, 6$. From Eqs. (4) and (5), we arrive at the Cauchy stress tensor $\boldsymbol{\tau}$ and electric field vector $\mathbf{E}$ as

$$\begin{aligned} &\tau = J^{-1}\mathbf{F}\mathbf{T} = J^{-1}\mathbf{F}\frac{\partial\Omega}{\partial\mathbf{F}} = 2J^{-1}\left[\Omega_1\mathbf{b} + \Omega_2\left(\mathscr{I}_1\mathbf{b} - \mathbf{b}^2\right) + \mathscr{I}_3\Omega_3\widetilde{\mathbb{I}} + \mathscr{I}_3\Omega_5\mathbf{D}\otimes\mathbf{D} + \mathscr{I}_3\Omega_6(\mathbf{D}\otimes\mathbf{bD} + \mathbf{bD}\otimes\mathbf{D})\right], \\ &\mathbf{E} = \mathbf{F}^{-\mathrm{T}}\mathscr{E} = \mathbf{F}^{-\mathrm{T}}\frac{\partial\Omega}{\partial\mathscr{D}} = 2J\left(\Omega_4\mathbf{b}^{-1}\mathbf{D} + \Omega_5\mathbf{D} + \Omega_6\mathbf{bD}\right), \end{aligned} \tag{6}$$

respectively, where "$\otimes$" represents the tensor product.

For significantly smaller load and displacement further applied on the electroactive body compared to the biasing fields, an infinitesimal incremental perturbation is superimposed on the initial configuration. According to Dorfmann and Ogden (2010), an incremental deformation $\dot{\mathbf{x}}(\mathbf{X})$ and an incremental electric displacement $\dot{\mathbf{D}}_0$ are applied to $\overline{\mathbb{B}}$, leading to the current configuration $\overline{\mathbb{B}}_c$. Here, dotted variables denote incremental quantities (not time derivatives). The incremental equilibrium equations in Eulerian form are derived as

$$\mathrm{div}\dot{\mathbf{T}}_0 = \mathbf{0}, \quad \mathrm{div}\dot{\mathbf{D}}_0 = 0, \quad \mathrm{curl}\dot{\mathbf{E}}_0 = \mathbf{0}, \tag{7}$$

where $\dot{\mathbf{T}}_0 = J^{-1}\mathbf{F}\dot{\mathbf{T}}$, $\dot{\mathbf{D}}_0 = J^{-1}\mathbf{F}\dot{\mathscr{D}}$, and $\dot{\mathbf{E}}_0 = \mathbf{F}^{-\mathrm{T}}\dot{\mathscr{E}}$ represent the push-forward versions of the incremental stress, electric displacement vector, and electric field vector, respectively.

The constitutive relations are linearized via Taylor expansion as

$$\begin{aligned} &\dot{\mathbf{T}}_0 = J^{-1}\mathbf{F}\frac{\partial^2\Omega}{\partial\mathbf{F}\partial\mathbf{F}}\cdot\cdot\dot{\mathbf{F}} + J^{-1}\mathbf{F}\frac{\partial^2\Omega}{\partial\mathbf{F}\partial\mathscr{D}}\dot{\mathscr{D}} := \mathbf{A}_0\cdot\cdot\mathbf{L} + \mathbf{M}_0\dot{\mathbf{D}}_0, \\ &\dot{\mathbf{E}}_0 = \mathbf{F}^{-\mathrm{T}}\frac{\partial^2\Omega}{\partial\mathscr{D}\partial\mathbf{F}}\cdot\cdot\dot{\mathbf{F}} + \mathbf{F}^{-\mathrm{T}}\frac{\partial^2\Omega}{\partial\mathscr{D}\partial\mathscr{D}}\dot{\mathscr{D}} := \mathbf{M}_0^{\mathrm{T}}\cdot\cdot\mathbf{L} + \mathbf{K}_0\dot{\mathbf{D}}_0, \end{aligned} \tag{8}$$

where $\mathbf{L} = \left([I_{\circledast}]^{\mathrm{T}}\widetilde{\mathbf{F}} - \mathbf{F}\right)\mathbf{F}^{-1} := \dot{\mathbf{F}}\mathbf{F}^{-1} = \mathrm{grad}\mathbf{u}$ is the displacement gradient tensor, with $\mathbf{u}(\mathbf{x}) = \mathbf{u}(\chi(\mathbf{X})) = \dot{\mathbf{x}}(\mathbf{X})$. It should be noted that $I_{\circledast}$ is a two-point unit tensor used to transform bases across configurations and will be omitted hereafter when no ambiguity arises. The double inner products follow the rules of $\boldsymbol{\Xi}_1 : \boldsymbol{\Xi}_2 = (\Xi_1)_{ij}(\Xi_2)_{ij}$ and $\boldsymbol{\Xi}_1\cdot\cdot\boldsymbol{\Xi}_2 = (\Xi_1)_{ij}(\Xi_2)_{ji}$, respectively (where $\boldsymbol{\Xi}_1$ and $\boldsymbol{\Xi}_2$ are two distinct second-order tensors); while the product "$\underset{2}{\circ}$" follows $\mathbf{A}\underset{2}{\circ}\mathbf{F}^{\mathrm{T}} = A_{\alpha i\beta j}\boldsymbol{E}^r_\alpha\otimes\boldsymbol{e}_i\otimes\boldsymbol{E}^r_\beta\otimes\boldsymbol{e}_j\underset{2}{\circ}F_{k\gamma}\boldsymbol{E}^r_\gamma\otimes\boldsymbol{e}_k = A_{\alpha i\beta j}F_{k\beta}\boldsymbol{E}^r_\alpha\otimes\boldsymbol{e}_i\otimes\boldsymbol{e}_k\otimes\boldsymbol{e}_j$, where $\{\boldsymbol{E}^r_\alpha\}$ and $\{\boldsymbol{e}_i\}$ are the bases in the reference and initial configurations, respectively. The instantaneous material tensors $\mathbf{A}_0$, $\mathbf{M}_0$, and $\mathbf{K}_0$ have components given by

$$\begin{aligned} &\mathrm{A}_{0jigk} = J^{-1}\mathrm{F}_{j\alpha}\mathrm{F}_{g\beta}\left(\sum_{m=1, m\neq 4}^{6}\sum_{n=1, n\neq 4}^{6}\Omega_{mn}\frac{\partial\mathscr{I}_m}{\partial\mathrm{F}_{i\alpha}}\frac{\partial\mathscr{I}_n}{\partial\mathrm{F}_{k\beta}} + \sum_{m=1, m\neq 4}^{6}\Omega_m\frac{\partial^2\mathscr{I}_m}{\partial\mathrm{F}_{i\alpha}\partial\mathrm{F}_{k\beta}}\right) = \mathrm{A}_{0gkji}, \\ &\mathrm{M}_{0jik} = \mathrm{F}_{j\alpha}\mathrm{F}^{-1}_{\beta k}\left(\sum_{m=1, m\neq 4}^{6}\sum_{n=4}^{6}\Omega_{mn}\frac{\partial\mathscr{I}_m}{\partial\mathrm{F}_{i\alpha}}\frac{\partial\mathscr{I}_n}{\partial\mathscr{D}_\beta} + \sum_{m=5}^{6}\Omega_m\frac{\partial^2\mathscr{I}_m}{\partial\mathrm{F}_{i\alpha}\partial\mathscr{D}_\beta}\right) = \mathrm{M}_{0kji}, \\ &K_{0jk} = J\mathrm{F}^{-1}_{\alpha j}\mathrm{F}^{-1}_{\beta k}\left(\sum_{m=4}^{6}\sum_{n=4}^{6}\Omega_{mn}\frac{\partial\mathscr{I}_m}{\partial\mathscr{D}_\alpha}\frac{\partial\mathscr{I}_n}{\partial\mathscr{D}_\beta} + \sum_{m=4}^{6}\Omega_m\frac{\partial^2\mathscr{I}_m}{\partial\mathscr{D}_\alpha\partial\mathscr{D}_\beta}\right) = \mathrm{K}_{0kj}, \end{aligned} \tag{9}$$

where $\Omega_{mn} = \partial^2\Omega / (\partial\mathscr{I}_m\partial\mathscr{I}_n)$. Here, we use the Einstein summation convention to express the instantaneous material tensors. If the external electric field is neglected, the incremental boundary conditions yield

$$\dot{\mathbf{T}}_0^{\mathrm{T}}\mathbf{n} = \dot{\mathbf{t}}_{\hat{a}}, \quad \mathbf{n}\cdot\dot{\mathbf{D}}_0 = \dot{q}_{\hat{a}}, \quad \mathbf{n}\times\dot{\mathbf{E}}_0 = \mathbf{0}, \tag{10}$$

where $\dot{\mathbf{t}}_{\hat{a}}$ and $\dot{q}_{\hat{a}}$ denote the incremental mechanical traction and incremental electric charge per unit area on $\partial\overline{\mathbb{B}}$, satisfying $\dot{\mathbf{t}}_{\hat{a}}\mathrm{d}\hat{a} = \dot{\mathbf{t}}_{\hat{A}}\mathrm{d}\hat{A}$ and $\dot{q}_{\hat{a}}\mathrm{d}\hat{a} = \dot{q}_{\hat{A}}\mathrm{d}\hat{A}$, respectively.

3. Governing equations and general solutions

We consider that an electroactive body undergoes a uniform, finite deformation, consisting of an equi-biaxial stretch λ_1 within the plane perpendicular to the z-axis (i.e., $\lambda_2 = \lambda_1$) and a transverse stretch λ_3 parallel to the z-axis. Given the symmetry of the problem with respect to the plane $z = 0$, it is sufficient to analyse only the $z \geq 0$ half-space, as illustrated in Fig. 3. This deformed configuration is also accompanied by an electric displacement field that is purely normal to the plane $z = 0$, with D_3 as its only non-zero component. Thus, we have

$$\mathbf{F} = \begin{bmatrix} \lambda_1 & 0 & 0 \\ 0 & \lambda_1 & 0 \\ 0 & 0 & \lambda_3 \end{bmatrix}, \quad \mathbf{D} = \begin{Bmatrix} 0 \\ 0 \\ D_3 \end{Bmatrix}. \tag{11}$$

Substituting the deformation gradient and electric displacement field into the linearized equilibrium equations displayed in Eq. (8), we have

$$\begin{aligned}
&\dot{\mathrm{T}}_{0xx} = A_{01111}\frac{\partial u_x}{\partial x} + A_{01122}\frac{\partial u_y}{\partial y} + A_{01133}\frac{\partial u_z}{\partial z} + M_{0113}\dot{D}_{0z},\\
&\dot{\mathrm{T}}_{0yy} = A_{01122}\frac{\partial u_x}{\partial x} + A_{01111}\frac{\partial u_y}{\partial y} + A_{01133}\frac{\partial u_z}{\partial z} + M_{0113}\dot{D}_{0z},\\
&\dot{\mathrm{T}}_{0zz} = A_{01133}\frac{\partial u_x}{\partial x} + A_{01133}\frac{\partial u_y}{\partial y} + A_{03333}\frac{\partial u_z}{\partial z} + M_{0333}\dot{D}_{0z},\\
&\dot{\mathrm{T}}_{0xy} = A_{01221}\frac{\partial u_x}{\partial y} + A_{01212}\frac{\partial u_y}{\partial x}, \quad \dot{\mathrm{T}}_{0yx} = A_{01212}\frac{\partial u_x}{\partial y} + A_{01221}\frac{\partial u_y}{\partial x},\\
&\dot{\mathrm{T}}_{0xz} = A_{01331}\frac{\partial u_x}{\partial z} + A_{01313}\frac{\partial u_z}{\partial x} + M_{0131}\dot{D}_{0x}, \quad \dot{\mathrm{T}}_{0zx} = A_{03131}\frac{\partial u_x}{\partial z} + A_{01331}\frac{\partial u_z}{\partial x} + M_{0131}\dot{D}_{0x},\\
&\dot{\mathrm{T}}_{0yz} = A_{01331}\frac{\partial u_y}{\partial z} + A_{01313}\frac{\partial u_z}{\partial y} + M_{0131}\dot{D}_{0y}, \quad \dot{\mathrm{T}}_{0zy} = A_{03131}\frac{\partial u_y}{\partial z} + A_{01331}\frac{\partial u_z}{\partial y} + M_{0131}\dot{D}_{0y},
\end{aligned} \tag{12}$$

$$\begin{aligned}
&\dot{E}_{0x} = M_{0131}\left(\frac{\partial u_x}{\partial z} + \frac{\partial u_z}{\partial x}\right) + K_{011}\dot{D}_{0x}, \quad \dot{E}_{0y} = M_{0131}\left(\frac{\partial u_y}{\partial z} + \frac{\partial u_z}{\partial y}\right) + K_{011}\dot{D}_{0y},\\
&\dot{E}_{0z} = M_{0113}\left(\frac{\partial u_x}{\partial x} + \frac{\partial u_y}{\partial y}\right) + M_{0333}\frac{\partial u_z}{\partial z} + K_{033}\dot{D}_{0z},
\end{aligned} \tag{13}$$

which can be represented in terms of displacement components u_κ and electric potential $\widetilde{\varphi}$ by introducing $\dot{\mathrm{E}}_{0\kappa} = -\partial\widetilde{\varphi}/\partial\kappa$ ($\kappa = x, y, z$) according to Eq. $(7)_3$:

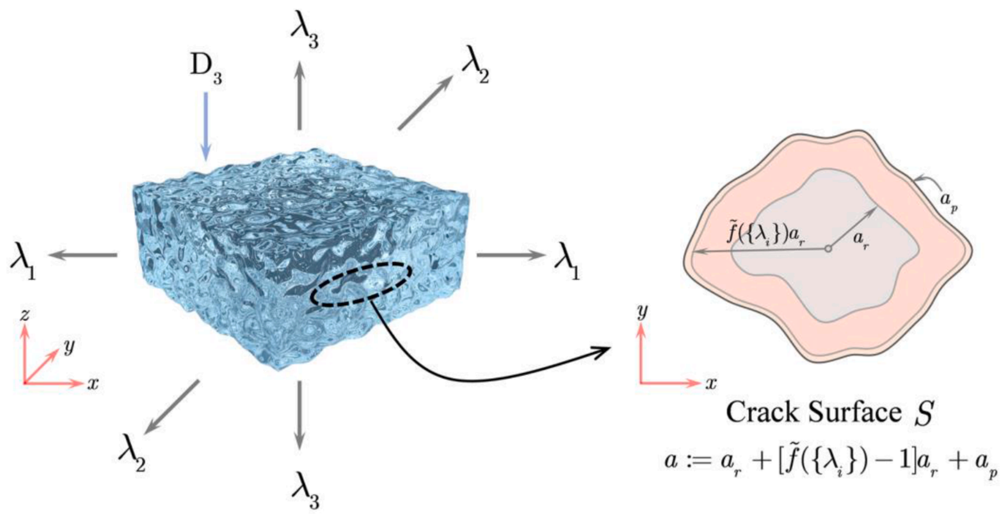

Fig. 3. Definitions of symmetric crack problem. The pre-stretches λ_1, λ_2, and λ_3 together with an electric displacement component D_3 are along the axes of the Cartesian coordinate system. A crack of general shape with surface area S in $\overline{\mathbb{B}}$ is embedded in the electroactive material. a_r and a represent the radius of the crack surface before and after pre-stretch, respectively. a_p denotes the radial length of crack propagation during pre-deformation. The function $\widetilde{f}(\{\lambda_i\})$ quantifies the proportional variation of the crack surface radius due to changes in the stretches λ_i ($i = 1, 2, 3$).

$$
\begin{aligned}
&\dot{\mathrm{T}}_{0xx} = c_{11}\frac{\partial u_x}{\partial x} + c_{12}\frac{\partial u_y}{\partial y} + c_{13}\frac{\partial u_z}{\partial z} + e_{31}\frac{\partial \widetilde{\varphi}}{\partial z},\\
&\dot{\mathrm{T}}_{0yy} = c_{12}\frac{\partial u_x}{\partial x} + c_{11}\frac{\partial u_y}{\partial y} + c_{13}\frac{\partial u_z}{\partial z} + e_{31}\frac{\partial \widetilde{\varphi}}{\partial z},\\
&\dot{\mathrm{T}}_{0zz} = c_{13}\frac{\partial u_x}{\partial x} + c_{13}\frac{\partial u_y}{\partial y} + c_{33}\frac{\partial u_z}{\partial z} + e_{33}\frac{\partial \widetilde{\varphi}}{\partial z},\\
&\dot{\mathrm{T}}_{0xy} = c_{69}\frac{\partial u_x}{\partial y} + c_{66}\frac{\partial u_y}{\partial x}, \quad \dot{\mathrm{T}}_{0yx} = c_{66}\frac{\partial u_x}{\partial y} + c_{69}\frac{\partial u_y}{\partial x},\\
&\dot{\mathrm{T}}_{0xz} = c_{58}\frac{\partial u_x}{\partial z} + c_{55}\frac{\partial u_z}{\partial x} + e_{15}\frac{\partial \widetilde{\varphi}}{\partial x}, \quad \dot{\mathrm{T}}_{0zx} = c_{88}\frac{\partial u_x}{\partial z} + c_{58}\frac{\partial u_z}{\partial x} + e_{15}\frac{\partial \widetilde{\varphi}}{\partial x},\\
&\dot{\mathrm{T}}_{0yz} = c_{58}\frac{\partial u_y}{\partial z} + c_{55}\frac{\partial u_z}{\partial y} + e_{15}\frac{\partial \widetilde{\varphi}}{\partial y}, \quad \dot{\mathrm{T}}_{0zy} = c_{88}\frac{\partial u_y}{\partial z} + c_{58}\frac{\partial u_z}{\partial y} + e_{15}\frac{\partial \widetilde{\varphi}}{\partial y},
\end{aligned}
\tag{14}
$$

$$
\begin{aligned}
&\dot{\mathrm{D}}_{0x} = e_{15}\left(\frac{\partial u_x}{\partial z} + \frac{\partial u_z}{\partial x}\right) - \varepsilon_{11}\frac{\partial \widetilde{\varphi}}{\partial x}, \quad \dot{\mathrm{D}}_{0y} = e_{15}\left(\frac{\partial u_y}{\partial z} + \frac{\partial u_z}{\partial y}\right) - \varepsilon_{11}\frac{\partial \widetilde{\varphi}}{\partial y},\\
&\dot{\mathrm{D}}_{0z} = e_{31}\left(\frac{\partial u_x}{\partial x} + \frac{\partial u_y}{\partial y}\right) + e_{33}\frac{\partial u_z}{\partial z} - \varepsilon_{33}\frac{\partial \widetilde{\varphi}}{\partial z},
\end{aligned}
\tag{15}
$$

where the instantaneous material tensors A_{0jigk}, M_{0jik}, and K_{0jk} ($i,j,k,g = 1,2,3$) together with equivalent constants c_{mn}, e_{mn}, and ε_{mn} (m, $n = \{1,2,3,5,6,8,9\}$) are presented in Appendix A. Note that relation $c_{11} - c_{12} = c_{69} + c_{66}$ is applied in the derivation process. Substituting Eqs. (14) and (15) into Eq. $(7)_{1\text{-}2}$, the governing equations are derived as

$$
\begin{aligned}
&\left(c_{11}\frac{\partial^2}{\partial x^2} + c_{66}\frac{\partial^2}{\partial y^2} + c_{88}\frac{\partial^2}{\partial z^2}\right)u_x + (c_{12}+c_{69})\frac{\partial^2 u_y}{\partial x \partial y} + (c_{13}+c_{58})\frac{\partial^2 u_z}{\partial x \partial z} + (e_{15}+e_{31})\frac{\partial^2 \widetilde{\varphi}}{\partial x \partial z} = 0,\\
&(c_{12}+c_{69})\frac{\partial^2 u_x}{\partial x \partial y} + \left(c_{66}\frac{\partial^2}{\partial x^2} + c_{11}\frac{\partial^2}{\partial y^2} + c_{88}\frac{\partial^2}{\partial z^2}\right)u_y + (c_{13}+c_{58})\frac{\partial^2 u_z}{\partial y \partial z} + (e_{15}+e_{31})\frac{\partial^2 \widetilde{\varphi}}{\partial y \partial z} = 0,\\
&(c_{13}+c_{58})\frac{\partial}{\partial z}\left(\frac{\partial u_x}{\partial x} + \frac{\partial u_y}{\partial y}\right) + \left(c_{55}\Delta + c_{33}\frac{\partial^2}{\partial z^2}\right)u_z + \left(e_{15}\Delta + e_{33}\frac{\partial^2}{\partial z^2}\right)\widetilde{\varphi} = 0,\\
&(e_{15}+e_{31})\frac{\partial}{\partial z}\left(\frac{\partial u_x}{\partial x} + \frac{\partial u_y}{\partial y}\right) + \left(e_{15}\Delta + e_{33}\frac{\partial^2}{\partial z^2}\right)u_z - \left(\varepsilon_{11}\Delta + \varepsilon_{33}\frac{\partial^2}{\partial z^2}\right)\widetilde{\varphi} = 0,
\end{aligned}
\tag{16}
$$

where $\Delta = \partial^2/\partial x^2 + \partial^2/\partial y^2$ is the planar Laplacian. If we set

$$
u_x = \frac{\partial(\psi_0 + \widetilde{\psi})}{\partial y} - \frac{\partial(\Phi_0 + \widetilde{\Phi})}{\partial x}, \quad u_y = -\frac{\partial(\psi_0 + \widetilde{\psi})}{\partial x} - \frac{\partial(\Phi_0 + \widetilde{\Phi})}{\partial y},
\tag{17}
$$

Eq. $(16)_{1\text{-}2}$ can be expressed as

$$
\begin{aligned}
&\frac{\partial}{\partial y}\left[\left(c_{66}\Delta + c_{88}\frac{\partial^2}{\partial z^2}\right)(\psi_0 + \widetilde{\psi})\right] - \frac{\partial}{\partial x}\left[\left(c_{11}\Delta + c_{88}\frac{\partial^2}{\partial z^2}\right)(\Phi_0 + \widetilde{\Phi}) - (c_{13}+c_{58})\frac{\partial u_z}{\partial z} - (e_{15}+e_{31})\frac{\partial \widetilde{\varphi}}{\partial z}\right] = 0,\\
&\frac{\partial}{\partial x}\left[\left(c_{66}\Delta + c_{88}\frac{\partial^2}{\partial z^2}\right)(\psi_0 + \widetilde{\psi})\right] + \frac{\partial}{\partial y}\left[\left(c_{11}\Delta + c_{88}\frac{\partial^2}{\partial z^2}\right)(\Phi_0 + \widetilde{\Phi}) - (c_{13}+c_{58})\frac{\partial u_z}{\partial z} - (e_{15}+e_{31})\frac{\partial \widetilde{\varphi}}{\partial z}\right] = 0.
\end{aligned}
\tag{18}
$$

The solutions are obtained by introducing Ψ that fulfils

$$
\begin{aligned}
&\frac{\partial \Psi}{\partial x} = \left(c_{66}\Delta + c_{88}\frac{\partial^2}{\partial z^2}\right)(\psi_0 + \widetilde{\psi}),\\
&\frac{\partial \Psi}{\partial y} = \left(c_{11}\Delta + c_{88}\frac{\partial^2}{\partial z^2}\right)(\Phi_0 + \widetilde{\Phi}) - (c_{13}+c_{58})\frac{\partial u_z}{\partial z} - (e_{15}+e_{31})\frac{\partial \widetilde{\varphi}}{\partial z},
\end{aligned}
\tag{19}
$$

and $\Delta\Psi = 0$, where $\widetilde{\psi}$ and $\widetilde{\Phi}$ are nontrivial solutions of $\partial\widetilde{\psi}/\partial y - \partial\widetilde{\Phi}/\partial x = 0$ and $\partial\widetilde{\psi}/\partial x + \partial\widetilde{\Phi}/\partial y = 0$, leading to $\Delta\widetilde{\psi} = 0$ and $\Delta\widetilde{\Phi} = 0$. Assuming $c_{88}\partial^2\widetilde{\psi}/\partial z^2 = \partial\Psi/\partial x$ and $c_{88}\partial^2\widetilde{\Phi}/\partial z^2 = \partial\Psi/\partial y$, then Eq. (19) simplifies as

$$
\begin{aligned}
&\left(c_{66}\Delta + c_{88}\frac{\partial^2}{\partial z^2}\right)\psi_0 = 0,\\
&\left(c_{11}\Delta + c_{88}\frac{\partial^2}{\partial z^2}\right)\Phi_0 - (c_{13}+c_{58})\frac{\partial u_z}{\partial z} - (e_{15}+e_{31})\frac{\partial \widetilde{\varphi}}{\partial z} = 0.
\end{aligned}
\tag{20}
$$

Substituting Eq. (17) into Eq. $(16)_{3\text{-}4}$ and combining Eq. $(20)_2$, the governing equations for Φ_0, u_z, and $\widetilde{\varphi}$ can be organized in a matrix form as

$$\mathfrak{D}\left\{\begin{array}{c}\Phi_0\\ u_z\\ \widetilde{\varphi}\end{array}\right\}=\begin{bmatrix} c_{11}\Delta+c_{88}\dfrac{\partial^2}{\partial z^2} & -(c_{13}+c_{58})\dfrac{\partial}{\partial z} & -(e_{15}+e_{31})\dfrac{\partial}{\partial z}\\ -(c_{13}+c_{58})\Delta\dfrac{\partial}{\partial z} & c_{55}\Delta+c_{33}\dfrac{\partial^2}{\partial z^2} & e_{15}\Delta+e_{33}\dfrac{\partial^2}{\partial z^2}\\ (e_{15}+e_{31})\Delta\dfrac{\partial}{\partial z} & -\left(e_{15}\Delta+e_{33}\dfrac{\partial^2}{\partial z^2}\right) & \varepsilon_{11}\Delta+\varepsilon_{33}\dfrac{\partial^2}{\partial z^2}\end{bmatrix}\left\{\begin{array}{c}\Phi_0\\ u_z\\ \widetilde{\varphi}\end{array}\right\}=\mathbf{0}. \tag{21}$$

Then, the solution is assumed to be

$$\left\{\begin{array}{c}\Phi_0\\ u_z\\ \widetilde{\varphi}\end{array}\right\}=\mathfrak{D}^{\dagger}\boldsymbol{\xi}=\begin{bmatrix}\mathfrak{F}_{11} & \mathfrak{F}_{21} & \mathfrak{F}_{31}\\ \mathfrak{F}_{12} & \mathfrak{F}_{22} & \mathfrak{F}_{32}\\ \mathfrak{F}_{13} & \mathfrak{F}_{23} & \mathfrak{F}_{33}\end{bmatrix}\left\{\begin{array}{c}\xi^{(1)}\\ \xi^{(2)}\\ \xi^{(3)}\end{array}\right\}, \tag{22}$$

where $\mathfrak{D}^{\dagger}$ is the adjugate of $\mathfrak{D}$; $\mathfrak{F}_{ij}\quad(i,j=1,2,3)$ are the cofactors of the operator matrix $\mathfrak{D}$; $\boldsymbol{\xi}=\left[\xi^{(1)},\xi^{(2)},\xi^{(3)}\right]^{\mathrm{T}}$ is a vector function that satisfies

$$\mathfrak{D}\mathfrak{D}^{\dagger}\boldsymbol{\xi}=(\det\mathfrak{D})\boldsymbol{\xi}=\left(\hbar_0\frac{\partial^6}{\partial z^6}+\hbar_1\Delta\frac{\partial^4}{\partial z^4}+\hbar_2\Delta^2\frac{\partial^2}{\partial z^2}+\hbar_3\Delta^3\right)\boldsymbol{\xi}=\hbar_3\left(\Delta+\frac{\partial^2}{\partial z_1^2}\right)\left(\Delta+\frac{\partial^2}{\partial z_2^2}\right)\left(\Delta+\frac{\partial^2}{\partial z_3^2}\right)\boldsymbol{\xi}=\mathbf{0}, \tag{23}$$

where $\hbar_i(i=0,1,2,3)$ are presented in Appendix A; $z_j^2=s_j^2z^2(j=1,2,3)$, and s_j^2 are the roots of the bicubic $\hbar_0s^6-\hbar_1s^4+\hbar_2s^2-\hbar_3=0$, as derived in Appendix A. It is noted that $\xi^{(1)}$, $\xi^{(2)}$, and $\xi^{(3)}$ are not independent, which indicates that any one of them, e.g., $\xi^{(i)}(i=1,2,3)$, can be selected for convenience. According to the generalized Almansi's theorem (Ding et al., 1996), the solutions of Eq. (22) may be classified into three cases:

$$\begin{cases}\xi^{(i)}=\xi_1^{(i)}+\xi_2^{(i)}+\xi_3^{(i)}, & (\text{when}\, s_1^2\neq s_2^2\neq s_3^2\neq s_1^2)\\ \xi^{(i)}=\xi_1^{(i)}+\xi_2^{(i)}+z\xi_3^{(i)}, & (\text{when}\, s_1^2\neq s_2^2=s_3^2)\\ \xi^{(i)}=\xi_1^{(i)}+z\xi_2^{(i)}+z^2\xi_3^{(i)}, & (\text{when}\, s_1^2=s_2^2=s_3^2)\end{cases} \tag{24}$$

where $\xi_k^{(i)}\ (k=1,2,3)$ are governed by

$$\left(\Delta+\frac{\partial^2}{\partial z_k^2}\right)\xi_k^{(i)}=0,\ \text{no summation over}\, k. \tag{25}$$

It is important to note that the roots of $\hbar_0s^6-\hbar_1s^4+\hbar_2s^2-\hbar_3=0$ may become imaginary, leading to instability of the electroactive material induced by pre-deformation. For brevity, we may simply assume that the roots are distinct hereinafter.

Without loss of generality, we may adopt $\Phi_0=\mathfrak{F}_{21}\xi^{(2)}$, $u_z=\mathfrak{F}_{22}\xi^{(2)}$, and $\varphi=\mathfrak{F}_{23}\xi^{(2)}$. Then

$$\begin{aligned}\Phi_0&=\left[(c_{13}+c_{58})\left(\varepsilon_{11}\Delta+\varepsilon_{33}\frac{\partial^2}{\partial z^2}\right)+(e_{15}+e_{31})\left(e_{15}\Delta+e_{33}\frac{\partial^2}{\partial z^2}\right)\right]\frac{\partial\xi^{(2)}}{\partial z}\\&=\left(a_1\frac{\partial^2}{\partial z^2}+b_1\Delta\right)\frac{\partial\xi^{(2)}}{\partial z}=\sum_{k=1}^{3}\left(a_1s_k^3-b_1s_k^2\right)\frac{\partial^3\xi_k^{(2)}}{\partial z_k^3}:=\sum_{k=1}^{3}\psi_k,\\u_z&=\left[\left(c_{11}\Delta+c_{88}\frac{\partial^2}{\partial z^2}\right)\left(\varepsilon_{11}\Delta+\varepsilon_{33}\frac{\partial^2}{\partial z^2}\right)+(e_{15}+e_{31})^2\Delta\frac{\partial^2}{\partial z^2}\right]\xi^{(2)}\\&=\left(a_2\frac{\partial^4}{\partial z^4}+b_2\Delta\frac{\partial^2}{\partial z^2}+d_2\Delta^2\right)\xi^{(2)}=\sum_{k=1}^{3}\left(a_2s_k^4-b_2s_k^2+d_2\right)\frac{\partial^4\xi_k^{(2)}}{\partial z_k^4}:=\sum_{k=1}^{3}\alpha_{1k}\frac{\partial\psi_k}{\partial z_k},\\\varphi&=\left[\left(c_{11}\Delta+c_{88}\frac{\partial^2}{\partial z^2}\right)\left(e_{15}\Delta+e_{33}\frac{\partial^2}{\partial z^2}\right)-(c_{13}+c_{58})(e_{15}+e_{31})\Delta\frac{\partial^2}{\partial z^2}\right]\xi^{(2)}\\&=\left(a_3\frac{\partial^4}{\partial z^4}+b_3\Delta\frac{\partial^2}{\partial z^2}+d_3\Delta^2\right)\xi^{(2)}=\sum_{k=1}^{3}\left(a_3s_k^4-b_3s_k^2+d_3\right)\frac{\partial^4\xi_k^{(2)}}{\partial z_k^4}:=\sum_{k=1}^{3}\alpha_{2k}\frac{\partial\psi_k}{\partial z_k},\end{aligned} \tag{26}$$

where

$$\begin{aligned}
&a_1 = (c_{13} + c_{58})\varepsilon_{33} + (e_{15} + e_{31})e_{33},\\
&b_1 = (c_{13} + c_{58})\varepsilon_{11} + (e_{15} + e_{31})e_{15},\\
&a_2 = c_{88}\varepsilon_{33}, \quad b_2 = c_{11}\varepsilon_{33} + c_{88}\varepsilon_{11} + (e_{15} + e_{31})^2, \quad d_2 = c_{11}\varepsilon_{11},\\
&a_3 = c_{88}e_{33}, \quad b_3 = c_{11}e_{33} + c_{88}e_{15} - (c_{13} + c_{58})(e_{15} + e_{31}), \quad d_3 = c_{11}e_{15},\\
&\alpha_{1k} = \frac{a_2 s_k^4 - b_2 s_k^2 + d_2}{s_k(a_1 s_k^2 - b_1)}, \quad \alpha_{2k} = \frac{a_3 s_k^4 - b_3 s_k^2 + d_3}{s_k(a_1 s_k^2 - b_1)}.
\end{aligned} \tag{27}$$

In view of Eqs. $(20)_1$ and (25), ψ_i $(i = 0, 1, 2, 3)$ satisfies

$$\left(\Delta + \frac{\partial^2}{\partial z_i^2}\right)\psi_i = 0, \text{ no summation over } i \tag{28}$$

where $s_0^2 = c_{66}/c_{88}$. In Cartesian coordinates (x, y, z), the mechanical displacement components and the electric potential are thus expressed as

$$u_x = \frac{\partial \psi_0}{\partial y} - \sum_{k=1}^{3}\frac{\partial \psi_k}{\partial x}, \quad u_y = -\frac{\partial \psi_0}{\partial x} - \sum_{k=1}^{3}\frac{\partial \psi_k}{\partial y}, \quad u_z = \sum_{k=1}^{3}\alpha_{1k}\frac{\partial \psi_k}{\partial z_k}, \quad \tilde{\varphi} = \sum_{k=1}^{3}\alpha_{2k}\frac{\partial \psi_k}{\partial z_k}, \tag{29}$$

which is the general solution to the governing equations. To facilitate later derivation steps, it can be rewritten in cylindrical coordinates (ρ, ϕ, z) as

$$u_\rho = \frac{1}{\rho}\frac{\partial \psi_0}{\partial \phi} - \sum_{k=1}^{3}\frac{\partial \psi_k}{\partial \rho}, \quad u_\phi = -\frac{\partial \psi_0}{\partial \rho} - \frac{1}{\rho}\sum_{k=1}^{3}\frac{\partial \psi_k}{\partial \phi}, \quad u_z = \sum_{k=1}^{3}\alpha_{1k}\frac{\partial \psi_k}{\partial z_k} := w_1, \quad \tilde{\varphi} = \sum_{k=1}^{3}\alpha_{2k}\frac{\partial \psi_k}{\partial z_k} := w_2\,. \tag{30}$$

Therefore, the equivalent incremental stress and electric displacement components are

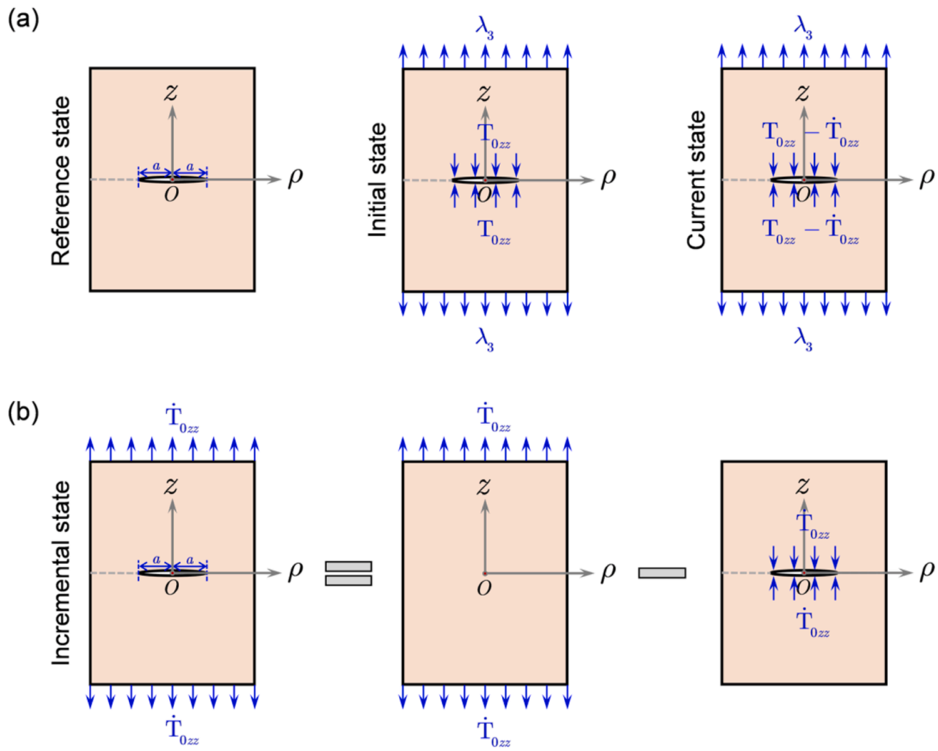

Fig. 4. Schematic of a soft electroactive solid containing a flat crack under mechanical loading in the z-direction: (a) the reference, initial, and current states together with the corresponding boundary conditions, and (b) the equivalent boundary conditions in the incremental state.

$$
\begin{aligned}
&\dot{\mathrm{T}}_{0zz}=\sum_{k=1}^{3}\gamma_{1k}\frac{\partial^2\psi_k}{\partial z_k^2}:=\sigma_{z1},\quad \dot{\mathrm{D}}_{0z}=\sum_{k=1}^{3}\gamma_{2k}\frac{\partial^2\psi_k}{\partial z_k^2}:=\sigma_{z2},\quad \dot{\mathrm{T}}_{0\rho\rho}+\dot{\mathrm{T}}_{0\phi\phi}=\sum_{k=1}^{3}\gamma_{3k}\frac{\partial^2\psi_k}{\partial z_k^2}:=\sigma_{z3},\\
&\dot{\mathrm{T}}_{0\rho\rho}-\dot{\mathrm{T}}_{0\phi\phi}=(c_{12}-c_{11})\left[\frac{2}{\rho}\left(\frac{1}{\rho}\frac{\partial\psi_0}{\partial\phi}-\frac{\partial^2\psi_0}{\partial\rho\partial\phi}\right)+\sum_{k=1}^{3}\left(\frac{\partial^2\psi_k}{\partial\rho^2}-\frac{1}{\rho}\frac{\partial\psi_k}{\partial\rho}-\frac{1}{\rho^2}\frac{\partial^2\psi_k}{\partial\phi^2}\right)\right]:=\sigma_{\rho t},\\
&\dot{\mathrm{T}}_{0\rho\phi}+\dot{\mathrm{T}}_{0\phi\rho}=(c_{66}+c_{69})\left[\left(-\frac{\partial^2\psi_0}{\partial\rho^2}+\frac{1}{\rho}\frac{\partial\psi_0}{\partial\rho}+\frac{1}{\rho^2}\frac{\partial^2\psi_0}{\partial\phi^2}\right)+\sum_{k=1}^{3}\frac{2}{\rho}\left(\frac{1}{\rho}\frac{\partial\psi_k}{\partial\phi}-\frac{\partial^2\psi_k}{\partial\rho\partial\phi}\right)\right]:=\sigma_{\phi t},\quad \dot{\mathrm{T}}_{0\rho\phi}-\dot{\mathrm{T}}_{0\phi\rho}=(c_{69}-c_{66})\Delta\psi_0:=\sigma_{zt},\\
&\dot{\mathrm{T}}_{0z\rho}=c_{88}\frac{1}{\rho}\frac{\partial^2\psi_0}{\partial\phi\partial z}+\sum_{k=1}^{3}\varpi_{1k}\frac{\partial^2\psi_k}{\partial\rho\partial z_k}:=\sigma_{\rho1},\quad \dot{\mathrm{T}}_{0\rho z}=c_{58}\frac{1}{\rho}\frac{\partial^2\psi_0}{\partial\phi\partial z}+\sum_{k=1}^{3}\varpi_{2k}\frac{\partial^2\psi_k}{\partial\rho\partial z_k}:=\sigma_{\rho2},\quad \dot{\mathrm{D}}_{0\rho}=e_{15}\frac{1}{\rho}\frac{\partial^2\psi_0}{\partial\phi\partial z}+\sum_{k=1}^{3}\varpi_{3k}\frac{\partial^2\psi_k}{\partial\rho\partial z_k}:=\sigma_{\rho3},\\
&\dot{\mathrm{T}}_{0z\phi}=-c_{88}\frac{\partial^2\psi_0}{\partial\rho\partial z}+\sum_{k=1}^{3}\varpi_{1k}\frac{1}{\rho}\frac{\partial^2\psi_k}{\partial\phi\partial z_k}:=\sigma_{\phi1},\quad \dot{\mathrm{T}}_{0\phi z}=-c_{58}\frac{\partial^2\psi_0}{\partial\rho\partial z}+\sum_{k=1}^{3}\varpi_{2k}\frac{1}{\rho}\frac{\partial^2\psi_k}{\partial\phi\partial z_k}:=\sigma_{\phi2},\quad \dot{\mathrm{D}}_{0\phi}=-e_{15}\frac{\partial^2\psi_0}{\partial\rho\partial z}+\sum_{k=1}^{3}\varpi_{3k}\frac{1}{\rho}\frac{\partial^2\psi_k}{\partial\phi\partial z_k}:=\sigma_{\phi3},
\end{aligned}
\tag{31}
$$

where

$$
\begin{aligned}
&\gamma_{1k}=c_{13}+s_k(c_{33}\alpha_{1k}+e_{33}\alpha_{2k}),\quad \gamma_{2k}=e_{31}+s_k(e_{33}\alpha_{1k}-\varepsilon_{33}\alpha_{2k}),\quad \gamma_{3k}=c_{11}+c_{12}+2s_k(c_{13}\alpha_{1k}+e_{31}\alpha_{2k}),\\
&\varpi_{1k}=-c_{88}s_k+c_{58}\alpha_{1k}+e_{15}\alpha_{2k},\quad \varpi_{2k}=-c_{58}s_k+c_{55}\alpha_{1k}+e_{15}\alpha_{2k},\quad \varpi_{3k}=-e_{15}s_k+e_{15}\alpha_{1k}-\varepsilon_{11}\alpha_{2k}.
\end{aligned}
\tag{32}
$$

4. Potential theory method for complete solutions

In general, maintaining a flat crack under pre-deformation usually necessitates applying external loads on the crack surfaces. In the absence of such loads, an initial crack opening is likely to develop. Physically, the case of zero crack-face stress and electric displacement can be interpreted via superimposing a surface load that is equal in magnitude but opposite in direction. As an illustrative example, a schematic of the mechanical loading condition in the z-direction is provided in Fig. 4.

The incremental boundary conditions of a flat crack at $z=0$ read

$$
\begin{array}{lll}
\sigma_{z1}=P_1(\rho,\phi), & \sigma_{z2}=P_2(\rho,\phi), & (\rho,\phi)\in S\\
w_1=0, & w_2=0, & (\rho,\phi)\notin S\\
\sigma_{\rho1}=0, & \sigma_{\phi1}=0, & (\rho,\phi)\in[0,+\infty)\times[0,2\pi]
\end{array}
\tag{33}
$$

and the potentials are assumed as

$$
\begin{cases}
\psi_0=0,\\
\psi_k=\sum_{i=1}^{2}\varsigma_{ki}\widehat{H}_i(\rho,\phi,z_k),\quad (k=1,2,3)
\end{cases}
\tag{34}
$$

where $\widehat{H}_i(\rho,\phi,z_k)$ are established over the crack surface S, as

$$
\widehat{H}_i(\rho,\phi,z_k)=\iint_S\frac{\omega_i(\rho_0,\phi_0)}{\sqrt{\rho^2+\rho_0^2-2\rho\rho_0\cos(\phi-\phi_0)+z_k^2}}\rho_0\mathrm{d}\rho_0\mathrm{d}\phi_0,\quad (i=1,2;k=1,2,3)
\tag{35}
$$

in which $\omega_1(\rho,\phi)$ and $\omega_2(\rho,\phi)$ represent the densities of crack face displacement $w_1(\rho,\phi,0)$ and electric potential $w_2(\rho,\phi,0)$, respectively. We emphasize that the crack surface $S\subset\partial\overline{\mathbb{B}}$ differs from $S_r\subset\partial\overline{\mathbb{B}}_r$ due to the evolving crack size during pre-deformation and the potential crack propagation. According to the property of single layer potential (Fabrikant, 1989), we have

$$
\begin{aligned}
&\lim_{z_k\to0^+}\frac{\partial\widehat{H}_i(\rho,\phi,z_k)}{\partial z_k}=-2\pi\omega_i(\rho,\phi)=-2\pi w_i(\rho,\phi,0),\quad (\rho,\phi)\in S\\
&\lim_{z_k\to0^+}\frac{\partial\widehat{H}_i(\rho,\phi,z_k)}{\partial z_k}=0,\quad (\rho,\phi)\notin S
\end{aligned}
\tag{36}
$$

for $i=1,2,3$. With Eqs. (30), (31), $(33)_{2\text{-}3}$, (34), and (36), we arrive at

$$
\begin{aligned}
&\sigma_{\rho1}(\rho,\phi,0)=\sum_{i=1}^{2}\left(\sum_{k=1}^{3}\varpi_{1k}\varsigma_{ki}\right)\lim_{z_k\to0^+}\frac{\partial^2\widehat{H}_i(\rho,\phi,z_k)}{\partial\rho\partial z_k}=0\Rightarrow\sum_{k=1}^{3}\varpi_{1k}\varsigma_{ki}=0,\\
&w_j(\rho,\phi,0)=\sum_{i=1}^{2}\left(\sum_{k=1}^{3}\alpha_{jk}\varsigma_{ki}\right)\lim_{z_k\to0^+}\frac{\partial\widehat{H}_i(\rho,\phi,z_k)}{\partial z_k}=-2\pi\sum_{i=1}^{2}\left(\sum_{k=1}^{3}\alpha_{jk}\varsigma_{ki}\right)w_i\Rightarrow\sum_{k=1}^{3}\alpha_{jk}\varsigma_{ki}=-\frac{\delta_{ji}}{2\pi},
\end{aligned}
\tag{37}
$$

where $j = 1, 2$, and δ_{ji} is the Kronecker delta. It is noted that the summations are interchanged in Eq. (37), and the terms with $\widehat{H}_i$ are independent of z_k when $z_k \to 0^+$. Besides, $\sigma_{\phi 1}(\rho, \phi, 0) = 0$ gives the same equation as that derived from $\sigma_{\rho 1}(\rho, \phi, 0) = 0$, because ψ_0 is assumed to be zero. Hence, we only claim $\sigma_{\rho 1}(\rho, \phi, 0) = 0$ in Eq. (37). Eventually, ς_{ki} can be determined as

$$\begin{Bmatrix} \varsigma_{1i} \\ \varsigma_{2i} \\ \varsigma_{3i} \end{Bmatrix} = -\frac{1}{2\pi} \begin{bmatrix} \varpi_{11} & \varpi_{12} & \varpi_{13} \\ \alpha_{11} & \alpha_{12} & \alpha_{13} \\ \alpha_{21} & \alpha_{22} & \alpha_{23} \end{bmatrix}^{-1} \begin{Bmatrix} 0 \\ \delta_{1i} \\ \delta_{2i} \end{Bmatrix}. \tag{38}$$

From Eq. $(33)_1$, the integro-differential equations are derived as

$$\sum_{i=1}^{2} \left(\sum_{k=1}^{3} \gamma_{jk} \varsigma_{ki} \right) \lim_{z_k \to 0} \frac{\partial^2}{\partial z_k^2} \iint_S \frac{\omega_i(\rho_0, \phi_0)}{\sqrt{\rho^2 + \rho_0^2 - 2\rho\rho_0 \cos(\phi - \phi_0) + z_k^2}} \rho_0 \mathrm{d}\rho_0 \mathrm{d}\phi_0 = P_j(\rho, \phi), \quad (j = 1, 2) \tag{39}$$

leading to

$$\lim_{z_k \to 0} \frac{\partial^2}{\partial z_k^2} \iint_S \frac{\omega_i(\rho_0, \phi_0)}{\sqrt{\rho^2 + \rho_0^2 - 2\rho\rho_0 \cos(\phi - \phi_0) + z_k^2}} \rho_0 \mathrm{d}\rho_0 \mathrm{d}\phi_0 = \sum_{j=1}^{2} \eta_{ij} P_j(\rho, \phi), \quad (i = 1, 2) \tag{40}$$

where

$$\begin{bmatrix} \eta_{11} & \eta_{12} \\ \eta_{21} & \eta_{22} \end{bmatrix} = \begin{bmatrix} \sum_{k=1}^{3} \gamma_{1k} \varsigma_{k1} & \sum_{k=1}^{3} \gamma_{1k} \varsigma_{k2} \\ \sum_{k=1}^{3} \gamma_{2k} \varsigma_{k1} & \sum_{k=1}^{3} \gamma_{2k} \varsigma_{k2} \end{bmatrix}^{-1}. \tag{41}$$

In torsionless axisymmetric problems, $\partial(\#)/\partial\phi = 0$, $u_\phi = 0$, and $\sigma_{\phi m} = 0 (m = 1,2,3)$. The terms in $\sigma_{\rho t}$, $\sigma_{\phi t}$, and σ_{zt} are also modified accordingly. As shown in Appendix B, Eq. (40) is a type-A integro-differential equation, with solution

$$\omega_i(\rho, \phi) = \frac{1}{\pi^2} \int_\rho^a \frac{\mathrm{d}x}{\sqrt{x^2 - \rho^2}} \int_0^x \frac{\rho_0 \mathrm{d}\rho_0}{\sqrt{x^2 - \rho_0^2}} \mathscr{L}\left(\frac{\rho\rho_0}{x^2}\right) \sum_{j=1}^{2} \eta_{ij} P_j(\rho_0, \phi), \quad (i = 1, 2) \tag{42}$$

when $S = \{(\rho, \phi) | 0 \le \rho \le a; 0 \le \phi \le 2\pi\}$. Here, $a := a(\lambda_1) = a_r + (\lambda_1 - 1)a_r + a_p$, where a_r represents the radius of the crack surface S_r in reference configuration, and a_p denotes the radial length of the crack propagation during pre-deformation ($a_p = 0$ if no crack propagation occurs). It is noted that the crack is assumed to grow along its initial path according to the kinking stability. Thus, the potential functions are in the form of

$$\widehat{H}_i(\rho, \phi, z_k) = 4 \int_0^{l_1(a)} \frac{\mathrm{d}x}{\sqrt{\rho^2 - x^2}} \int_{g(x)}^a \frac{\rho_0 \mathrm{d}\rho_0}{\sqrt{\rho_0^2 - g^2(x)}} \mathscr{L}\left(\frac{x^2}{\rho\rho_0}\right) \omega_i(\rho_0, \phi), \quad (i = 1, 2; k = 1, 2, 3) \tag{43}$$

where $\mathscr{L}(\#)$, $g(x)$, and $l_1(a)$ are defined in Appendix B. When the integral is intractable by analytical approaches, we employ semi-analytical or numerical methods, with the densities formulated as

$$\omega_i(\rho, \phi) = \frac{1}{2\pi^3} \int_0^{2\pi} \int_0^a \frac{1}{R_0} \arctan\left(\frac{\sqrt{l_2^2(a) - \rho^2} \sqrt{a^2 - \rho_0^2}}{l_2(a) R_0} \right) \sum_{j=1}^{2} \eta_{ij} P_j(\rho_0, \phi_0) \rho_0 \mathrm{d}\rho_0 \mathrm{d}\phi_0 \tag{44}$$

according to Eq. (B.44), where R_0 is elucidated in Appendix B. In the following subsections, we present several representative examples for verification and application.

4.1. Penny-shaped cracks

For axisymmetric uniform loads applied on the crack surface S, i.e., $P_j(\rho, \phi) \equiv P_j (j = 1, 2)$, Eqs. (42) and (43) yield

$$\omega_i(\rho) = \frac{1}{\pi^2} \int_\rho^a \frac{\mathrm{d}x}{\sqrt{x^2 - \rho^2}} \int_0^x \frac{\rho_0 \mathrm{d}\rho_0}{\sqrt{x^2 - \rho_0^2}} \mathscr{L}\left(\frac{\rho\rho_0}{x^2}\right) \sum_{j=1}^{2} \eta_{ij} P_j = \frac{1}{\pi^2} \left(\sum_{j=1}^{2} \eta_{ij} P_j \right) \sqrt{a^2 - \rho^2}, \tag{45}$$

$$\widehat{H}_i(\rho, z_k) = \frac{\sum_{j=1}^{2} \eta_{ij} P_j}{2\pi} \left\{ \left[2\left(a^2 + z_k^2\right) - \rho^2 \right] \arctan\left[\frac{l_1(a)}{\sqrt{\rho^2 - l_1^2(a)}} \right] + \frac{l_1(a) \left[\rho^2 - l_1^2(a) - 2z_k^2 \right]}{\sqrt{\rho^2 - l_1^2(a)}} \right\}. \tag{46}$$

Using the identities

$$\arctan\left[\frac{l_1(a)}{\sqrt{\rho^2 - l_1^2(a)}}\right] = \arcsin\left[\frac{l_1(a)}{\rho}\right] = \arcsin\left[\frac{a}{l_2(a)}\right] \tag{47}$$

and

$$\frac{l_1(a)\left[\rho^2 - l_1^2(a) - 2z_k^2\right]}{\sqrt{\rho^2 - l_1^2(a)}} = \frac{3l_1^2(a) - 2a^2}{a}\sqrt{l_2^2(a) - a^2}, \tag{48}$$

yields another form of Eq. (46) as

$$\widehat{H}_i(\rho, z_k) = \frac{\sum_{j=1}^{2}\eta_{ij}P_j}{2\pi}\left\{\left[2\left(a^2 + z_k^2\right) - \rho^2\right]\arcsin\left[\frac{a}{l_2(a)}\right] - \frac{2a^2 - 3l_1^2(a)}{a}\sqrt{l_2^2(a) - a^2}\right\}, \tag{49}$$

where $l_2(a)$ is defined in Appendix B, that satisfies $l_1(a)l_2(a) = \rho a$ and $l_1^2(a) + l_2^2(a) = \rho^2 + a^2 + z_k^2$. Within an incremental field framework, the potential function in Eq. (49) matches the published linear-case result except for the involved material parameters (Chen et al., 2004), and hence the proposed theory is validated. Substituting Eq. (46) into Eqs. (30) and (31), the nonzero mechanical displacement, electric potential, equivalent incremental stress, and electric displacement components are derived in Appendix D. By letting $z = 0$, $\sigma_{zm}(m = 1, 2)$ can be simplified as

$$\lim_{z\to 0}\sigma_{zm} = \begin{cases} \sum_{k=1}^{3}\sum_{i=1}^{2}\gamma_{mk}\varsigma_{ki}\sum_{j=1}^{2}\eta_{ij}P_j, & (\rho \le a) \\ \frac{2}{\pi}\sum_{k=1}^{3}\sum_{i=1}^{2}\gamma_{mk}\varsigma_{ki}\sum_{j=1}^{2}\eta_{ij}P_j\left[\arctan\left(\frac{a}{\sqrt{\rho^2 - a^2}}\right) - \frac{a}{\sqrt{\rho^2 - a^2}}\right]. & (\rho > a) \end{cases} \tag{50}$$

In view of Eq. (41), it readily follows that $\sum_{k=1}^{3}\sum_{i=1}^{2}\gamma_{mk}\varsigma_{ki}\sum_{j=1}^{2}\eta_{ij}P_j = P_m$, which is identical to the boundary conditions $P_j(\rho, \phi) \equiv P_j(j = 1, 2)$ when $\rho \le a$, thus confirming the validity of analytical solutions. Besides, the incremental intensity factors (mode I) are obtained as

$$\begin{aligned} \dot{K}_{\mathrm{IT}} &= \lim_{\rho\to a}\left[\sqrt{2(\rho - a)}\dot{\mathrm{T}}_{0zz}|_{z=0}\right] = -\frac{2}{\pi}\sqrt{a}P_1, \\ \dot{K}_{\mathrm{ID}} &= \lim_{\rho\to a}\left[\sqrt{2(\rho - a)}\dot{D}_{0z}|_{z=0}\right] = -\frac{2}{\pi}\sqrt{a}P_2, \end{aligned} \tag{51}$$

from which we find that $\dot{K}_{\mathrm{IT}}$ and $\dot{K}_{\mathrm{ID}}$ are independent of material properties and are solely governed by the crack geometry and the applied loads in the respective fields.

We also conducted finite element (FE) simulations for a special case with the energy density function (Zhao et al., 2007)

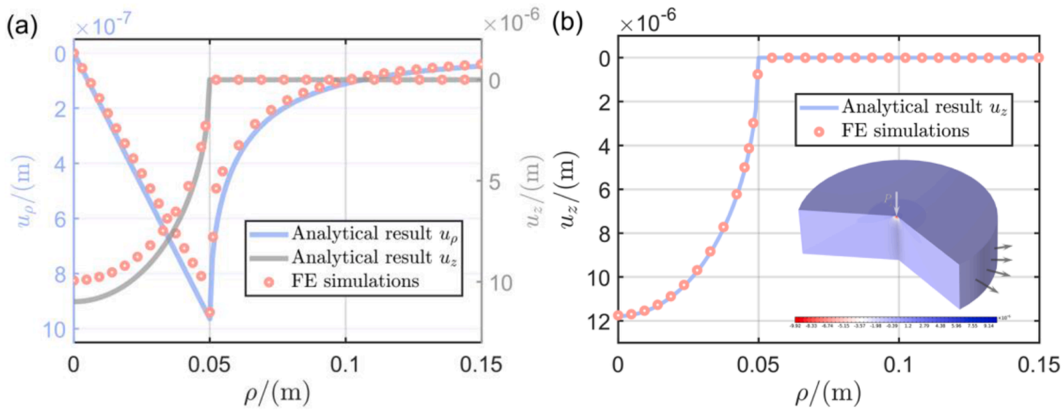

Fig. 5. Finite element simulations and verifications for axial displacement u_z at $z = 0(\mathrm{m})$ under (a) purely mechanical loading and (b) coupled electromechanical loading. The finite element model is a cylinder with a radius and height of 1 m each, which is significantly larger than the loading zone to represent a half-space. Given the decay of physical fields away from the loaded region, where they approach zero, the comparative analysis is confined to the vicinity of the loaded region specifically for $\rho \in [0, 0.15](\mathrm{m})$. Taking advantage of the axisymmetry of the problem, the finite element model was simplified and discretized with a mesh consisting of 57,600 quadrilateral elements and 58,081 nodes.

$$\Omega(\mathbf{F}, \mathscr{D}) = \frac{\mu}{2\Lambda}\left(J^{-2\Lambda} - 1\right) + \frac{\mu}{2}(\mathscr{I}_1 - 3) + \frac{1}{J\varepsilon_0}(\zeta_1 \mathscr{I}_4 + \zeta_2 \mathscr{I}_5), \tag{52}$$

where $\Lambda = \nu/(1-2\nu)$ is a material coefficient; μ, ν, ε_0, ζ_1, and ζ_2 are shear modulus, Poisson's ratio, dielectric permittivity ($\varepsilon_0 = 8.854 \times 10^{-12}(\mathrm{F/m})$ in vacuum), and two dimensionless coefficients describing the electromechanical coupling effect, respectively. As displayed in Fig. 5, we consider a purely mechanical case and an electromechanical case to validate our analytical solutions. In the electromechanical case, $\lambda_1 = 1.1, \lambda_3 = 0.832, D_3 = \sqrt{\mu\varepsilon_0}(\mathrm{C/m^2}), \mu = 1.0(\mathrm{MPa}), \nu = 0.49, \zeta_1 = 0.0, \zeta_2 = 0.05, P_1 = -700(\mathrm{Pa}), P_2 = \sqrt{\mu\varepsilon_0} \times 10^{-3}(\mathrm{C/m^2})$, and $a = 0.05(\mathrm{m})$ are adopted in the electromechanical loading case. Under purely mechanical loading, $\lambda_3 = 0.832$, $D_3 = 0(\mathrm{C/m^2})$, $\zeta_2 = 0.0$, and $P_2 = 0.0(\mathrm{C/m^2})$ are substituted for the corresponding parameters listed above, while the other parameters remain unchanged, so as to preserve physical compatibility.

The results confirm a close match between theoretical predictions and finite element numerical simulations. It is important to note, however, that the incremental theory provides accurate predictions primarily under relatively small incremental external loads. For large loadings, the analysis necessitates a multi-step incremental procedure. The spatial distributions of selected mechanical and electrical quantities along $\rho \in [0, 0.3](\mathrm{m})$ are illustrated at different depths in Fig. 6, with representative parameters $\lambda_1 = 1.1$, $\lambda_3 = 0.832$, $\mathrm{D}_3 = \sqrt{\mu\varepsilon_0}(\mathrm{C/m^2})$, $\mu = 1.0(\mathrm{MPa})$, $\nu = 0.49$, $\zeta_1 = 0.0$, $\zeta_2 = 0.05$, $P_1 = -1000\,(\mathrm{Pa})$, $P_2 = 2.976 \times 10^{-7}(C/\mathrm{m^2})$, and $a = 0.05(\mathrm{m})$. It should be emphasized that, prior to numerical computation, the analytical solution should be nondimensionalized. This treatment mitigates the accumulation of round-off errors caused by large discrepancies in the orders of magnitude among terms during floating-point arithmetic, thereby enhancing both the accuracy and robustness of the numerical solution. The results show that the curves exhibit greater similarity with increasing depth, whereas the crack singularity and applied loads display more pronounced effects on the field distributions near the surface. All physical quantities approach zero in the far-field region, away from the crack and the loaded area.

To investigate the effects of parametric variations and stability on physical field distributions, the z-direction displacement component is presented as an illustrative example in Fig. 7. The parameters are set initially as $\lambda_1 = 1.1$, $\lambda_3 = 0.832$, $\mathrm{D}_3 = \sqrt{\mu\varepsilon_0}(\mathrm{C/m^2})$, $\mu = 1(\mathrm{MPa})$, $\nu = 0.49$, $\zeta_1 = 0.0$, $\zeta_2 = 0.05$, $P_1 = -700(\mathrm{Pa})$, $P_2 = \sqrt{\mu\varepsilon_0} \times 10^{-3}(\mathrm{C/m^2})$, and $a = 0.05(\mathrm{m})$. With the exception of the varying parameter, the other quantities remain unchanged at their initial values.

The figure reveals a nonlinear relationship between u_z and the parameters studied, with u_z being notably sensitive to specific

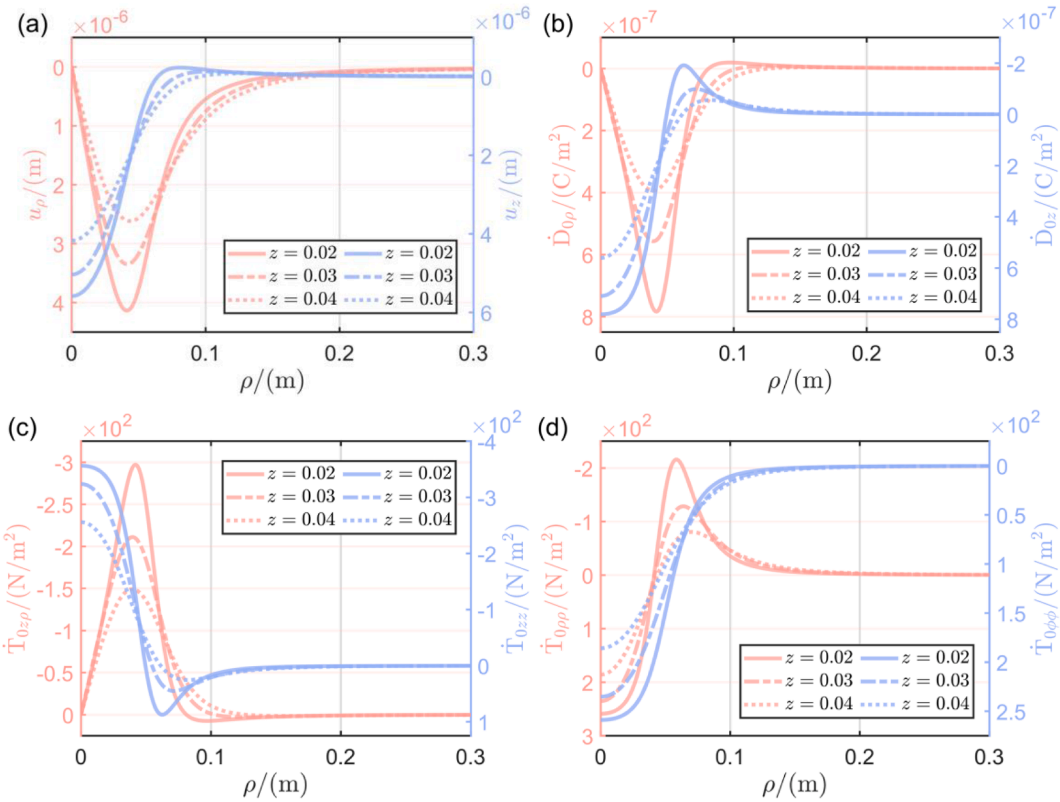

Fig. 6. Spatial distributions of selected mechanical and electrical quantities for (a) radial displacement u_ρ and axial displacement u_z; (b) radial incremental electric displacement $\dot{D}_{0\rho}$ and axial incremental electric displacement $\dot{D}_{0z}$; (c) the push-forward version of the incremental stress components $\dot{\mathrm{T}}_{0z\rho}$ and $\dot{\mathrm{T}}_{0zz}$; and (d) the push-forward version of the incremental stress components $\dot{\mathrm{T}}_{0\rho\rho}$ and $\dot{\mathrm{T}}_{0\phi\phi}$.

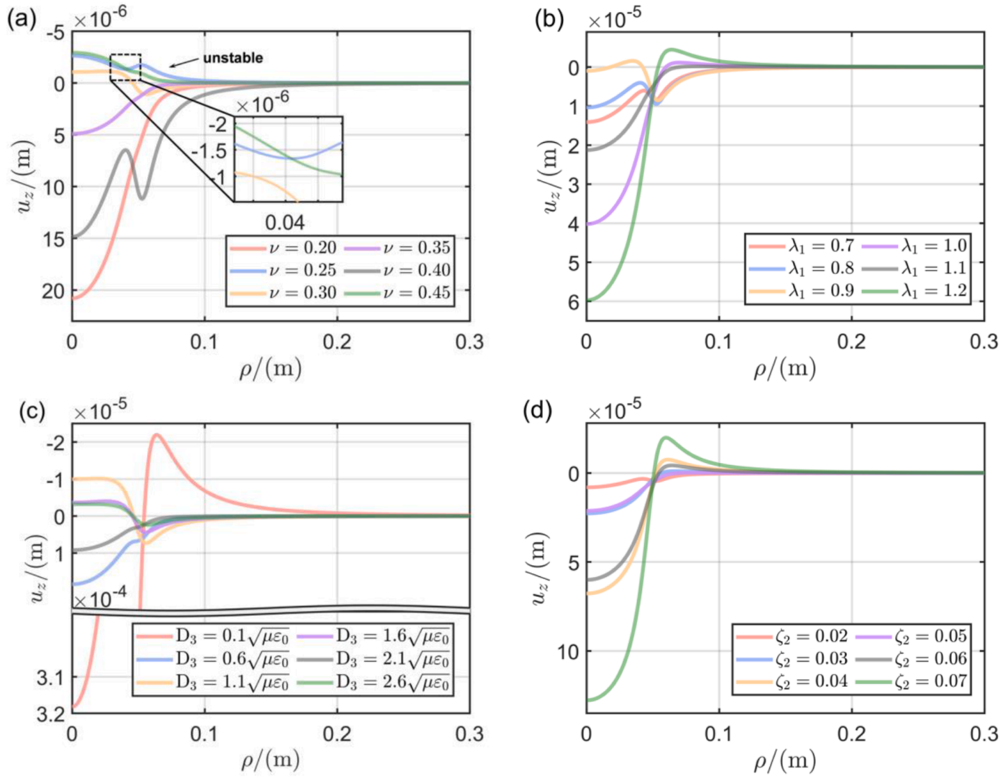

Fig. 7. Parametric dependence of u_z distribution at $z = 0.01(\mathrm{m})$ along $\rho \in [0, 0.15](\mathrm{m})$ for (a) variation of Poisson's ratio ν; (b) variation of stretch λ_1; (c) variation of electrical displacement D_3; and (d) variation of parameter ζ_2.

parameter changes. For example, in Fig. 7(a), increasing Poisson's ratio from 0.40 to 0.45 causes a pronounced shift in u_z. This nonlinearity stems not only from the explicit mathematical form relating u_z to the parameters, but also from the stability behavior of soft electroactive materials under finite pre-deformation. The surface instability within a penny-shaped crack is identified via the bifurcation equation in the subsequent section. Here, the onset of instability is indicated by curves annotated "unstable" in Fig. 7. Nevertheless, buckling may occur and yet remain stable due to the presence of external loads in some cases. It is noted that solutions for penny-shaped cracks subjected to alternative loadings are provided in Appendix E.

4.2. Flat cracks of general shape

The densities and potential functions shown in Eqs. (42) and (43) are designed for the case where S is a circular domain. For a flat crack of general shape with contour $\partial S : \rho = a(\phi)$, we may express Eq. (40) via Eq. (B.5) as

$$\frac{2}{\pi}\lim_{z_k\to 0}\frac{\partial^2}{\partial z_k^2}\int_0^{l_1[a(\phi_0)]}\frac{\mathrm{d}x}{\sqrt{\rho^2 - x^2}}\int_0^{2\pi}\mathrm{d}\phi_0\int_{g(x)}^{a(\phi_0)}\frac{\rho_0\mathrm{d}\rho_0}{\sqrt{\rho_0^2 - g^2(x)}}\mathscr{G}\left(\frac{x^2}{\rho\rho_0}, \phi - \phi_0\right)\omega_i(\rho_0, \phi_0) = \sum_{j=1}^{2}\eta_{ij}P_j(\rho, \phi). \tag{53}$$

We point out that the order of integration has been interchanged in the equation above, and this operation is valid only if $\rho \le \min[a(\phi)]$. For uniform loading (Fabrikant, 1989), we may take

$$\omega_i(\rho, \phi) = \frac{\Theta_i}{a(\phi)}\sqrt{a^2(\phi) - \rho^2} \tag{54}$$

in the analytical solution obtained in Eq. (45), where Θ_i are undetermined constants. Then, Eq. (53) may be further simplified by expanding $\mathscr{G}(\#, \#)$ and integrating over ρ_0 as

$$
\begin{aligned}
\sum_{j=1}^{2}\eta_{ij}P_j &= \frac{2\Theta_i}{\pi}\lim_{z_k\to 0}\frac{\partial^2}{\partial z_k^2}\int_0^{l_1[a(\phi_0)]}\frac{\mathrm{d}x}{\sqrt{\rho^2-x^2}}\int_0^{2\pi}\mathrm{d}\phi_0\int_{g(x)}^{a(\phi_0)}\sum_{n=-\infty}^{+\infty}\left(\frac{x^2}{\rho\rho_0}\right)^{|n|}\mathrm{e}^{\mathrm{i}n(\phi-\phi_0)}\frac{\sqrt{a^2(\phi_0)-\rho_0^2}}{a(\phi_0)}\frac{\rho_0\mathrm{d}\rho_0}{\sqrt{\rho_0^2-g^2(x)}} \\
&= \frac{\Theta_i}{2\sqrt{\pi}}\lim_{z_k\to 0}\frac{\partial^2}{\partial z_k^2}\sum_{n=-\infty}^{+\infty}\int_0^{l_1[a(\phi_0)]}\left(\frac{x^2}{\rho}\right)^{|n|}\frac{\mathrm{d}x}{g(x)\sqrt{\rho^2-x^2}}\int_0^{2\pi}\Gamma\left(1-\frac{|n|}{2}\right)\left[\frac{a^{2-|n|}(\phi_0)}{\Gamma\left(\frac{5}{2}-\frac{|n|}{2}\right)}{}_2\widetilde{F}_1\left(\frac{1}{2},1-\frac{|n|}{2};\frac{5}{2}-\frac{|n|}{2};\frac{a^2(\phi_0)}{g^2(x)}\right)\right. \\
&\quad \left.-\frac{2g^{2-|n|}(x)}{\Gamma\left(\frac{3}{2}-\frac{|n|}{2}\right)}{}_2\widetilde{F}_1\left(-\frac{1}{2},1-\frac{|n|}{2};\frac{3}{2}-\frac{|n|}{2};\frac{g^2(x)}{a^2(\phi_0)}\right)\right]\mathrm{i}\mathrm{e}^{\mathrm{i}n(\phi-\phi_0)}\mathrm{d}\phi_0.
\end{aligned}
\tag{55}
$$

Therefore, we can determine Θ_i via $\sum_{j=1}^{2}\eta_{ij}P_j$.

4.3. Anti-crack problems

The anti-crack problem is defined as a boundary value problem where the incremental displacement components within the crack are prescribed due to the presence of a perfectly embedded rigid inclusion, and the corresponding incremental stress components are to be determined. This is also a typical scenario in the puncture mechanics of soft matter (Fakhouri et al., 2015; Jiang et al., 2025). For simplicity, the rigid inclusion is assumed to be symmetric with respect to the z-axis and the plane $z = 0$. Given its symmetry, the boundary value problem in cylindrical coordinates takes the following mathematical form:

$$
\begin{array}{lll}
w_1 = W_1(\rho,\phi), & w_2 = W_2(\rho,\phi), & (\rho,\phi)\in S \\
w_1 = 0, & w_2 = 0, & (\rho,\phi)\notin S \\
\sigma_{\rho 1} = 0, & \sigma_{\phi 1} = 0, & (\rho,\phi)\in[0,+\infty)\times[0,2\pi]
\end{array}
\tag{56}
$$

where W_1 and W_2 denote the prescribed incremental displacement and electric potential within the crack surface, respectively. We take the same assumptions as those shown in Eq. (34) for potentials, hence the analytical solutions established in Eq. (35) are derived by replacing ω_i with W_i directly, as

$$
\begin{aligned}
\widehat{H}_i(\rho,\phi,z_k) &= \iint_s \frac{W_i(\rho_0,\phi_0)}{\sqrt{\rho^2+\rho_0^2-2\rho\rho_0\cos(\phi-\phi_0)+z_k^2}}\rho_0\mathrm{d}\rho_0\mathrm{d}\phi_0 \\
&= 4\int_0^{l_1(a)}\frac{\mathrm{d}x}{\sqrt{\rho^2-x^2}}\int_{g(x)}^{a}\frac{\rho_0\mathrm{d}\rho_0}{\sqrt{\rho_0^2-g^2(x)}}\mathscr{L}\left(\frac{x^2}{\rho\rho_0}\right)W_i(\rho_0,\phi)
\end{aligned}
\quad (i=1,2;k=1,2,3)
\tag{57}
$$

according to Eq. (36), where the second equality is a simplification resulting from the axisymmetric crack surface assumption. All previous analytical results designed for ω_i still hold in this case and are omitted for brevity.

Apart from the direct method, the primary interest in inclusion and puncture problems often lies in the surface stress distribution on the crack surface,

$$
\begin{aligned}
\sigma_{zi}(\rho,\phi) &= -\frac{1}{\pi^2\rho}\mathscr{L}\left(\frac{1}{\rho}\right)\frac{\mathrm{d}}{\mathrm{d}\rho}\int_0^{\rho}\frac{x\mathrm{d}x}{\sqrt{\rho^2-x^2}}\mathscr{L}(x^2)\frac{\mathrm{d}}{\mathrm{d}x}\int_x^a\frac{\rho_0\mathrm{d}\rho_0}{\sqrt{\rho_0^2-x^2}}\mathscr{L}\left(\frac{1}{\rho_0}\right)W_i(\rho_0,\phi), \quad (0\le\rho<a;i=1,2) \\
\sigma_{zi}(\rho,\phi) &= -\frac{1}{\pi^2\rho}\mathscr{L}\left(\frac{1}{\rho}\right)\frac{\mathrm{d}}{\mathrm{d}\rho}\int_0^{a}\frac{x\mathrm{d}x}{\sqrt{\rho^2-x^2}}\mathscr{L}(x^2)\frac{\mathrm{d}}{\mathrm{d}x}\int_x^a\frac{\rho_0\mathrm{d}\rho_0}{\sqrt{\rho_0^2-x^2}}\mathscr{L}\left(\frac{1}{\rho_0}\right)W_i(\rho_0,\phi), \quad (\rho\ge a;i=1,2)
\end{aligned}
\tag{58}
$$

where details of derivations are presented in Appendix F. Interestingly, the difference between the results inside and outside the crack lies solely in the upper limit of the integration with respect to x.

5. Crack-face stability analysis

The analysis in Section 4 quantitatively captures the incremental response of cracked electroactive materials under various mechanical and electrical loadings. However, once the pre-deformation or initial electric displacement exceeds a critical threshold, instability may occur at the crack faces. For the stability analysis of an axisymmetric crack problem, the governing equations remain identical to those in Eqs. $(7)_{1\text{-}2}$, (14), and (15), except for the boundary conditions at $z = 0$, which now read

$$
\begin{array}{lll}
\sigma_{z1} = 0, & \sigma_{z2} = 0, & (\rho,\phi)\in S \\
w_1 = 0, & w_2 = 0, & (\rho,\phi)\notin S \\
\sigma_{\rho 1} = 0, & \sigma_{\phi 1} = 0. & (\rho,\phi)\in[0,+\infty)\times[0,2\pi]
\end{array}
\tag{59}
$$

The trivial solution $u_\kappa = 0$, $\widetilde{\varphi} = 0$ $(\kappa = \rho,\phi,z)$ is clearly one possible case. However, a non-trivial solution that satisfies the conditions above is possible. While the preceding equations are described in cylindrical coordinates, a similar form holds in Cartesian coordinates.

5.1. Stability in the x–z plane

Within the x-z plane, $u_y = 0$ and $\partial(\#)/\partial y = 0$ are adopted for simplification. Without loss of generality, we assume that the non-trivial solution has the following form

$$u_x = \vartheta_1(\hat{k}z)\mathrm{e}^{\mathrm{i}\hat{k}x}, \quad u_z = \vartheta_2(\hat{k}z)\mathrm{e}^{\mathrm{i}\hat{k}x}, \quad \tilde{\varphi} = \vartheta_3(\hat{k}z)\mathrm{e}^{\mathrm{i}\hat{k}x}, \tag{60}$$

where $\hat{k}$ is the wavenumber, and $\vartheta_i(\hat{k}z)$ $(i = 1,2,3)$ are three yet unknown functions. To satisfy the boundary conditions in Eq. (59), the uniformly pre-deformed electroactive material, with a crack inside, calls for a standing-wave-like condition where the crack width $2a$ should be equal to an integer multiple of the half-wavelength, i.e.,

$$2a_r\lambda_1 + 2a_p = \frac{n}{2}\frac{2\pi}{\hat{k}}, \tag{61}$$

where $n \in \mathbb{N}$. Substituting Eq. (60) into Eq. (16) yields

$$u_x = \sum_{j=1}^{3} \mathrm{i}\mathfrak{A}_j \mathrm{e}^{-\hat{k}\mathfrak{s}_j z}\mathrm{e}^{\mathrm{i}\hat{k}x}, \quad u_z = \sum_{j=1}^{3} \mathfrak{B}_j \mathrm{e}^{-\hat{k}\mathfrak{s}_j z}\mathrm{e}^{\mathrm{i}\hat{k}x}, \quad \tilde{\varphi} = \sum_{j=1}^{3} \mathfrak{C}_j \mathrm{e}^{-\hat{k}\mathfrak{s}_j z}\mathrm{e}^{\mathrm{i}\hat{k}x}, \tag{62}$$

where $\mathfrak{s}_j$ $(j = 1,2,3)$ are the eigenvalues derived from

$$\det\begin{bmatrix} c_{88}\mathfrak{s}^2 - c_{11} & -(c_{13}+c_{58})\mathfrak{s} & -(e_{15}+e_{31})\mathfrak{s} \\ (c_{13}+c_{58})\mathfrak{s} & c_{33}\mathfrak{s}^2 - c_{55} & e_{33}\mathfrak{s}^2 - e_{15} \\ (e_{15}+e_{31})\mathfrak{s} & e_{33}\mathfrak{s}^2 - e_{15} & \varepsilon_{11} - \varepsilon_{33}\mathfrak{s}^2 \end{bmatrix} = 0. \tag{63}$$

Note that the conditions $\mathrm{Re}(\mathfrak{s}_j) > 0$ are required to satisfy $\lim_{z\to\infty}\vartheta_i(\hat{k}z) = 0 (i = 1,2,3)$. In Eq. (62), $\mathfrak{A}_j$, $\mathfrak{B}_j$, and $\mathfrak{C}_j$ $(j = 1,2,3)$ are constants, which are connected via

$$\begin{cases} \left(c_{88}\mathfrak{s}_j^2 - c_{11}\right)\mathfrak{A}_j - (c_{13}+c_{58})\mathfrak{s}_j\mathfrak{B}_j - (e_{15}+e_{31})\mathfrak{s}_j\mathfrak{C}_j = 0, \\ (c_{13}+c_{58})\mathfrak{s}_j\mathfrak{A}_j + \left(c_{33}\mathfrak{s}_j^2 - c_{55}\right)\mathfrak{B}_j + \left(e_{33}\mathfrak{s}_j^2 - e_{15}\right)\mathfrak{C}_j = 0. \end{cases} \tag{64}$$

The boundary conditions shown in Eq. (59) can be reduced to

$$\dot{\mathrm{T}}_{0zz} = 0, \quad \dot{\mathrm{T}}_{0zx} = 0, \quad \dot{\mathrm{D}}_{0z} = 0 \tag{65}$$

within the crack surface, leading to the homogeneous system

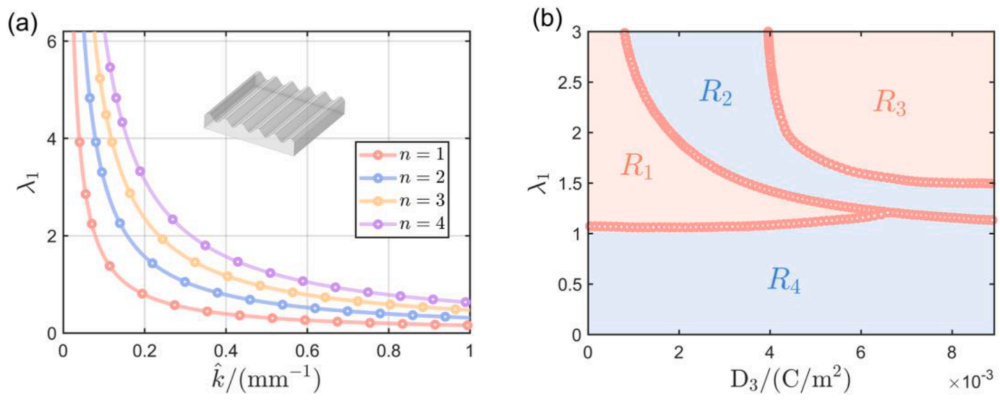

Fig. 8. Bifurcation curves of the x–z plane stability analysis: (a) stretch λ_1 dependence on wave number $\hat{k}$ for various modes n; and (b) critical stretch and electric displacement for $\lambda_3 = 0.6$, $\mu = 1(\mathrm{MPa})$, $\nu = 0.25$, $\zeta_1 = 0$, and $\zeta_2 = 0.5$. Here R_1 and R_3 are the stable regions, while R_2 and R_4 correspond to the unstable regions.

$$\begin{cases} \sum_{j=1}^{3} \left(c_{13}\mathfrak{A}_j + c_{33}\mathfrak{s}_j\mathfrak{B}_j + e_{33}\mathfrak{s}_j\mathfrak{C}_j\right) = 0, \\ \sum_{j=1}^{3} \left(-c_{88}\mathfrak{s}_j\mathfrak{A}_j + c_{58}\mathfrak{B}_j + e_{15}\mathfrak{C}_j\right) = 0, \\ \sum_{j=1}^{3} \left(e_{31}\mathfrak{A}_j + e_{33}\mathfrak{s}_j\mathfrak{B}_j - \varepsilon_{33}\mathfrak{s}_j\mathfrak{C}_j\right) = 0. \end{cases} \tag{66}$$

Combining Eqs. (64) and (66), we arrive at the following bifurcation equation

$$\det(\mathfrak{M}_x) = 0, \tag{67}$$

where $\mathfrak{M}_x$ is presented in Appendix G.

Without crack growth (i.e., $a_p = 0$), the energy release rate satisfies $G < G^*$, where the critical energy release rate G^* reflects the material property. An incremental energy release rate $\dot{G} := G_c - G = -\partial\dot{\Pi}/\partial S$ is further defined to determine whether crack propagation has occurred in the current configuration. Here $\dot{\Pi} := \dot{\mathscr{U}} - \dot{\mathscr{W}}$ is the incremental total potential energy governed by the principle of incremental minimum potential energy $\delta\dot{\Pi} = \delta(\Pi_c - \Pi) = 0$, where Π_c and Π are the total potential energies defined in $\overline{\mathbb{B}}_c$ and $\overline{\mathbb{B}}$, respectively; $\dot{\mathscr{U}}$ is the incremental internal energy; $\dot{\mathscr{W}}$ is the incremental work performed by the applied loads; while G_c and G are the energy release rates defined in $\overline{\mathbb{B}}_c$ and $\overline{\mathbb{B}}$, respectively. Under these assumptions, the bifurcation curves are presented in Fig. 8 for $a_r = 1(\mathrm{cm})$.

When crack propagation occurs, the relation among a_p, λ_1, and λ_3 can be fitted experimentally, under the constraint that $a_p = 0$ when $\lambda_1 = 1$ and $\lambda_3 = 1$. Generally, the energy density function $\Omega(\mathbf{F}, \mathscr{D})$, geometric characteristics of the specimen, and the crack are incorporated into the fracture criterion. This renders the relationship between $\lambda_i (i = 1, 2)$ and $\widehat{k}$ more intricate compared to the case of a non-propagating crack.

The conditions for the persistent stability of the crack-face buckling are further investigated. To this end, we define a buckling topological number as

$$\mathscr{C}_{n^+,n^-} := \mathscr{C}^+_{n^+} + \mathscr{C}^-_{n^-}, \tag{68}$$

where $n^\natural \geq 0$ ($\natural = +, -$) characterizes the number of half-wavelengths within the crack surface radius in the buckling mode, and superscripts "$+$" and "$-$" correspond to the upper and lower crack faces, respectively. A mode is referred to as a simple mode when n^+

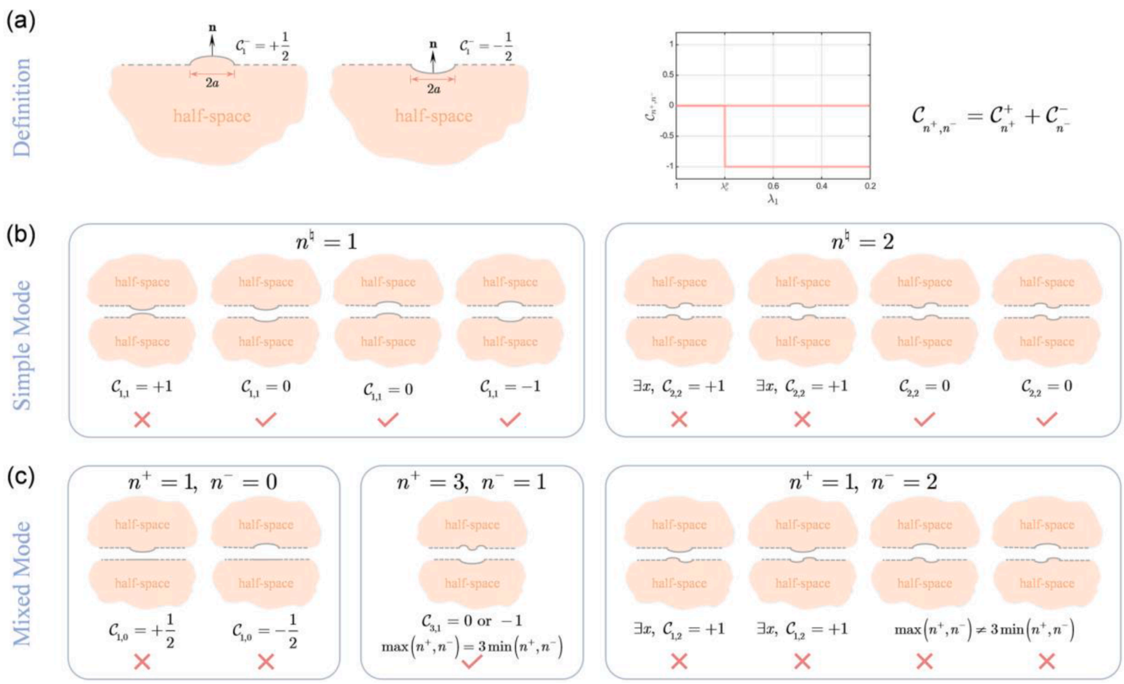

Fig. 9. Criteria for persistent crack-face buckling stability: (a) definition of bulking topological number where λ_c^p is the critical transition point; (b) examples for the simple mode case; and (c) examples for the mixed mode case. In subfigures (b) and (c), the check marks (✓) and cross marks (×) indicate physically admissible and inadmissible modes, respectively.

$= n^-$, and as a mixed mode otherwise. The buckling amplitude is quantified by assigning $\mathscr{C}^{\natural}_{n^{\natural}} = +\frac{1}{2}$ for displacement along the outward normal of the crack surface, and $\mathscr{C}^{\natural}_{n^{\natural}} = -\frac{1}{2}$ for displacement in the opposite direction. An analogous definition is adopted for the electric potential, where $\mathscr{C}^{\natural}_{n^{\natural}} = +\frac{1}{2}$ or $\mathscr{C}^{\natural}_{n^{\natural}} = -\frac{1}{2}$ depending on whether its sign matches or opposes the direction of the outward normal of the crack surface. If all stretches $\lambda_i (i = 1, 3)$ exceed their critical values obtained from the bifurcation equation, buckling is absent ($n = 0$ and $\mathscr{C}_{0,0} = \mathscr{C}_0^+ = \mathscr{C}_0^- = 0$), resulting in the trivial solution. Once buckling emerges, persistent stability is achieved if and only if $\mathscr{C}_{n^+,n^-} = 0$ or -1 for $\forall x \in (-a, a) \setminus \left\{a\left(4\frac{m}{n^{\natural}} - 1\right)\right\}$ when $m, n^{\natural} \in \mathbb{N}^+$ and $2m < n^{\natural}$ in simple mode, while for mixed mode, an additional condition $\max(n^+, n^-) = 3\min(n^+, n^-)$ is required. In Fig. 9, representative examples are presented to illustrate the buckling topological number for cases with penny-shaped cracks. Although the stability criterion remains identical for a crack with an initial opening displacement, the critical transition point from unstable to stable modes shifts.

For mixed-mode buckling, it is important to note that displacement continuity of u_x (i.e., $u_x(a, 0^+) - u_x(a, 0^-) = \mathrm{Re}\left[\mathrm{i}\mathrm{e}^{\mathrm{i}\frac{n\pi}{2}} \sum_{j=1}^{3} \mathfrak{A}_j^{0^+}\right] - \mathrm{Re}\left[\mathrm{i}\mathrm{e}^{\mathrm{i}\frac{n\pi}{2}} \sum_{j=1}^{3} \mathfrak{A}_j^{0^-}\right] = 0$) requires equal buckling amplitude (i.e., $\mathfrak{A}_j^{0^+} = \mathfrak{A}_j^{0^-}$, $\mathfrak{B}_j^{0^+} = \mathfrak{B}_j^{0^-}$, and $\mathfrak{C}_j^{0^+} = \mathfrak{C}_j^{0^-}$), because there is only one independent buckling amplitude according to Eq. (67). Without loss of generality, we may take $\mathfrak{A}_1$ as the independent amplitude. However, different buckling modes possess distinct energy levels, making such a configuration physically unrealistic. For instance, the incremental internal energy defined above is in the form

$$\dot{\mathscr{U}} = \mathscr{U}_c - \mathscr{U} \approx \iiint_{\overline{\mathbb{B}}} (\tau : \epsilon - \mathbf{D} \cdot \dot{\mathbf{E}}_0) \mathrm{d}v, \tag{69}$$

where $\epsilon = \mathrm{sym}(\mathbf{L}) := (\mathbf{L} + \mathbf{L}^{\mathrm{T}})/2$. For simplicity, the discussion here may be confined to an incremental internal energy in the upper and lower bounded half-spaces embedded with the crack in $\overline{\mathbb{B}}$ ($\mathfrak{S}_x^{\pm} = \{(x, y, z) | x \in [-a, a]; y \in (-\infty, +\infty); z \in (-\infty, 0^-)$ or $z \in (0^+, +\infty)\}$). Hence, Eq. (69) may be further analyzed in terms of the independent amplitude as

$$\dot{\mathscr{U}}_{\mathscr{S}_x^{\pm}} \sim \mathrm{Re}\left[\left(\int_0^{\pm\infty} \mathrm{e}^{\mp \hat{k} s z} \mathrm{d}\hat{k} z\right) \frac{2a}{n\pi} \int_{-\frac{n\pi}{2}}^{\frac{n\pi}{2}} \mathscr{A}_1^{0^{\pm}} \mathrm{e}^{i\hat{k}x} \mathrm{d}\hat{k}x\right], \tag{70}$$

leading to $\dot{\mathscr{U}}_{\mathscr{S}_x^{\pm}} = \mathscr{O}\left(\frac{1}{n}\sin\left(\frac{n\pi}{2}\right)\mathscr{A}_1^{0^{\pm}}\right)$. Although geometrically plausible mixed-mode buckling exists, it is precluded by physical constraints. Note that the contributions of incremental stress and electric displacement to the energy change are neglected in Eq. (69), which yields

$$\frac{1}{2} \iiint_{\mathscr{S}_x^{\pm}} (\dot{\mathbf{T}}_0 : \epsilon - \dot{\mathbf{D}}_0 \cdot \dot{\mathbf{E}}_0) \mathrm{d}v = \mathscr{O}\left[n\left(\mathscr{A}_1^{\pm}\right)^2\right]. \tag{71}$$

5.2. Stability in the ρ-z plane

Within the ρ-z plane, $u_\phi = 0$ and $\partial(\#)/\partial\phi = 0$ are adopted to express Eq. (16) as

$$\begin{aligned}
&\left[c_{11}\left(\frac{\partial^2}{\partial\rho^2} + \frac{1}{\rho}\frac{\partial}{\partial\rho} - \frac{1}{\rho^2}\right) + c_{88}\frac{\partial^2}{\partial z^2}\right]u_\rho + (c_{13} + c_{58})\frac{\partial^2 u_z}{\partial\rho\partial z} + (e_{15} + e_{31})\frac{\partial^2 \widetilde{\varphi}}{\partial\rho\partial z} = 0,\\
&(c_{13} + c_{58})\frac{\partial}{\partial z}\left(\frac{\partial}{\partial\rho} + \frac{1}{\rho}\right)u_\rho + \left[c_{55}\left(\frac{\partial^2}{\partial\rho^2} + \frac{1}{\rho}\frac{\partial}{\partial\rho}\right) + c_{33}\frac{\partial^2}{\partial z^2}\right]u_z + \left[e_{15}\left(\frac{\partial^2}{\partial\rho^2} + \frac{1}{\rho}\frac{\partial}{\partial\rho}\right) + e_{33}\frac{\partial^2}{\partial z^2}\right]\widetilde{\varphi} = 0,\\
&(e_{15} + e_{31})\frac{\partial}{\partial z}\left(\frac{\partial}{\partial\rho} + \frac{1}{\rho}\right)u_\rho + \left[e_{15}\left(\frac{\partial^2}{\partial\rho^2} + \frac{1}{\rho}\frac{\partial}{\partial\rho}\right) + e_{33}\frac{\partial^2}{\partial z^2}\right]u_z - \left[\varepsilon_{11}\left(\frac{\partial^2}{\partial\rho^2} + \frac{1}{\rho}\frac{\partial}{\partial\rho}\right) + \varepsilon_{33}\frac{\partial^2}{\partial z^2}\right]\widetilde{\varphi} = 0,
\end{aligned} \tag{72}$$

from which we have

$$u_\rho = \sum_{j=1}^{3} \mathfrak{A}_j \widetilde{J}_1\left(\hat{k}\rho\right) \mathrm{e}^{-\hat{k}\mathfrak{s}_j z}, \quad u_z = \sum_{j=1}^{3} \mathfrak{B}_j \widetilde{J}_0\left(\hat{k}\rho\right) \mathrm{e}^{-\hat{k}\mathfrak{s}_j z}, \quad \widetilde{\varphi} = \sum_{j=1}^{3} \mathfrak{C}_j \widetilde{J}_0\left(\hat{k}\rho\right) \mathrm{e}^{-\hat{k}\mathfrak{s}_j z}, \tag{73}$$

where $\mathfrak{s}_j (j = 1, 2, 3)$ are the roots of

$$\det\begin{bmatrix} c_{88}\mathfrak{s}^2 - c_{11} & (c_{13}+c_{58})\mathfrak{s} & (e_{15}+e_{31})\mathfrak{s} \\ -(c_{13}+c_{58})\mathfrak{s} & c_{33}\mathfrak{s}^2 - c_{55} & e_{33}\mathfrak{s}^2 - e_{15} \\ -(e_{15}+e_{31})\mathfrak{s} & e_{33}\mathfrak{s}^2 - e_{15} & \varepsilon_{11} - \varepsilon_{33}\mathfrak{s}^2 \end{bmatrix} = 0, \tag{74}$$

which is identical to Eq. (63), because the transpose of a matrix leaves its determinant unchanged. Here, the conditions $\mathrm{Re}(\mathfrak{s}_j) > 0$ are required to satisfy $\lim_{z\to\infty} u_\kappa = 0$ $(\kappa = \rho, z)$ and $\lim_{z\to\infty} \widetilde{\varphi} = 0$. $\widetilde{J}_v(\#)$ is the Bessel function of the first kind. The boundary conditions in Eq. (59) are simplified as

$$\begin{aligned} \dot{\mathrm{T}}_{0zz} &= c_{13}\left(\frac{\partial u_\rho}{\partial \rho} + \frac{u_\rho}{\rho}\right) + c_{33}\frac{\partial u_z}{\partial z} + e_{33}\frac{\partial \widetilde{\varphi}}{\partial z} = 0, \\ \dot{\mathrm{T}}_{0z\rho} &= c_{88}\frac{\partial u_\rho}{\partial z} + c_{58}\frac{\partial u_z}{\partial \rho} + e_{15}\frac{\partial \widetilde{\varphi}}{\partial \rho} = 0, \\ \dot{\mathrm{D}}_{0z} &= e_{31}\left(\frac{\partial u_\rho}{\partial \rho} + \frac{u_\rho}{\rho}\right) + e_{33}\frac{\partial u_z}{\partial z} - \varepsilon_{33}\frac{\partial \widetilde{\varphi}}{\partial z} = 0, \end{aligned} \tag{75}$$

together with

$$\widetilde{J}_0\left[\widehat{k}\left(a_r\lambda_1 + a_p\right)\right] = 0 \tag{76}$$

within the crack surface. It is noted that the wavenumber can be derived via the zeros of the Bessel function of the first kind. Finally, the bifurcation equation is obtained after substituting Eq. (73) into Eq. (75) as

$$\det(\mathfrak{M}_\rho) = 0, \tag{77}$$

where $\mathfrak{M}_\rho$ is also presented in Appendix G. Remarkably, the expression in Eq. (77) coincides with that of Eq. (67). Fig. 10 shows the bifurcation curves for the ρ-z plane case, with the same parameters as those described in Section 5.1. We further observe that when the energy release rate remains below the fracture toughness, crack-face buckling precedes crack propagation in systems falling into the unstable regions. Conversely, when systems lie within the stable regions, crack propagation occurs prior to buckling if the energy release rate exceeds the critical threshold. Moreover, a coupled regime where both crack-face instability and crack propagation coexist can occur. For instance, in region R_4, the crack-face instability may induce crack opening and further promote crack propagation when $\lambda_1 < 1$.

Owing to the identical bifurcation equations, a comparison between Figs. 8(b) and 10(b) reveals that the stable region under compression (where $\lambda_3 < 1$) is smaller than that under tension (where $\lambda_3 > 1$), which is consistent with our physical intuition. Besides, the figure suggests the possible emergence of a re-entrant phenomenon for a fixed D_3. For decreasing λ_1, the system may undergo a sequence of transitions from stable to unstable, back to stable, and finally to an unstable region again, which is a fascinating phenomenon. Note also that the consideration of re-entrant behavior yields a rich analysis of crack-face stability. We further analyze the influence of parameter variations on the bifurcation behavior, with the result presented in Fig. 11. All parameters remain identical to those in Fig. 8(b), except for the case under investigation. The comparison shows that the stable region expands as Poisson's ratio approaches zero. This indicates that when the compressive effect in the z-direction (i.e., $\lambda_3 = 0.6$) has less influence on the in-plane deformation in the x-y plane, the overall system becomes more stable, which also aligns well with physical intuition. For $\zeta_2 = 0.6$, the re-entrant phenomenon is no longer observed across the range of analysis.

The topological number $\mathscr{C}_{n^+,n^-}$ is extended here in a direct analogy with the previous section. It follows that for the simple mode,

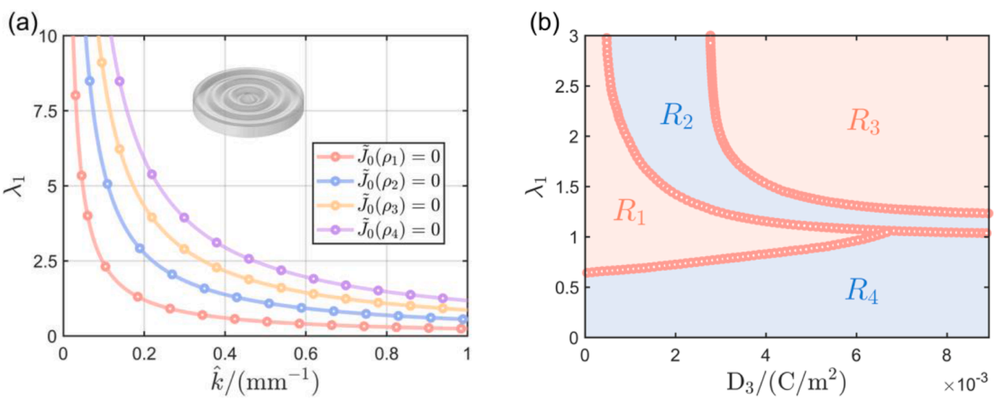

Fig. 10. Bifurcation curves of the ρ–z plane stability analysis: (a) stretch λ_1 dependence on wave number $\widehat{k}$ for various modes n; and (b) critical stretch and electric displacement for $\lambda_3 = 1.2$, $\mu = 1(\mathrm{MPa})$, $\nu = 0.25$, $\zeta_1 = 0$, and $\zeta_2 = 0.5$. Here R_1 and R_3 are the stable regions, while R_2 and R_4 correspond to the unstable regions.

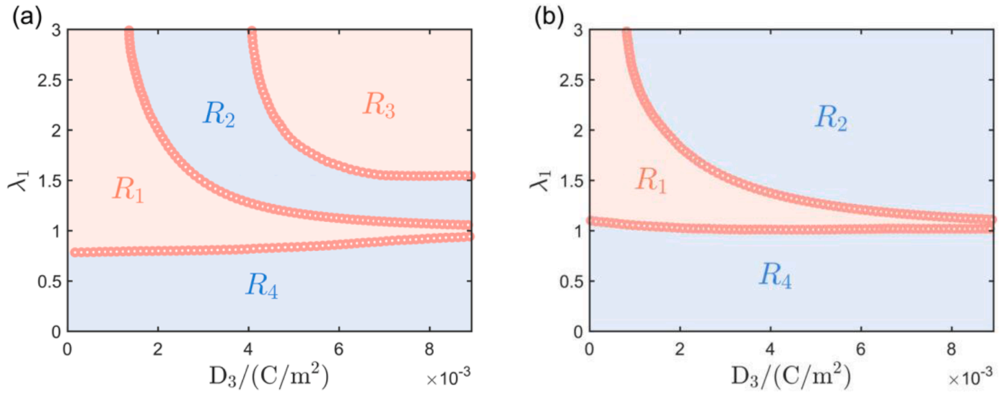

Fig. 11. Parametric dependence of bifurcation equation where R_1 and R_3 are the stable regions, while R_2 and R_4 correspond to the unstable regions: (a) Poisson's ratio $\nu = 0.05$; and (b) parameter $\zeta_2 = 0.6$.

buckling is persistently stable when $\mathscr{C}_{n^+,n^-} = 0$ or -1 for $\forall \rho \in (0,a) \setminus \{\rho_n\}$, where ρ_n is the n-th zero of $\widetilde{J}_0(\rho)$. Similarly, the continuity condition for u_ρ requires the buckling amplitude to be identical. Therefore, the incremental internal energy in $\mathfrak{S}_\rho^\pm$ of the initial configuration can be evaluated as

$$\begin{aligned}
\dot{\mathscr{U}}_{\mathscr{S}_\rho^\pm} &\sim \mathrm{Y}_1 \widehat{k} \int_0^{2\pi} \mathrm{d}\phi \int_0^a \int_0^{\pm\infty} \mathscr{A}_1^{0^\pm} \mathrm{e}^{\mp \hat{k} s z} \widetilde{J}_0(\widehat{k}\rho) \rho \mathrm{d}z \mathrm{d}\rho + \mathrm{Y}_2 \widehat{k} \int_0^{2\pi} \mathrm{d}\phi \int_0^a \int_0^{\pm\infty} \mathscr{A}_1^{0^\pm} \mathrm{e}^{\mp \hat{k} s z} \widetilde{J}_1(\widehat{k}\rho) \rho \mathrm{d}z \mathrm{d}\rho \\
&\sim \mathrm{Y}_1 \left(\int_0^{\pm\infty} e^{\mp \hat{k} s z} d\widehat{k} z \right) \frac{1}{\widehat{k}^2} \int_0^{\hat{k}a} \mathscr{A}_1^{0^\pm} \widetilde{J}_0(\widehat{k}\rho) \widehat{k}\rho d\widehat{k}\rho + \mathrm{Y}_2 \left(\int_0^{\pm\infty} e^{\mp \hat{k} s z} d\widehat{k} z \right) \frac{1}{\widehat{k}^2} \int_0^{\hat{k}a} \mathscr{A}_1^{0^\pm} \widetilde{J}_1(\widehat{k}\rho) \widehat{k}\rho d\widehat{k}\rho \\
&\sim \mathrm{Y}_1 \mathscr{A}_1^{0^\pm} \frac{a^2}{\rho_n} \widetilde{J}_1(\rho_n) + \mathrm{Y}_2 \mathscr{A}_1^{0^\pm} \frac{\pi}{2} \frac{a^2}{\rho_n} \widetilde{J}_1(\rho_n) \widetilde{H}_0(\rho_n),
\end{aligned} \tag{78}$$

where Y_1 and Y_2 are two constants; $\mathfrak{S}_\rho^\pm = \{(\rho,\phi,z) | \rho \in [0,a]; \phi \in [0,2\pi]; z \in (-\infty, 0^-) \text{ or } z \in (0^+, +\infty)\}$; and $\widetilde{H}_\upsilon(\#)$ is the Struve function. Consequently, these findings imply that mixed-mode buckling is also physically precluded. In addition, the term in energy variation arising from the incremental stress and electric displacement is analyzed by

$$\frac{1}{2} \iiint_{\mathfrak{S}_\rho^\pm} (\dot{\mathbf{T}}_0 : \epsilon - \dot{\mathbf{D}}_0 \cdot \dot{\mathbf{E}}_0) \mathrm{d}v \sim \rho_n a [\widetilde{J}_1(\rho_n)]^2 \left(\mathfrak{A}_1^{0^\pm}\right)^2. \tag{79}$$

A comparison between the results in Eqs. (78) and (79) and those in Eqs. (70) and (71) reveal their similar mathematical structure with respect to n and ρ_n. Notably, both Eqs. (70) and (78) indicate that the incremental energy is inversely proportional to n or ρ_n, implying that higher buckling modes involve smaller energy changes. This behavior originates from the decay characteristics in the z-direction, where, for higher-order modes, the displacement field decays more rapidly, confining the deformation to a region near the surface. This physical mechanism is also reflected in the evaluation of the integral $\int_0^{+\infty} \mathrm{e}^{-\hat{k}z} \mathrm{d}z = 1/\widehat{k}$.

6. Conclusions

Dielectric elastomers hold great promise for actuators, sensors, and soft robotics, yet their performance is severely limited by electromechanical failures such as material fracture and electromechanical instability. Accurately characterizing and quantitatively analyzing these failure behaviors is essential for engineering applications and demands rigorous theoretical models, which directly motivates the fracture and crack-face stability analysis of a cracked electroactive solid established in this work. Based on the proposed model, we can analytically determine the incremental mechanical and electrical responses of dielectric elastomers under combined external mechanical and electrical loads, and quantitatively evaluate fracture and crack-surface instability. Based on the nonlinear theory of electroelasticity and incremental field theory, we derived general solutions for type-A and type-B integro-differential equations appearing in the potential theory method. We also put forward complete solutions for analyzing electromechanical behaviors of soft electroelastic bodies containing penny-shaped or arbitrarily shaped flat cracks, subjected to axisymmetric or non-axisymmetric loadings. Represented in terms of special functions, we derived explicit analytical solutions for a penny-shaped crack under various loading conditions and validated against finite element simulations at a high precision level. Besides, the incremental intensity factors for mode I were analytically determined and presented. We emphasized that neither $\dot{\mathbf{T}}$ nor $\dot{\mathbf{T}}_0$ is objective. Hence, an objective stress rate $\overset{\star}{\mathbf{T}} = \dot{\mathbf{T}} - \mathbf{T}\mathbf{L}^{\mathrm{T}}$ was defined based on the Truesdell regime, so that $\overset{\star}{\mathbf{T}}_0 = J^{-1}\mathbf{F}\overset{\star}{\mathbf{T}} = J^{-1}\mathbf{F}(\dot{\mathbf{T}} - \mathbf{T}\mathbf{L}^{\mathrm{T}})$, which is identical to the Truesdell rate of the Cauchy stress tensor $\overset{\circ}{\boldsymbol{\tau}} = \dot{\boldsymbol{\tau}} - \mathbf{L}\boldsymbol{\tau} - \boldsymbol{\tau}\mathbf{L}^{\mathrm{T}} + \mathrm{tr}(\mathbf{L})\boldsymbol{\tau}$.

We also provided general solutions for anti-crack problems. The stability of pre-deformed cracked electroactive bodies was analyzed with respect to two types of surface instabilities, namely, in the x-z and ρ-z planes, accompanied by the derivation of the corresponding bifurcation equations. Besides, our results demonstrate that, for specific material parameters and under a fixed electric displacement, varying the pre-stretch can induce re-entrant phenomena, manifested as repeated alternating transitions between stable and unstable regimes. To evaluate crack propagation, the incremental energy release rate governed by the principle of incremental minimum potential energy was introduced. We also introduced a buckling topological number to characterize persistent stability, along with an estimate of incremental energy in the buckling state, thus providing a unified theoretical framework for addressing crack and stability problems in soft electroelastic materials under finite deformation and analytically prescribed mechanical and electrical loadings.

CRediT authorship contribution statement

Lizichen Chen: Writing – original draft, Validation, Methodology, Investigation, Conceptualization. **Yangkun Du:** Writing – review & editing, Conceptualization. **Rongqiao Xu:** Writing – review & editing, Conceptualization. **Michel Destrade:** Writing – review & editing. **C.W. Lim:** Writing – review & editing. **Weiqiu Chen:** Writing – review & editing, Supervision, Funding acquisition, Conceptualization.

Declaration of competing interest

The authors declare that they have no known competing financial interests or personal relationships that could have appeared to influence the work reported in this paper.

Acknowledgments

The work was supported by the National Natural Science Foundation of China (Nos. 125B2042, 12192211 and 12192210), the 111 Project, PR China (No. B21034), the China Association for Science and Technology Young Elite Scientist Sponsorship Program (Doctoral Student Special Plan), the Qiushi Rising Star Program of Zhejiang University, Hangzhou, Zhejiang Province, and the specialized research projects of Huanjiang Laboratory, Zhuji, Zhejiang Province.

Appendix A. Essential constants and parameters

Nonzero components of the instantaneous material tensors are listed below:

$$
\begin{aligned}
&\mathrm{A}_{01111} = 2\lambda_3^{-1}\{\Omega_1 + \lambda_1^2[(2\Omega_{11} + \Omega_2) + 4\Omega_{12}\lambda_1^2 + 2\Omega_{22}\lambda_1^4] \\
&+\Omega_2\lambda_3^2 + 2\lambda_1^2\lambda_3^2[2\Omega_{12} + 2(\Omega_{13} + \Omega_{22})\lambda_1^2 + \Omega_3/2 \\
&+2\Omega_{23}\lambda_1^4 + \Omega_{22}\lambda_3^2 + 2\Omega_{23}\lambda_1^2\lambda_3^2 + \Omega_{33}\lambda_1^4\lambda_3^2]\}, \\
&\mathrm{A}_{01122} = 4\lambda_1^2\lambda_3^{-1}\{\Omega_{11} + \Omega_2 + 2\Omega_{12}\lambda_1^2 + \Omega_{22}\lambda_1^4 + (2\Omega_{12} + \Omega_3)\lambda_3^2 \\
&+\Omega_{22}\lambda_3^4 + \lambda_1^2\lambda_3^2[2\Omega_{13} + 2\Omega_{22} + 2\Omega_{23}(\lambda_1^2 + \lambda_3^2) + \Omega_{33}\lambda_1^2\lambda_3^2]\}, \\
&\mathrm{A}_{01133} = 4\lambda_3[\Omega_{11} + \Omega_2 + (3\Omega_{12} + \Omega_3)\lambda_1^2 + (\Omega_{13} + 2\Omega_{22})\lambda_1^4 + \Omega_{23}\lambda_1^6 \\
&+\Omega_{12}\lambda_3^2 + (\Omega_{13} + 2\Omega_{22})\lambda_1^2\lambda_3^2 + 3\Omega_{23}\lambda_1^4\lambda_3^2 + \Omega_{33}\lambda_1^6\lambda_3^2] \\
&+4\lambda_1^{-2}\lambda_3^{-1}D_3^2\{\lambda_1^8\lambda_3^4(\Omega_{35} + 2\Omega_{36}\lambda_3^2) + \lambda_1^6\lambda_3^2[\Omega_{15} + 2\Omega_{16}\lambda_3^2 \\
&+(\Omega_{25} + 2\Omega_{26}\lambda_3^2)(\lambda_1^2 + \lambda_3^2)]\}, \\
&\mathrm{A}_{03333} = 2\lambda_1^{-2}\lambda_3\{\Omega_1 + 2\Omega_2\lambda_1^2 + \Omega_3\lambda_1^4 + 2\lambda_3^2[\Omega_{11} + 4\Omega_{12}\lambda_1^2 \\
&+\lambda_1^4(2\Omega_{13} + 4\Omega_{22} + 4\Omega_{23}\lambda_1^2 + \Omega_{33}\lambda_1^4)]\} + 2\lambda_1^{-2}\lambda_3^{-1}D_3^2\{4\Omega_{35}\lambda_1^8\lambda_3^4 \\
&+\lambda_3^2[8\Omega_{36}\lambda_1^8\lambda_3^4 + \Omega_5\lambda_1^4 + 2\lambda_1^4\lambda_3^2(2\Omega_{15} + 3\Omega_6 + 4\Omega_{25}\lambda_1^2 + 4\Omega_{16}\lambda_3^2 \\
&+8\Omega_{26}\lambda_1^2\lambda_3^2)]\} + 4\lambda_1^6\lambda_3^3D_3^4[\Omega_{55} + 4\lambda_3^2(\Omega_{56} + \Omega_{66}\lambda_3^2)], \\
&\mathrm{A}_{01212} = 2\lambda_3^{-1}(\Omega_1 + \Omega_2\lambda_3^2), \mathrm{A}_{01221} = -2\lambda_1^2\lambda_3^{-1}(\Omega_2 + \Omega_3\lambda_3^2), \\
&\mathrm{A}_{01313} = 2\lambda_3^{-1}(\Omega_1 + \Omega_2\lambda_1^2 + \Omega_6\lambda_1^4\lambda_3^2D_3^2), \\
&\mathrm{A}_{01331} = -2\lambda_3(\Omega_2 + \Omega_3\lambda_1^2 - \Omega_6\lambda_1^4D_3^2), \\
&\mathrm{A}_{03131} = 2\lambda_1^{-2}\lambda_3\{\Omega_1 + \Omega_2\lambda_1^2 + \lambda_1^4D_3^2[\Omega_5 + \Omega_6(\lambda_1^2 + 2\lambda_3^2)]\},
\end{aligned}
\tag{A.1}
$$

$$\begin{aligned}
&\mathrm{M}_{0113}=4\lambda_1^4\lambda_3^{-1}D_3\{\Omega_{14}+\Omega_{24}(\lambda_1^2+\lambda_3^2)+\lambda_3^2[\Omega_{15}+\Omega_{34}\lambda_1^2+\Omega_{16}\lambda_3^2\\
&+(\Omega_{26}+\Omega_{35})\lambda_1^2\lambda_3^2+\Omega_{26}\lambda_3^4+\Omega_{36}\lambda_1^2\lambda_3^4+\Omega_{25}(\lambda_1^2+\lambda_3^2)]\},\\
&\mathrm{M}_{0131}=2\lambda_1^2\lambda_3D_3[\Omega_5+\Omega_6(\lambda_1^2+\lambda_3^2)],\\
&\mathrm{M}_{0333}=4\lambda_1^2\lambda_3D_3\{\Omega_{14}+\Omega_5+2\Omega_{24}\lambda_1^2+\Omega_{34}\lambda_1^4+(\Omega_{15}+2\Omega_6)\lambda_3^2\\
&+\Omega_{16}\lambda_3^4+\lambda_1^2\lambda_3^2(2\Omega_{25}+2\Omega_{26}\lambda_3^2+\Omega_{35}\lambda_1^2+\Omega_{36}\lambda_1^2\lambda_3^2)\\
&+\lambda_1^4D_3^2[\Omega_{45}+(2\Omega_{46}+\Omega_{55})\lambda_3^2+3\Omega_{56}\lambda_3^4+2\Omega_{66}\lambda_3^6]\},
\end{aligned}\tag{A.2}$$

$$\begin{aligned}
&\mathrm{K}_{011}=2\lambda_3(\Omega_4+\Omega_5\lambda_1^2+\Omega_6\lambda_1^4),\\
&\mathrm{K}_{033}=2\lambda_1^2\lambda_3^{-1}\{\Omega_4+\lambda_3^2(\Omega_5+\Omega_6\lambda_3^2)+2\lambda_1^4D_3^2[2\Omega_{45}\lambda_3^2\\
&+\lambda_3^4(\Omega_{44}+2\Omega_{46}+\Omega_{55}+2\Omega_{56}\lambda_3^2+\Omega_{66}\lambda_3^4)]\},
\end{aligned}\tag{A.3}$$

and the equivalent constants are expressed as

$$\begin{array}{lll}
c_{11}=\mathrm{A}_{01111}+\mathrm{M}_{0113}e_{31}, & c_{12}=\mathrm{A}_{01122}+\mathrm{M}_{0113}e_{31}, & c_{13}=\mathrm{A}_{01133}+\mathrm{M}_{0113}e_{33},\\
c_{33}=\mathrm{A}_{03333}+\mathrm{M}_{0333}e_{33}, & c_{55}=\mathrm{A}_{01313}+\mathrm{M}_{0131}e_{15}, & c_{58}=\mathrm{A}_{01331}+\mathrm{M}_{0131}e_{15},\\
c_{66}=\mathrm{A}_{01212}, & c_{69}=\mathrm{A}_{01221}, & c_{88}=\mathrm{A}_{03131}+\mathrm{M}_{0131}e_{15},\\
e_{15}=-\mathrm{M}_{0131}\varepsilon_{11}, & e_{31}=-\mathrm{M}_{0113}\varepsilon_{33}, & e_{33}=-\mathrm{M}_{0333}\varepsilon_{33},\\
\varepsilon_{11}=1/\mathrm{K}_{011}, & \varepsilon_{33}=1/\mathrm{K}_{033}. &
\end{array}\tag{A.4}$$

The coefficients of the equation $\hbar_0s^6-\hbar_1s^4+\hbar_2s^2-\hbar_3=0$ are in the form of

$$\begin{aligned}
&\hbar_0=c_{88}(c_{33}\varepsilon_{33}+e_{33}^2),\\
&\hbar_1=c_{33}[c_{88}\varepsilon_{11}+(e_{15}+e_{31})^2]+e_{33}[c_{11}e_{33}+2c_{88}e_{15}-2(c_{13}+c_{58})(e_{15}+e_{31})]+\varepsilon_{33}[c_{11}c_{33}+c_{55}c_{88}-(c_{13}+c_{58})^2],\\
&\hbar_2=c_{55}[c_{11}\varepsilon_{33}+(e_{15}+e_{31})^2]+e_{15}[2c_{11}e_{33}+c_{88}e_{15}-2(c_{13}+c_{58})(e_{15}+e_{31})]+\varepsilon_{11}[c_{11}c_{33}+c_{55}c_{88}-(c_{13}+c_{58})^2],\\
&\hbar_3=c_{11}(c_{55}\varepsilon_{11}+e_{15}^2),
\end{aligned}\tag{A.5}$$

and the roots are

$$\begin{aligned}
&s_1^2=\frac{\hbar_1}{3\hbar_0}-\frac{\sqrt[3]{2}(3\hbar_0\hbar_2-\hbar_1^2)}{3\hbar_0\sqrt[3]{\mho}}+\frac{\sqrt[3]{\mho}}{3\sqrt[3]{2}\hbar_0},\\
&s_2^2=\frac{\hbar_1}{3\hbar_0}+\frac{(1+\mathrm{i}\sqrt{3})(3\hbar_0\hbar_2-\hbar_1^2)}{3\sqrt[3]{4}\hbar_0\sqrt[3]{\mho}}-\frac{(1-\mathrm{i}\sqrt{3})\sqrt[3]{\mho}}{6\sqrt[3]{2}\hbar_0},\\
&s_3^2=\frac{\hbar_1}{3\hbar_0}+\frac{(1-\mathrm{i}\sqrt{3})(3\hbar_0\hbar_2-\hbar_1^2)}{3\sqrt[3]{4}\hbar_0\sqrt[3]{\mho}}-\frac{(1+\mathrm{i}\sqrt{3})\sqrt[3]{\mho}}{6\sqrt[3]{2}\hbar_0},
\end{aligned}\tag{A.6}$$

where $\mho=2\hbar_1^3-9\hbar_0\hbar_1\hbar_2+27\hbar_0^2\hbar_3+\sqrt{4(3\hbar_0\hbar_2-\hbar_1^2)^3+(2\hbar_1^3-9\hbar_0\hbar_1\hbar_2+27\hbar_0^2\hbar_3)^2}$.

Appendix B. Potential theory method and typical integro-differential equations

A mixed boundary value problem described in cylindrical coordinates (ρ,ϕ,z) for a half-space is considered. Assuming that the boundary conditions (only the potential function and its first derivatives are considered) are distinct on $\partial\Omega_{\mathrm{in}}=\{(\rho,\phi,z)|0\le\rho\le a,0\le\phi\le2\pi,z=0\}$ and $\partial\Omega_{\mathrm{out}}=\{(\rho,\phi,z)|\rho>a,0\le\phi\le2\pi,z=0\}$, a potential function $H(\rho,\phi,z)$ can be represented via the single layer potential as

$$H(\rho,\phi,z)=\int_0^{2\pi}\int_0^a\frac{\omega(\rho_0,\phi_0)}{R_0}\rho_0\mathrm{d}\rho_0\mathrm{d}\phi_0+\int_0^{2\pi}\int_a^\infty\frac{\omega(\rho_0,\phi_0)}{R_0}\rho_0\mathrm{d}\rho_0\mathrm{d}\phi_0,\tag{B.1}$$

where $R_0=\sqrt{\rho^2+\rho_0^2-2\rho\rho_0\cos(\phi-\phi_0)+z^2}$ and $\lim_{z\to0^+}\frac{\partial H}{\partial z}=-2\pi\omega$. According to Fabrikant (1989), we may denote $R=\lim_{z\to0}R_0$ and express $1/R^{1+\lambda}$ as

$$\begin{aligned}
\frac{1}{R^{1+\lambda}}&=\sum_{n=-\infty}^{+\infty}\frac{\mathrm{e}^{\mathrm{i}n(\phi-\phi_0)}}{[\max(\rho,\rho_0)]^{1+\lambda}}\frac{\Gamma[|n|+(1+\lambda)/2]}{\Gamma[(1+\lambda)/2]\Gamma(|n|+1)}\left[\frac{\min(\rho,\rho_0)}{\max(\rho,\rho_0)}\right]^{|n|}{}_2\widetilde{F}_1\left(\frac{1+\lambda}{2},|n|+\frac{1+\lambda}{2};|n|+1;\left[\frac{\min(\rho,\rho_0)}{\max(\rho,\rho_0)}\right]^2\right)\\
&=\frac{2}{\pi}\cos\frac{\pi\lambda}{2}\int_0^{\min(\rho,\rho_0)}\frac{\mathscr{G}\left(\frac{x^2}{\rho\rho_0},\phi-\phi_0\right)x^\lambda\mathrm{d}x}{(\rho^2-x^2)^{\frac{1+\lambda}{2}}(\rho_0^2-x^2)^{\frac{1+\lambda}{2}}}=\frac{2}{\pi}\cos\frac{\pi\lambda}{2}\int_0^\infty\frac{\mathscr{K}^{-\lambda}\mathrm{d}\mathscr{K}}{R^2+\mathscr{K}^2}
\end{aligned}\tag{B.2}$$

where $-1<\lambda<1$; $\Gamma(n)$ is the gamma function, and

$$
{}_2\widetilde{F}_1\left(\frac{1+\lambda}{2}, n+\frac{1+\lambda}{2}; n+1; z\right) = \frac{2\Gamma(n+1)}{\Gamma[n+(1+\lambda)/2]\Gamma[1-(1+\lambda)/2]}\int_0^1 \frac{t^{2n+\lambda}(1-t^2)^{-\frac{1+\lambda}{2}}}{(1-zt^2)^{\frac{1+\lambda}{2}}}\mathrm{d}t \tag{B.3}
$$

is the Gauss hypergeometric function, $\mathscr{G}(k,\varphi) := \sum_{n=-\infty}^{+\infty} k^{|n|}\mathrm{e}^{\mathrm{i}n\varphi} = (1-k^2)/(1+k^2-2k\cos\varphi)$, and $\mathscr{K}(x) = \sqrt{(\rho^2-x^2)(\rho_0^2-x^2)}/x$. Similarly, $1/R_0^{1+\lambda}$ can be expressed as

$$
\begin{aligned}
\frac{1}{R_0^{1+\lambda}} &= \frac{2}{\pi}\cos\frac{\pi\lambda}{2}\int_0^{l_1(\rho_0)} \frac{\mathscr{G}\left(\frac{x^2}{\rho\rho_0}, \phi-\phi_0\right)x^{\lambda}\mathrm{d}x}{\left\{\left[l_1^2(\rho_0)-x^2\right]\left[l_2^2(\rho_0)-x^2\right]\right\}^{\frac{1+\lambda}{2}}} \quad ((-1<\lambda<1)) \\
&= \frac{2}{\pi}\cos\frac{\pi\lambda}{2}\int_{l_2(\rho_0)}^{\infty} \frac{\mathscr{G}\left(\frac{\rho\rho_0}{x^2}, \phi-\phi_0\right)x^{\lambda}\mathrm{d}x}{\left\{\left[x^2-l_1^2(\rho_0)\right]\left[x^2-l_2^2(\rho_0)\right]\right\}^{\frac{1+\lambda}{2}}},
\end{aligned} \tag{B.4}
$$

from which Eq. (B.1) can be further simplified as

$$
\begin{aligned}
H(\rho,\phi,z) &= 4\int_0^{l_1(a)} \frac{\mathrm{d}x}{\sqrt{\rho^2-x^2}}\int_{g(x)}^{a} \frac{\rho_0\mathrm{d}\rho_0}{\sqrt{\rho_0^2-g^2(x)}}\mathscr{L}\left(\frac{x^2}{\rho\rho_0}\right)\omega(\rho_0,\phi) \\
&+4\int_{l_2(a)}^{\infty} \frac{\mathrm{d}x}{\sqrt{x^2-\rho^2}}\int_a^{g(x)} \frac{\rho_0\mathrm{d}\rho_0}{\sqrt{g^2(x)-\rho_0^2}}\mathscr{L}\left(\frac{\rho\rho_0}{x^2}\right)\omega(\rho_0,\phi),
\end{aligned} \tag{B.5}
$$

where the Poisson operator $\mathscr{L}(k)$, together with $g(x)$, $l_1(\rho_0)$, and $l_2(\rho_0)$ are in the form of

$$
\begin{aligned}
&\mathscr{L}(k)f(\phi) := \frac{1}{2\pi}\sum_{n=-\infty}^{+\infty} k^{|n|}\mathrm{e}^{\mathrm{i}n\phi}\int_0^{2\pi} \mathrm{e}^{-\mathrm{i}n\phi_0}f(\phi_0)\mathrm{d}\phi_0 = \frac{1}{2\pi}\int_0^{2\pi}\mathscr{G}(k,\phi-\phi_0)f(\phi_0)\mathrm{d}\phi_0, \\
&g(x) = x\sqrt{1+\frac{z^2}{\rho^2-x^2}}, \\
&l_1(\rho_0) := l_1(\rho_0,\rho,z) = \frac{1}{2}\left[\sqrt{(\rho+\rho_0)^2+z^2}-\sqrt{(\rho-\rho_0)^2+z^2}\right], \\
&l_2(\rho_0) := l_2(\rho_0,\rho,z) = \frac{1}{2}\left[\sqrt{(\rho+\rho_0)^2+z^2}+\sqrt{(\rho-\rho_0)^2+z^2}\right].
\end{aligned} \tag{B.6}
$$

Here, $\int_0^a(\#)\mathrm{d}\rho_0\int_0^{l_1(\rho_0)}(\#)\mathrm{d}x = \int_0^{l_1(a)}(\#)\mathrm{d}x\int_{g(x)}^a(\#)\mathrm{d}\rho_0$ and $\int_a^{\infty}(\#)\mathrm{d}\rho_0\int_{l_2(\rho_0)}^{\infty}(\#)\mathrm{d}x = \int_{l_2(a)}^{\infty}(\#)\mathrm{d}x\int_a^{g(x)}(\#)\mathrm{d}\rho_0$ are adopted. Besides, $(\rho^2-x^2)\left[\rho_0^2-g^2(x)\right] = \left[l_1^2(\rho_0)-x^2\right]\left[l_2^2(\rho_0)-x^2\right]$ is also applied in Eq. (B.5). It is important to note that $g(x)$ is inverse to $l_1(x)$ for $x^2<\rho^2$, while it is inverse to $l_2(x)$ for $x^2>\rho^2+z^2$. The problems are ultimately boiled down to the following two types of equations:

$$
\begin{aligned}
&\lim_{z_0\to 0}\frac{\partial^2}{\partial z_0^2}\left[\iint_S \frac{\omega_B(N)}{R_0(M_0,N)}\mathrm{d}S_N\right] = -2\pi P_B(N_0), \quad (\text{type}-\text{A}) \\
&\iint_S \frac{\omega_A(N)}{R(N_0,N)}\mathrm{d}S_N = P_A(N_0), \quad (\text{type}-\text{B})
\end{aligned} \tag{B.7}
$$

where $\lim\limits_{z_0\to 0} M_0(\rho_0,\phi_0,z_0) = N_0(\rho_0,\phi_0,0)$, $N = N(\rho,\phi,0)$, and both $N,N_0\in S$. Thereafter, the type-B is addressed first and subsequently turn to the type-A.

For a type-B integro-differential equation, Eq. $(\text{B.7})_1$ can be expressed as $4\int_0^{\rho}\frac{\mathrm{d}x}{\sqrt{\rho^2-x^2}}\int_x^a\frac{\rho_0\mathrm{d}\rho_0}{\sqrt{\rho_0^2-x^2}}\mathscr{L}\left(\frac{x^2}{\rho\rho_0}\right)\omega_A(\rho_0,\phi) = P_A(\rho,\phi)$ concerning Eq. (B.4). With the Abel integral equation and its solution

$$
\begin{aligned}
&\int_0^{\rho}\frac{\mathscr{F}(x)\mathrm{d}x}{\sqrt{\rho^2-x^2}} = f(\rho) \Rightarrow \mathscr{F}(x) = \frac{2}{\pi}\frac{\mathrm{d}}{\mathrm{d}x}\int_0^x\frac{f(\rho)\rho\mathrm{d}\rho}{\sqrt{x^2-\rho^2}}, \\
&\int_{\rho}^{a}\frac{\mathscr{F}(x)\mathrm{d}x}{\sqrt{x^2-\rho^2}} = f(\rho) \Rightarrow \mathscr{F}(x) = -\frac{2}{\pi}\frac{\mathrm{d}}{\mathrm{d}x}\int_x^a\frac{f(\rho)\rho\mathrm{d}\rho}{\sqrt{\rho^2-x^2}},
\end{aligned} \tag{B.8}
$$

we can invert Eq. $(\text{B.7})_1$ by applying $\mathscr{L}\left(\frac{1}{t}\right)\frac{\mathrm{d}}{\mathrm{d}t}\int_0^t\frac{\rho\mathrm{d}\rho}{\sqrt{t^2-\rho^2}}\mathscr{L}(\rho)$ and $\mathscr{L}(y)\frac{\mathrm{d}}{\mathrm{d}y}\int_y^a\frac{t\mathrm{d}t}{\sqrt{t^2-y^2}}\mathscr{L}\left(\frac{1}{t}\right)$ sequentially, which yields

$$
2\pi\int_t^a\frac{\rho_0\mathrm{d}\rho_0}{\sqrt{\rho_0^2-t^2}}\mathscr{L}\left(\frac{t}{\rho_0}\right)\omega_A(\rho_0,\phi) = \mathscr{L}\left(\frac{1}{t}\right)\frac{\mathrm{d}}{\mathrm{d}t}\int_0^t\frac{\rho\mathrm{d}\rho}{\sqrt{t^2-\rho^2}}\mathscr{L}(\rho)P_A(\rho,\phi), \tag{B.9}
$$

and

$$\omega_A(y,\phi) = -\frac{1}{\pi^2 y}\mathscr{L}(y)\frac{\mathrm{d}}{\mathrm{d}y}\int_y^a \frac{t\mathrm{d}t}{\sqrt{t^2-y^2}}\mathscr{L}\left(\frac{1}{t^2}\right)\frac{\mathrm{d}}{\mathrm{d}t}\int_0^t \frac{\rho\mathrm{d}\rho}{\sqrt{t^2-\rho^2}}\mathscr{L}(\rho)P_A(\rho,\phi). \tag{B.10}$$

Substituting Eq. (B.10) into the corresponding terms in Eq. (B.5), we have

$$H(\rho,\phi,z) = -\frac{4}{\pi^2}\int_0^{l_1(a)} \frac{\mathrm{d}x}{\sqrt{\rho^2-x^2}}\mathscr{L}\left(\frac{x^2}{\rho}\right)\int_{g(x)}^a \frac{\mathrm{d}\rho_0}{\sqrt{\rho_0^2-g^2(x)}}\frac{\mathrm{d}}{\mathrm{d}\rho_0}\int_{\rho_0}^a \frac{t\mathrm{d}t}{\sqrt{t^2-\rho_0^2}}\mathscr{L}\left(\frac{1}{t^2}\right)\frac{\mathrm{d}}{\mathrm{d}t}\int_0^t \frac{s\mathrm{d}s}{\sqrt{t^2-s^2}}\mathscr{L}(s)P_A(s,\phi). \tag{B.11}$$

It is noteworthy that the other terms in the potential function are omitted here. With the property of the Abel operator

$$\int_y^a \frac{\mathrm{d}r}{\sqrt{r^2-y^2}}\frac{\mathrm{d}}{\mathrm{d}r}\int_r^a \frac{tf(t)\mathrm{d}t}{\sqrt{t^2-r^2}} = -\frac{\pi}{2}f(y), \tag{B.12}$$

Eq. (B.11) can be further simplified to

$$H(\rho,\phi,z) = \frac{2}{\pi}\int_0^{l_1(a)} \frac{\mathrm{d}x}{\sqrt{\rho^2-x^2}}\mathscr{L}\left(\frac{x^2}{\rho g^2(x)}\right)\frac{\mathrm{d}}{\mathrm{d}g(x)}\int_0^{g(x)} \frac{\rho_0\mathrm{d}\rho_0}{\sqrt{g^2(x)-\rho_0^2}}\mathscr{L}(\rho_0)P_A(\rho_0,\phi). \tag{B.13}$$

If we set $t = g(x)$ and $x = l_1(t)$,

$$H(\rho,\phi,z) = \frac{2}{\pi}\int_0^{t=a} \frac{\mathrm{d}l_1(t)}{\sqrt{\rho^2-l_1^2(t)}}\mathscr{L}\left(\frac{l_1^2(t)}{\rho t^2}\right)\frac{\mathrm{d}}{\mathrm{d}t}\int_0^t \frac{\rho_0\mathrm{d}\rho_0}{\sqrt{t^2-\rho_0^2}}\mathscr{L}(\rho_0)P_A(\rho_0,\phi). \tag{B.14}$$

According to

$$\int_0^a \mathscr{F}(r)\mathrm{d}r\frac{\mathrm{d}}{\mathrm{d}r}\int_0^r \frac{f(\rho)\rho\mathrm{d}\rho}{\sqrt{r^2-\rho^2}} = -\int_0^a f(\rho)\mathrm{d}\rho\frac{\mathrm{d}}{\mathrm{d}\rho}\int_\rho^a \frac{\mathscr{F}(r)r\mathrm{d}r}{\sqrt{r^2-\rho^2}}, \tag{B.15}$$

Eq. (B.14) is reformulated by changing the order of integration

$$H(\rho,\phi,z) = \frac{1}{\pi^2}\int_0^{2\pi}\int_0^a \left\{-\frac{1}{\rho_0}\mathscr{L}(\rho_0)\frac{\mathrm{d}}{\mathrm{d}\rho_0}\int_{\rho_0}^a \frac{t\mathrm{d}t}{\sqrt{t^2-\rho_0^2}}\frac{\sqrt{l_2^2(t)-t^2}}{l_2^2(t)-l_1^2(t)}\mathscr{G}\left(\frac{\rho}{l_2^2(t)},\phi-\phi_0\right)\right\}P_A(\rho_0,\phi_0)\rho_0\mathrm{d}\rho_0\mathrm{d}\phi_0 \tag{B.16}$$

where

$$\frac{t\mathrm{d}l_1(t)}{\sqrt{t^2-\rho_0^2}\sqrt{\rho^2-l_1^2(t)}} = \frac{t\mathrm{d}t}{\sqrt{t^2-\rho_0^2}}\frac{\sqrt{l_2^2(t)-t^2}}{l_2^2(t)-l_1^2(t)}. \tag{B.17}$$

For clarity, the derivation details of Eq. (B.8), Eq. (B.12), and Eq. (B.15) are shown in Appendix C. Consider the following identities

$$\begin{aligned}&\frac{\mathrm{d}}{\mathrm{d}x}\int_x^a \frac{\mathscr{F}(\rho)\mathrm{d}\rho}{\sqrt{\rho^2-x^2}} = -\frac{\mathscr{F}(a)x}{a\sqrt{a^2-x^2}} + x\int_x^a \frac{\mathrm{d}\rho}{\sqrt{\rho^2-x^2}}\frac{\mathrm{d}}{\mathrm{d}\rho}\left[\frac{\mathscr{F}(\rho)}{\rho}\right]\\&= -\frac{\mathscr{F}(a)a}{x\sqrt{a^2-x^2}} + \frac{1}{x}\int_x^a \frac{\rho\mathrm{d}\rho}{\sqrt{\rho^2-x^2}}\frac{\mathrm{d}}{\mathrm{d}\rho}\mathscr{F}(\rho),\end{aligned} \tag{B.18}$$

the expression inside the curly braces in Eq. (B.16) gives

$$\begin{aligned}&-\frac{1}{\rho_0}\mathscr{L}(\rho_0)\frac{\mathrm{d}}{\mathrm{d}\rho_0}\int_{\rho_0}^a \frac{t\mathrm{d}t}{\sqrt{t^2-\rho_0^2}}\frac{\sqrt{l_2^2(t)-t^2}}{l_2^2(t)-l_1^2(t)}\mathscr{G}\left(\frac{\rho}{l_2^2(t)},\phi-\phi_0\right)\\&= \frac{\sqrt{l_2^2(a)-a^2}}{\sqrt{a^2-\rho_0^2}\left[l_2^2(a)-l_1^2(a)\right]}\mathscr{G}\left(\frac{\rho\rho_0}{l_2^2(a)},\phi-\phi_0\right) - \int_{\rho_0}^a \frac{\mathrm{d}x}{\sqrt{x^2-\rho_0^2}}\frac{\mathrm{d}}{\mathrm{d}x}\left[\frac{\sqrt{l_2^2(x)-x^2}}{l_2^2(x)-l_1^2(x)}\mathscr{G}\left(\frac{\rho\rho_0}{l_2^2(x)},\phi-\phi_0\right)\right].\end{aligned} \tag{B.19}$$

If we denote $h(x) = \left[\sqrt{x^2-\rho_0^2}\sqrt{x^2-l_1^2(x)}\right]/x$, the derivative with respect to x is computed as

$$h'(x) = \frac{\sqrt{x^2-l_1^2(x)}\left[x^2 l_2^2(x)-\rho_0^2 l_1^2(x)\right]}{x^2\sqrt{x^2-\rho_0^2}\left[l_2^2(x)-l_1^2(x)\right]}, \tag{B.20}$$

which leads to

$$\mathscr{G}\left(\frac{\rho\rho_0}{l_2^2(x)},\phi-\phi_0\right)=\frac{\left[l_2^2(x)-l_1^2(x)\right]\sqrt{x^2-\rho_0^2}}{\sqrt{x^2-l_1^2(x)}}\frac{h'(x)}{R_0^2+h^2(x)}. \tag{B.21}$$

Substituting Eq. (B.21) into Eq. (B.19), the modified expression is derived as

$$\frac{\sqrt{l_2^2(a)-a^2}}{\sqrt{a^2-\rho_0^2}\left[l_2^2(a)-l_1^2(a)\right]}\mathscr{G}\left(\frac{\rho\rho_0}{l_2^2(a)},\phi-\phi_0\right)-\int_{\rho_0}^{a}\frac{\mathrm{d}x}{\sqrt{x^2-\rho_0^2}}\frac{\mathrm{d}}{\mathrm{d}x}\left[\frac{xz\sqrt{x^2-\rho_0^2}}{x^2-l_1^2(x)}\frac{h'(x)}{R_0^2+h^2(x)}\right]=\frac{z}{R_0^3}\left[\frac{R_0}{h(a)}+\arctan\left(\frac{h(a)}{R_0}\right)\right]. \tag{B.22}$$

Finally, we may represent the potential function in terms of Eq. (B.22) as

$$H(\rho,\phi,z)=\frac{1}{\pi^2}\int_0^{2\pi}\int_0^{a}\left[\frac{R_0}{h(a)}+\arctan\left(\frac{h(a)}{R_0}\right)\right]\frac{z}{R_0^3}P_A(\rho_0,\phi_0)\rho_0\mathrm{d}\rho_0\mathrm{d}\phi_0. \tag{B.23}$$

Generally, type-B integral equations commonly arise in contact problems. The analysis above suffices if the zeroth and first-order derivatives of a potential function $H(\rho,\phi,z)$ are assumed to relate to displacement and stress components, respectively. When displacement and stress components are expressed in terms of the first and second-order derivatives of a new potential function $\widehat{H}(\rho,\phi,z):=\int H\mathrm{d}z$, this leading to $\lim_{z\to0^+}\partial^2\widehat{H}/\partial z^2=-2\pi\omega$, which indicates that the potential function should be prescribed as $\widehat{H}(\rho,\phi,z)=\iint_S\ln(R_0+z)\omega(\rho_0,\phi_0)\rho_0\mathrm{d}\rho_0\mathrm{d}\phi_0$. Consequently, the evaluation of the integral $\int\frac{z}{R_0^3}\left[\frac{R_0}{h(a)}+\arctan\left(\frac{h(a)}{R_0}\right)\right]\mathrm{d}z$ becomes particularly critical. We may express this integral as

$$\int\frac{z\mathrm{d}z}{R_0^2h(a)}+\int\frac{z}{R_0^3}\arctan\left(\frac{h(a)}{R_0}\right)\mathrm{d}z=-\frac{1}{R_0}\arctan\left(\frac{h(a)}{R_0}\right)+\frac{1}{\sqrt{a^2-\rho_0^2}}\int\frac{\sqrt{l_2^2(a)-a^2}\left[l_2^4(a)-\rho^2\rho_0^2\right]}{\left[R_0^2+h^2(a)\right]\left[l_2^2(a)-l_1^2(a)\right]l_2^2(a)}\mathrm{d}z \tag{B.24}$$

Concerning $\left[R_0^2+h^2(a)\right]l_2^2(a)=\left[l_2^2(a)-\rho\rho_0\mathrm{e}^{\mathrm{i}(\phi-\phi_0)}\right]\left[l_2^2(a)-\rho\rho_0\mathrm{e}^{-\mathrm{i}(\phi-\phi_0)}\right]$, $\mathrm{d}l_2(a)/\mathrm{d}z=zl_2(a)/\left[l_2^2(a)-l_1^2(a)\right]$, and $\sqrt{l_2^2(a)-a^2}\sqrt{l_2^2(a)-\rho^2}=zl_2(a)$, we have

$$\int\frac{z}{R_0^3}\left[\frac{R_0}{h(a)}+\arctan\left(\frac{h(a)}{R_0}\right)\right]\mathrm{d}z=-\frac{1}{R_0}\arctan\left(\frac{h(a)}{R_0}\right)+\frac{1}{\sqrt{a^2-\rho_0^2}}\int\frac{\left[l_2^4(a)-\rho^2\rho_0^2\right]\mathrm{d}l_2(a)}{\sqrt{l_2^2(a)-\rho^2}\left[l_2^2(a)-\rho\rho_0\mathrm{e}^{\mathrm{i}(\phi-\phi_0)}\right]\left[l_2^2(a)-\rho\rho_0\mathrm{e}^{-\mathrm{i}(\phi-\phi_0)}\right]}. \tag{B.25}$$

The integral on the right-hand side can be further simplified to

$$\begin{aligned}&\int\frac{\left[l_2^2(a)-\rho\rho_0\right]\left[l_2^2(a)+\rho\rho_0\right]}{\sqrt{l_2^2(a)-\rho^2}}\frac{1}{2\rho\rho_0\mathrm{i}\sin(\phi-\phi_0)}\left[\frac{1}{l_2^2(a)-\rho\rho_0\mathrm{e}^{\mathrm{i}(\phi-\phi_0)}}-\frac{1}{l_2^2(a)-\rho\rho_0\mathrm{e}^{-\mathrm{i}(\phi-\phi_0)}}\right]\mathrm{d}l_2(a)\\&=\int\frac{\mathrm{d}\left(\frac{l_2(a)}{\rho}\right)}{\sqrt{\left(\frac{l_2(a)}{\rho}\right)^2-1}}-\int\mathrm{d}\left(\frac{a}{\sqrt{a^2-l_1^2(a)}}\right)\frac{1}{\rho^2}\left\{\frac{\frac{\rho\rho_0\mathrm{e}^{\mathrm{i}(\phi-\phi_0)}}{l_2^2(a)-\rho\rho_0\mathrm{e}^{\mathrm{i}(\phi-\phi_0)}}}{l_2^2(a)-\rho^2}+\frac{\frac{\rho\rho_0\mathrm{e}^{-\mathrm{i}(\phi-\phi_0)}}{l_2^2(a)-\rho\rho_0\mathrm{e}^{-\mathrm{i}(\phi-\phi_0)}}}{l_2^2(a)-\rho^2}\right\}.\end{aligned} \tag{B.26}$$

We can evaluate the first integral by applying $l_2(a)/\rho=\sec k$, leading to

$$\int\frac{\mathrm{d}\sec k}{\tan k}=\int\sec k\mathrm{d}k=\int\frac{\cos k\mathrm{d}k}{\cos^2k}=-\int\frac{\mathrm{d}\sin k}{\sin^2k-1}=\ln\sqrt{\frac{1+\sin k}{1-\sin k}}=\ln\frac{l_2(a)+\sqrt{l_2(a)-\rho^2}}{\rho}+f_1. \tag{B.27}$$

Without loss of generality, $\ln\rho$ can be absorbed into an arbitrary function f_1 independent of z. The second integral can be simplified as

$$\begin{aligned}&\int\mathrm{d}\left(\frac{a}{\sqrt{a^2-l_1^2(a)}}\right)\frac{1}{\rho^2}\left\{\frac{\frac{\rho\rho_0\mathrm{e}^{\mathrm{i}(\phi-\phi_0)}}{l_2^2(a)-\rho\rho_0\mathrm{e}^{\mathrm{i}(\phi-\phi_0)}}}{l_2^2(a)-\rho^2}+\frac{\frac{\rho\rho_0\mathrm{e}^{-\mathrm{i}(\phi-\phi_0)}}{l_2^2(a)-\rho\rho_0\mathrm{e}^{-\mathrm{i}(\phi-\phi_0)}}}{l_2^2(a)-\rho^2}\right\}\\&=\frac{1}{\sqrt{\mathscr{Z}-1}}\arctan\left(\frac{a\sqrt{\mathscr{Z}-1}}{\sqrt{a^2-l_1^2(a)}}\right)+\frac{1}{\sqrt{\overline{\mathscr{Z}}-1}}\arctan\left(\frac{a\sqrt{\overline{\mathscr{Z}}-1}}{\sqrt{a^2-l_1^2(a)}}\right)+f_2.\end{aligned} \tag{B.28}$$

where $\mathscr{Z}=\frac{\rho}{\rho_0}\mathrm{e}^{\mathrm{i}(\phi-\phi_0)}$. To avoid the logarithmic singularity at $\rho=0$, Eq. (B.25) is in the form of

$$\int \frac{z}{R_0^3}\left[\frac{R_0}{h(a)}+\arctan\left(\frac{h(a)}{R_0}\right)\right]\mathrm{d}z=-\frac{1}{R_0}\arctan\left(\frac{h(a)}{R_0}\right)$$
$$+\frac{1}{\sqrt{a^2-\rho_0^2}}\left\{\ln\left[l_2(a)+\sqrt{l_2^2(a)-\rho^2}\right]-2\mathrm{Re}\left[\frac{1}{\sqrt{\mathscr{Z}-1}}\left(\arctan\left(\frac{a\sqrt{\mathscr{Z}-1}}{\sqrt{a^2-l_1^2(a)}}\right)-\arctan\sqrt{\mathscr{Z}-1}\right)\right]\right\}. \tag{B.29}$$

where $\mathrm{Re}(\#)$ represents the real part of a complex-valued function. Additional explanations can be found in Appendix C.

While type-A integro-differential equations typically appear in crack problems, where displacement and stress components are generally expressed by the first and second-order derivatives of a potential function $\widehat{H}(\rho,\phi,z)$. To introduce a simplified formulation, the displacement and stress components are defined as the zeroth and first-order derivatives of another potential function $H(\rho,\phi,z):=\partial\widehat{H}/\partial z$, which satisfies the following conditions:

$$\begin{aligned}&\lim_{z\to 0^+}\frac{\partial H}{\partial z}=-2\pi P_B(\rho,\phi),\quad 0\le\rho<a;0\le\phi\le 2\pi\\ &H(\rho,\phi,0)=0.\qquad\qquad \rho\ge a;0\le\phi\le 2\pi\end{aligned} \tag{B.30}$$

Using Eq. (B.5) and Eq. $(\mathrm{B}.30)_1$, the following equation is obtained from Eq. $(\mathrm{B}.30)_2$ as

$$\int_0^a\frac{\mathrm{d}x}{\sqrt{\rho^2-x^2}}\int_x^a\frac{\rho_0\mathrm{d}\rho_0}{\sqrt{\rho_0^2-x^2}}\mathscr{L}\left(\frac{x^2}{\rho\rho_0}\right)P_B(\rho_0,\phi)+\int_\rho^\infty\frac{\mathrm{d}x}{\sqrt{x^2-\rho^2}}\int_a^x\frac{\rho_0\mathrm{d}\rho_0}{\sqrt{x^2-\rho_0^2}}\mathscr{L}\left(\frac{\rho\rho_0}{x^2}\right)\omega(\rho_0,\phi)=0, \tag{B.31}$$

leading to

$$\int_\rho^\infty\frac{\mathrm{d}x}{\sqrt{x^2-\rho^2}}\int_a^x\frac{\rho_0\mathrm{d}\rho_0}{\sqrt{x^2-\rho_0^2}}\mathscr{L}\left(\frac{\rho\rho_0}{x^2}\right)\omega(\rho_0,\phi)=-\int_\rho^\infty\frac{\mathrm{d}x}{\sqrt{x^2-\rho^2}}\int_0^a\frac{\rho_0\mathrm{d}\rho_0}{\sqrt{x^2-\rho_0^2}}\mathscr{L}\left(\frac{\rho\rho_0}{x^2}\right)P_B(\rho_0,\phi). \tag{B.32}$$

Applying $\mathscr{L}(t)\frac{\mathrm{d}}{\mathrm{d}t}\int_t^\infty\frac{\rho\mathrm{d}\rho}{\sqrt{\rho^2-t^2}}\mathscr{L}\left(\frac{1}{\rho}\right)$ and $\mathscr{L}\left(\frac{1}{\rho}\right)\frac{\mathrm{d}}{\mathrm{d}\rho}\int_a^\rho\frac{t\mathrm{d}t}{\sqrt{\rho^2-t^2}}\mathscr{L}(t)$ sequentially, we have

$$\int_a^t\frac{\rho_0\mathrm{d}\rho_0}{\sqrt{t^2-\rho_0^2}}\mathscr{L}\left(\frac{\rho_0}{t}\right)\omega(\rho_0,\phi)=-\int_0^a\frac{\rho_0\mathrm{d}\rho_0}{\sqrt{t^2-\rho_0^2}}\mathscr{L}\left(\frac{\rho_0}{t}\right)P_B(\rho_0,\phi), \tag{B.33}$$

and

$$\omega(\rho,\phi)=-\frac{2}{\pi}\frac{1}{\rho}\frac{\mathrm{d}}{\mathrm{d}\rho}\int_a^\rho\frac{t\mathrm{d}t}{\sqrt{\rho^2-t^2}}\int_0^a\frac{\rho_0\mathrm{d}\rho_0}{\sqrt{t^2-\rho_0^2}}\mathscr{L}\left(\frac{\rho_0}{\rho}\right)P_B(\rho_0,\phi), \tag{B.34}$$

respectively. It is possible to further simplify Eq. (B.34) as

$$\omega(\rho,\phi)=-\frac{2}{\pi}\frac{1}{\sqrt{\rho^2-a^2}}\int_0^a\frac{\rho_0\mathrm{d}\rho_0}{\sqrt{a^2-\rho_0^2}}\mathscr{L}\left(\frac{\rho_0}{\rho}\right)P_B(\rho_0,\phi)+\frac{2}{\pi}\int_0^a\int_a^\rho\frac{t\mathrm{d}t}{\sqrt{\rho^2-t^2}\left(\sqrt{t^2-\rho_0^2}\right)^3}\rho_0\mathrm{d}\rho_0\mathscr{L}\left(\frac{\rho_0}{\rho}\right)P_B(\rho_0,\phi). \tag{B.35}$$

With the integral elucidated in Appendix C:

$$\int_a^\rho\frac{t\mathrm{d}t}{\sqrt{\rho^2-t^2}\left(\sqrt{t^2-\rho_0^2}\right)^3}=\frac{\sqrt{\rho^2-a^2}}{(\rho^2-\rho_0^2)\sqrt{a^2-\rho_0^2}}, \tag{B.36}$$

the relation between $\omega(\rho,\phi)$ and $P_B(\rho,\phi)$ is derived as

$$\omega(\rho,\phi)=-\frac{1}{\pi^2}\frac{1}{\sqrt{\rho^2-a^2}}\int_0^{2\pi}\int_0^a\frac{\sqrt{a^2-\rho_0^2}P_B(\rho_0,\phi_0)}{\rho^2+\rho_0^2-2\rho\rho_0\cos(\phi-\phi_0)}\rho_0\mathrm{d}\rho_0\mathrm{d}\phi_0. \tag{B.37}$$

Substituting Eq. (B.37) into Eq. (B.5), we have

$$\begin{aligned}&H(\rho,\phi,z)=4\int_0^{l_1(a)}\frac{\mathrm{d}x}{\sqrt{\rho^2-x^2}}\int_{g(x)}^a\frac{\rho_0\mathrm{d}\rho_0}{\sqrt{\rho_0^2-g^2(x)}}\mathscr{L}\left(\frac{x^2}{\rho\rho_0}\right)P_B(\rho_0,\phi)\\ &-\frac{8}{\pi}\int_{l_2(a)}^\infty\frac{\mathrm{d}x}{\sqrt{x^2-\rho^2}}\int_a^{g(x)}\frac{\rho_0\mathrm{d}\rho_0}{\sqrt{g^2(x)-\rho_0^2}}\mathscr{L}\left(\frac{\rho\rho_0}{x^2}\right)\left[\frac{1}{\sqrt{\rho_0^2-a^2}}\int_0^a\frac{\sqrt{a^2-s^2}s\mathrm{d}s}{\rho_0^2-s^2}\mathscr{L}\left(\frac{s}{\rho_0}\right)P_B(s,\phi)\right],\end{aligned} \tag{B.38}$$

where

$$
\begin{aligned}
&4\int_0^{l_1(a)}\frac{\mathrm{d}x}{\sqrt{\rho^2-x^2}}\int_{g(x)}^{a}\frac{\rho_0\mathrm{d}\rho_0}{\sqrt{\rho_0^2-g^2(x)}}\mathscr{L}\left(\frac{x^2}{\rho\rho_0}\right)P_B(\rho_0,\phi)\\
&=4\int_{l_2(0)}^{l_2(a)}\frac{\mathrm{d}x}{\sqrt{x^2-\rho^2}}\int_0^{g(x)}\frac{\rho_0\mathrm{d}\rho_0}{\sqrt{g^2(x)-\rho_0^2}}\mathscr{L}\left(\frac{\rho\rho_0}{x^2}\right)P_B(\rho_0,\phi)+4\int_{l_2(a)}^{\infty}\frac{\mathrm{d}x}{\sqrt{x^2-\rho^2}}\int_0^{a}\frac{\rho_0\mathrm{d}\rho_0}{\sqrt{g^2(x)-\rho_0^2}}\mathscr{L}\left(\frac{\rho\rho_0}{x^2}\right)P_B(\rho_0,\phi),
\end{aligned}
\tag{B.39}
$$

and

$$
\begin{aligned}
&-\frac{8}{\pi}\int_{l_2(a)}^{\infty}\frac{\mathrm{d}x}{\sqrt{x^2-\rho^2}}\int_a^{g(x)}\frac{\rho_0\mathrm{d}\rho_0}{\sqrt{g^2(x)-\rho_0^2}}\mathscr{L}\left(\frac{\rho\rho_0}{x^2}\right)\left[\frac{1}{\sqrt{\rho_0^2-a^2}}\int_0^a\frac{\sqrt{a^2-s^2}s\mathrm{d}s}{\rho_0^2-s^2}\mathscr{L}\left(\frac{s}{\rho_0}\right)P_B(s,\phi)\right]\\
&=-4\int_{l_2(a)}^{\infty}\frac{\mathrm{d}x}{\sqrt{x^2-\rho^2}}\int_0^{a}\frac{\rho_0\mathrm{d}\rho_0}{\sqrt{g^2(x)-\rho_0^2}}\mathscr{L}\left(\frac{\rho\rho_0}{x^2}\right)P_B(\rho_0,\phi).
\end{aligned}
\tag{B.40}
$$

Then, Eq. (B.38) can be expressed as

$$
H(\rho,\phi,z)=4\int_{l_2(0)}^{l_2(a)}\frac{\mathrm{d}x}{\sqrt{x^2-\rho^2}}\int_0^{g(x)}\frac{\rho_0\mathrm{d}\rho_0}{\sqrt{g^2(x)-\rho_0^2}}\mathscr{L}\left(\frac{\rho\rho_0}{x^2}\right)P_B(\rho_0,\phi),
\tag{B.41}
$$

which leads to

$$
H(\rho,\phi,0)=4\int_\rho^{a}\frac{\mathrm{d}x}{\sqrt{x^2-\rho^2}}\int_0^{x}\frac{\rho_0\mathrm{d}\rho_0}{\sqrt{x^2-\rho_0^2}}\mathscr{L}\left(\frac{\rho\rho_0}{x^2}\right)P_B(\rho_0,\phi)=\frac{\partial\widehat{H}}{\partial z}=-2\pi\omega_B(\rho,\phi).
\tag{B.42}
$$

It is important to note that

$$
\int_a^\rho\frac{y\mathrm{d}y}{\sqrt{\rho^2-y^2}\sqrt{y^2-a^2}(y^2-r^2)}=\frac{\pi}{2\sqrt{\rho^2-r^2}\sqrt{a^2-r^2}}
\tag{B.43}
$$

is adopted in Eq. (B.40), which is presented in Appendix C. By setting $t=g(x)$ and $x=l_2(t)$, Eq. (B.41) is in the form of

$$
H(\rho,\phi,z)=\frac{2}{\pi}\int_0^{2\pi}\int_0^a\frac{1}{R_0}\arctan\left(\frac{\sqrt{l_2^2(a)-\rho^2}\sqrt{a^2-\rho_0^2}}{l_2(a)R_0}\right)P_B(\rho_0,\phi_0)\rho_0\mathrm{d}\rho_0\mathrm{d}\phi_0.
\tag{B.44}
$$

We then verify that Eq. (B.42) is a solution to the type-A integro-differential equations in Eq. (B.7). Applying $\mathscr{L}(t)\frac{\mathrm{d}}{\mathrm{d}t}\int_t^a\frac{\rho\mathrm{d}\rho}{\sqrt{\rho^2-t^2}}\mathscr{L}\left(\frac{1}{\rho}\right)$ and $\mathscr{L}\left(\frac{1}{y}\right)\frac{\mathrm{d}}{\mathrm{d}y}\int_0^y\frac{t\mathrm{d}t}{\sqrt{y^2-t^2}}\mathscr{L}(t)$ sequentially, Eq. (B.42) is inverted as

$$
P_B(\rho,\phi)=\frac{2}{\pi\rho}\mathscr{L}\left(\frac{1}{\rho}\right)\frac{\mathrm{d}}{\mathrm{d}\rho}\int_0^\rho\frac{x\mathrm{d}x}{\sqrt{\rho^2-x^2}}\mathscr{L}(x^2)\frac{\mathrm{d}}{\mathrm{d}x}\int_x^a\frac{\rho_0\mathrm{d}\rho_0}{\sqrt{\rho_0^2-x^2}}\mathscr{L}\left(\frac{1}{\rho_0}\right)\omega_B(\rho_0,\phi).
\tag{B.45}
$$

Concerning Eq. (B.18), Eq. (C.12), and $\omega_B(a,\phi)=-H(a,\phi,0)/2\pi=0$, Eq. (B.45) can be further simplified as

$$
\begin{aligned}
P_B(\rho,\phi)&=-\frac{1}{\pi^2}\int_0^{2\pi}\int_0^a\int_0^{\min(\rho,\rho_0)}\frac{\mathscr{G}\left(\frac{x^2}{\rho\rho_0},\phi-\phi_0\right)\omega_B(\rho_0,\phi_0)x^2\rho_0\mathrm{d}x\mathrm{d}\rho_0\mathrm{d}\phi_0}{\left(\sqrt{\rho^2-x^2}\right)^3\left(\sqrt{\rho_0^2-x^2}\right)^3}-\delta_L\\
&=-\frac{1}{2\pi}\lim_{z_0\to 0}\frac{\partial^2}{\partial z_0^2}\int_0^{2\pi}\int_0^a\frac{\omega_B(\rho_0,\phi_0)\rho_0\mathrm{d}\rho_0\mathrm{d}\phi_0}{\sqrt{\rho^2+\rho_0^2-2\rho\rho_0\cos(\phi-\phi_0)+z_0^2}},
\end{aligned}
\tag{B.46}
$$

where δ_L is a term with singularity when $N(\rho,\phi,0)=N_0(\rho_0,\phi_0,0)$; $\Delta=\partial^2/\partial\rho^2+\partial/\rho\partial\rho+\partial^2/\rho^2\partial\phi^2$. It is noteworthy that λ in Eq. (B.2) can be extended to 2, which is expressed as

$$
\frac{1}{R^3}=-\frac{2}{\pi}\int_0^{\min(\rho,\rho_0)}\frac{\mathscr{G}\left(\frac{x^2}{\rho\rho_0},\phi-\phi_0\right)x^2\mathrm{d}x}{\left(\sqrt{\rho^2-x^2}\right)^3\left(\sqrt{\rho_0^2-x^2}\right)^3}.
\tag{B.47}
$$

Appendix C. Essential integral equations and properties

(1) $\int_0^\rho\frac{\mathscr{F}(x)\mathrm{d}x}{\sqrt{\rho^2-x^2}}=f(\rho)\Rightarrow\mathscr{F}(x)=\frac{2}{\pi}\frac{\mathrm{d}}{\mathrm{d}x}\int_0^x\frac{f(\rho)\rho\mathrm{d}\rho}{\sqrt{x^2-\rho^2}}$

Concerning $\int_0^\rho \frac{\mathscr{F}(x)\mathrm{d}x}{\sqrt{\rho^2-x^2}} = f(\rho)$, the following integral equation can be expressed as

$$\int_0^x \frac{f(\rho)\rho\mathrm{d}\rho}{\sqrt{x^2-\rho^2}} = \int_0^x \frac{\rho\mathrm{d}\rho}{\sqrt{x^2-\rho^2}} \int_0^\rho \frac{\mathscr{F}(t)\mathrm{d}t}{\sqrt{\rho^2-t^2}} = \int_0^x \mathscr{F}(t)\mathrm{d}t \int_t^x \frac{\rho\mathrm{d}\rho}{\sqrt{(x^2-\rho^2)(\rho^2-t^2)}}. \tag{C.1}$$

On letting $\rho^2 = t^2 + (x^2-t^2)\sin^2\theta, \quad \theta \in \left[0, \frac{\pi}{2}\right]$, we have

$$\int_t^x \frac{\rho\mathrm{d}\rho}{\sqrt{(x^2-\rho^2)(\rho^2-t^2)}} = \frac{1}{2}\int_0^{\frac{\pi}{2}} \frac{2(x^2-t^2)\sin\theta\cos\theta\mathrm{d}\theta}{\sqrt{\left\{x^2-\left[t^2+(x^2-t^2)\sin^2\theta\right]\right\}\left\{\left[t^2+(x^2-t^2)\sin^2\theta\right]-t^2\right\}}} = \frac{\pi}{2}. \tag{C.2}$$

Then, Eq. (C.1) can be expressed as

$$\frac{\pi}{2}\int_0^x \mathscr{F}(t)\mathrm{d}t = \int_0^x \frac{f(\rho)\rho\mathrm{d}\rho}{\sqrt{x^2-\rho^2}}, \tag{C.3}$$

which leads to

$$\mathscr{F}(x) = \frac{2}{\pi}\frac{\mathrm{d}}{\mathrm{d}x}\int_0^x \frac{f(\rho)\rho\mathrm{d}\rho}{\sqrt{x^2-\rho^2}}. \tag{C.4}$$

(2) $\int_\rho^a \frac{\mathscr{F}(x)\mathrm{d}x}{\sqrt{x^2-\rho^2}} = f(\rho) \Rightarrow \mathscr{F}(x) = -\frac{2}{\pi}\frac{\mathrm{d}}{\mathrm{d}x}\int_x^a \frac{f(\rho)\rho\mathrm{d}\rho}{\sqrt{\rho^2-x^2}}$

Similarly, the integral equation is in the form of

$$\int_x^a \frac{f(\rho)\rho\mathrm{d}\rho}{\sqrt{\rho^2-x^2}} = \int_x^a \frac{\rho\mathrm{d}\rho}{\sqrt{\rho^2-x^2}} \int_\rho^a \frac{\mathscr{F}(t)\mathrm{d}t}{\sqrt{t^2-\rho^2}} = \int_x^a \mathscr{F}(t)\mathrm{d}t \int_x^t \frac{\rho\mathrm{d}\rho}{\sqrt{(\rho^2-x^2)(t^2-\rho^2)}} = \frac{\pi}{2}\int_x^a \mathscr{F}(t)\mathrm{d}t, \tag{C.5}$$

from which we arrive at

$$\mathscr{F}(x) = -\frac{2}{\pi}\frac{\mathrm{d}}{\mathrm{d}x}\int_x^a \frac{f(\rho)\rho\mathrm{d}\rho}{\sqrt{\rho^2-x^2}}. \tag{C.6}$$

(3) $\int_y^a \frac{\mathrm{d}r}{\sqrt{r^2-y^2}}\frac{\mathrm{d}}{\mathrm{d}r}\int_r^a \frac{tf(t)\mathrm{d}t}{\sqrt{t^2-r^2}} = -\frac{\pi}{2}f(y)$

From Eq. (C.6), we find that

$$\int_y^a \frac{\mathrm{d}r}{\sqrt{r^2-y^2}}\frac{\mathrm{d}}{\mathrm{d}r}\int_r^a \frac{tf(t)\mathrm{d}t}{\sqrt{t^2-r^2}} = \int_y^a \frac{\mathrm{d}r}{\sqrt{r^2-y^2}}\left[-\frac{\pi}{2}\mathscr{F}(r)\right] = -\frac{\pi}{2}f(y). \tag{C.7}$$

(4) $\int_0^a \mathscr{F}(r)\mathrm{d}r\frac{\mathrm{d}}{\mathrm{d}r}\int_0^r \frac{f(\rho)\rho\mathrm{d}\rho}{\sqrt{r^2-\rho^2}} = -\int_0^a f(\rho)\mathrm{d}\rho\frac{\mathrm{d}}{\mathrm{d}\rho}\int_\rho^a \frac{\mathscr{F}(r)r\mathrm{d}r}{\sqrt{r^2-\rho^2}}$

The expression is manipulated from the right-hand side to arrive at the left-hand side form of the equation:

$$\mathrm{RHS} = -\frac{2}{\pi}\int_0^a \left\{\left[\int_t^a \frac{1}{\sqrt{\rho^2-t^2}}\frac{\mathrm{d}}{\mathrm{d}\rho}\int_\rho^a \frac{\mathscr{F}(r)r\mathrm{d}r}{\sqrt{r^2-\rho^2}}\mathrm{d}\rho\right]\frac{\mathrm{d}}{\mathrm{d}t}\int_0^t \frac{f(s)s\mathrm{d}s}{\sqrt{t^2-s^2}}\right\}\mathrm{d}t = \mathrm{LHS}. \tag{C.8}$$

(5) $\frac{\mathrm{d}}{\mathrm{d}x}\int_x^a \frac{\mathscr{F}(\rho)\mathrm{d}\rho}{\sqrt{\rho^2-x^2}} = -\frac{\mathscr{F}(a)x}{a\sqrt{a^2-x^2}} + x\int_x^a \frac{\mathrm{d}\rho}{\sqrt{\rho^2-x^2}}\frac{\mathrm{d}}{\mathrm{d}\rho}\left[\frac{\mathscr{F}(\rho)}{\rho}\right] = -\frac{\mathscr{F}(a)a}{x\sqrt{a^2-x^2}} + \frac{1}{x}\int_x^a \frac{\rho\mathrm{d}\rho}{\sqrt{\rho^2-x^2}}\frac{\mathrm{d}}{\mathrm{d}\rho}\mathscr{F}(\rho)$

By applying the methods of integration by parts and the Leibniz integral rule, we may derive

$$\frac{\mathrm{d}}{\mathrm{d}x}\int_x^a \frac{\mathscr{F}(\rho)\mathrm{d}\rho}{\sqrt{\rho^2-x^2}} = -\frac{x\mathscr{F}(a)}{a\sqrt{a^2-x^2}} + \int_x^a \frac{x\mathrm{d}\rho}{\sqrt{\rho^2-x^2}}\frac{\mathrm{d}}{\mathrm{d}\rho}\left[\frac{\mathscr{F}(\rho)}{\rho}\right]. \tag{C.9}$$

Since

$$x\int_x^a \frac{\mathrm{d}\rho}{\sqrt{\rho^2-x^2}}\left[\frac{\mathscr{F}'(\rho)\rho-\mathscr{F}(\rho)}{\rho^2}\right] = -\frac{\mathscr{F}(a)\sqrt{a^2-x^2}}{xa} + \frac{1}{x}\int_x^a \frac{\rho\mathrm{d}\mathscr{F}(\rho)}{\sqrt{\rho^2-x^2}}, \tag{C.10}$$

then Eq. (C.9) is further expressed as

$$-\frac{x\mathscr{F}(a)}{a\sqrt{a^2-x^2}}+\int_x^a \frac{x\mathrm{d}\rho}{\sqrt{\rho^2-x^2}}\frac{\mathrm{d}}{\mathrm{d}\rho}\left[\frac{\mathscr{F}(\rho)}{\rho}\right]=-\frac{\mathscr{F}(a)a}{x\sqrt{a^2-x^2}}+\frac{1}{x}\int_x^a \frac{\rho\mathrm{d}\rho}{\sqrt{\rho^2-x^2}}\frac{\mathrm{d}}{\mathrm{d}\rho}\mathscr{F}(\rho). \tag{C.11}$$

If we take $a = 0$, Eq. (C.11) can be modified as

$$\frac{\mathrm{d}}{\mathrm{d}x}\int_0^x \frac{\mathscr{F}(\rho)\mathrm{d}\rho}{\sqrt{\rho^2-x^2}}=\frac{1}{x}\int_0^x \frac{\rho\mathrm{d}\rho}{\sqrt{x^2-\rho^2}}\frac{\mathrm{d}}{\mathrm{d}\rho}\mathscr{F}(\rho). \tag{C.12}$$

(6) $\arctan z = \frac{1}{2\mathrm{i}}\ln\frac{\mathrm{i}-z}{\mathrm{i}+z}$

Concerning

$$\arctan z=\int\frac{\mathrm{d}z}{1+z^2}=\frac{1}{2\mathrm{i}}\ln\frac{\mathrm{i}-z}{\mathrm{i}+z}, \tag{C.13}$$

then $\mathscr{Z} = 0$, $l_1(a) = 0$, and $\arctan\left(\frac{a\sqrt{\mathscr{Z}-1}}{\sqrt{a^2-l_1^2(a)}}\right) = \arctan\mathrm{i} = \infty$ when $\rho = 0$.

(7) $\int_a^\rho \frac{t\mathrm{d}t}{\sqrt{\rho^2-t^2}\left(\sqrt{t^2-\rho_0^2}\right)^3}=\frac{\sqrt{\rho^2-a^2}}{\left(\rho^2-\rho_0^2\right)\sqrt{a^2-\rho_0^2}}$ $(\rho_0 < a < \rho)$

If we set $u = \sqrt{t^2-\rho_0^2} = \sqrt{\rho^2-\rho_0^2}\sin k$, then

$$\int_a^\rho \frac{t\mathrm{d}t}{\sqrt{\rho^2-t^2}\left(\sqrt{t^2-\rho_0^2}\right)^3}=\frac{1}{\rho^2-\rho_0^2}\int_{\arcsin\left(\sqrt{\frac{a^2-\rho_0^2}{\rho^2-\rho_0^2}}\right)}^{\frac{\pi}{2}}\frac{\mathrm{d}k}{\sin^2 k}=\frac{\sqrt{\rho^2-a^2}}{\left(\rho^2-\rho_0^2\right)\sqrt{a^2-\rho_0^2}}. \tag{C.14}$$

(8) $\int_a^\rho \frac{y\mathrm{d}y}{\sqrt{\rho^2-y^2}\sqrt{y^2-a^2}(y^2-r^2)}=\frac{\pi}{2\sqrt{\rho^2-r^2}\sqrt{a^2-r^2}}$ $(0 < r < a < \rho)$

Let $y^2 = a^2\cos^2 k + \rho^2\sin^2 k$, then we have

$$\begin{aligned}&\int_a^\rho \frac{y\mathrm{d}y}{\sqrt{\rho^2-y^2}\sqrt{y^2-a^2}(y^2-r^2)}=\frac{1}{2}\int_0^{\frac{\pi}{2}}\frac{2(\rho^2-a^2)\sin k\cos k\mathrm{d}k}{\left(\sqrt{\rho^2-a^2}\cos k\right)\left(\sqrt{\rho^2-a^2}\sin k\right)\left(a^2\cos^2 k+\rho^2\sin^2 k-r^2\right)}\\&=\frac{\pi}{2}\frac{1}{\sqrt{\rho^2-r^2}\sqrt{a^2-r^2}}.\end{aligned} \tag{C.15}$$

Appendix D. Analytical solutions in the uniform loading case

The nonzero components are expressed as

$$\begin{aligned}u_\rho&=-\sum_{k=1}^{3}\sum_{i=1}^{2}\varsigma_{ki}\frac{\partial\widehat{H}_i(\rho,\phi,z_k)}{\partial\rho}\\&=-\frac{1}{2\pi}\sum_{k=1}^{3}\sum_{i=1}^{2}\varsigma_{ki}\sum_{j=1}^{2}\eta_{ij}P_j\left\{\frac{\left(\sqrt{(a+\rho)^2+z_k^2}-\sqrt{(a-\rho)^2+z_k^2}\right)\sqrt{\rho^2-a^2-z_k^2+\sqrt{(a+\rho)^2+z_k^2}\sqrt{(a-\rho)^2+z_k^2}}}{\sqrt{2}\rho}\right.\\&\left.-2\rho\arctan\left[\frac{\sqrt{(a+\rho)^2+z_k^2}-\sqrt{(a-\rho)^2+z_k^2}}{\sqrt{4\rho^2-\left[\sqrt{(a+\rho)^2+z_k^2}-\sqrt{(a-\rho)^2+z_k^2}\right]^2}}\right]\right\},\end{aligned} \tag{D.1}$$

$$
\begin{aligned}
w_s &= \sum_{k=1}^{3}\sum_{i=1}^{2}\alpha_{sk}\varsigma_{ki}\frac{\partial \widehat{H}_i(\rho,\phi,z_k)}{\partial z_k} \\
&= \frac{1}{2\pi}\sum_{k=1}^{3}\sum_{i=1}^{2}\alpha_{sk}\varsigma_{ki}\sum_{j=1}^{2}\eta_{ij}P_j\left\{4z_k\arctan\left[\frac{\sqrt{(a+\rho)^2+z_k^2}-\sqrt{(a-\rho)^2+z_k^2}}{\sqrt{4\rho^2-\left[\sqrt{(a+\rho)^2+z_k^2}-\sqrt{(a-\rho)^2+z_k^2}\right]^2}}\right]\right. \\
&\left.\quad-\frac{8\sqrt{2}a\rho z_k}{\left(\sqrt{(a+\rho)^2+z_k^2}+\sqrt{(a-\rho)^2+z_k^2}\right)\sqrt{\rho^2-a^2-z_k^2+\sqrt{(a+\rho)^2+z_k^2}\sqrt{(a-\rho)^2+z_k^2}}}\right\},
\end{aligned}
\tag{D.2}
$$

$$
\begin{aligned}
\sigma_{zm} &= \sum_{k=1}^{3}\sum_{i=1}^{2}\gamma_{mk}\varsigma_{ki}\frac{\partial^2 \widehat{H}_i(\rho,\phi,z_k)}{\partial z_k^2} \\
&= \frac{1}{2\pi}\sum_{k=1}^{3}\sum_{i=1}^{2}\gamma_{mk}\varsigma_{ki}\sum_{j=1}^{2}\eta_{ij}P_j\left\{4\arctan\left[\frac{\sqrt{(a+\rho)^2+z_k^2}-\sqrt{(a-\rho)^2+z_k^2}}{\sqrt{4\rho^2-\left[\sqrt{(a+\rho)^2+z_k^2}-\sqrt{(a-\rho)^2+z_k^2}\right]^2}}\right]\right. \\
&\left.\quad-\frac{\sqrt{2}a\left(\sqrt{(a+\rho)^2+z_k^2}+\sqrt{(a-\rho)^2+z_k^2}\right)\sqrt{\rho^2-a^2-z_k^2+\sqrt{(a+\rho)^2+z_k^2}\sqrt{(a-\rho)^2+z_k^2}}}{\rho\sqrt{(a+\rho)^2+z_k^2}\sqrt{(a-\rho)^2+z_k^2}}\right\},
\end{aligned}
\tag{D.3}
$$

$$
\begin{aligned}
\sigma_{\rho t} &= (c_{12}-c_{11})\sum_{k=1}^{3}\sum_{i=1}^{2}\varsigma_{ki}\left[\frac{\partial^2 \widehat{H}_i(\rho,\phi,z_k)}{\partial \rho^2}-\frac{1}{\rho}\frac{\partial \widehat{H}_i(\rho,\phi,z_k)}{\partial \rho}\right] \\
&= \frac{c_{12}-c_{11}}{2\pi}\sum_{k=1}^{3}\sum_{i=1}^{2}\varsigma_{ki}\sum_{j=1}^{2}\eta_{ij}P_j \\
&\quad\frac{2\sqrt{2}\left\{a\rho(a^2+z_k^2)\left(\sqrt{(a+\rho)^2+z_k^2}+\sqrt{(a-\rho)^2+z_k^2}\right)-\left[a^4+z_k^2(\rho^2+z_k^2+2a^2)\right]\left(\sqrt{(a+\rho)^2+z_k^2}-\sqrt{(a-\rho)^2+z_k^2}\right)\right\}}{\rho^2\sqrt{(a+\rho)^2+z_k^2}\sqrt{(a-\rho)^2+z_k^2}\sqrt{\rho^2-a^2-z_k^2+\sqrt{(a+\rho)^2+z_k^2}\sqrt{(a-\rho)^2+z_k^2}}},
\end{aligned}
\tag{D.4}
$$

$$
\begin{aligned}
\sigma_{\rho m} &= \sum_{k=1}^{3}\sum_{i=1}^{2}\varpi_{mk}\varsigma_{ki}\frac{\partial^2 \hat{H}_i(\rho,\phi,z_k)}{\partial\rho\partial z_k} \\
&= \frac{1}{2\pi}\sum_{k=1}^{3}\sum_{i=1}^{2}\varpi_{mk}\varsigma_{ki}\sum_{j=1}^{2}\eta_{ij}P_j\frac{2\sqrt{2}z_k\left(\sqrt{(a+\rho)^2+z_k^2}-\sqrt{(a-\rho)^2+z_k^2}\right)\left[a^2\left(\rho^2-2z_k^2+\sqrt{(a+\rho)^2+z_k^2}\sqrt{(a-\rho)^2+z_k^2}\right)-z_k^2\left(\rho^2+z_k^2-\sqrt{(a+\rho)^2+z_k^2}\sqrt{(a-\rho)^2+z_k^2}\right)-a^4\right]}{\rho\sqrt{(a+\rho)^2+z_k^2}\sqrt{(a-\rho)^2+z_k^2}\left(\sqrt{\rho^2-a^2-z_k^2+\sqrt{(a+\rho)^2+z_k^2}\sqrt{(a-\rho)^2+z_k^2}}\right)^3},
\end{aligned}
\tag{D.5}
$$

$$
\sigma_{\phi t}=\sigma_{zt}=0,
\tag{D.6}
$$

where $s=1,2$ and $m=1,2,3$; $\dot{\mathrm{T}}_{0\rho\rho}=(\sigma_{z3}+\sigma_{\rho t})/2$, while $\dot{\mathrm{T}}_{0\phi\phi}=(\sigma_{z3}-\sigma_{\rho t})/2$.

Appendix E. Penny-shaped cracks subjected to various loadings

While Section 4.1 presented solutions only for the case of uniform loading, we now proceed to derive solutions under various external loadings.

E.1. Axisymmetric linear loading

For $P_j(\rho,\phi)\equiv P_j\rho$, we may construct the densities and the corresponding potential functions as

$$
\omega_i(\rho)=\frac{\sum_{j=1}^{2}\eta_{ij}P_j}{8\pi}\left[a\sqrt{a^2-\rho^2}+\rho^2\ln\left(\frac{a+\sqrt{a^2-\rho^2}}{\rho}\right)\right]
\tag{E.1}
$$

and

$$\widehat{H}_i(\rho,z_k)=\frac{\sum_{j=1}^{2}\eta_{ij}P_j}{6}\left\{a^3\arcsin\left[\frac{l_1(a)}{\rho}\right]-z_k\left(3\rho^2-2z_k^2\right)\mathrm{arccoth}\left[\frac{\sqrt{l_2^2(a)-a^2}-\sqrt{\rho^2-l_1^2(a)}}{z_k}\right]\right.$$
$$-\frac{\sqrt{l_2^2(a)-a^2}\left[2l_1^4(a)+2l_1^2(a)\left(\rho^2-4z_k^2\right)+11\rho^2z_k^2-4\rho^4\right]}{6\left[\rho^2-l_1^2(a)\right]} \tag{E.2}$$
$$\left.+z_k\left(3\rho^2-2z_k^2\right)\mathrm{arccoth}\left[\frac{\sqrt{\rho^2+z_k^2}-\rho}{z_k}\right]+\frac{1}{6}\sqrt{\rho^2+z_k^2}\left(11z_k^2-4\rho^2\right)\right\},$$

respectively. The solution for $\widehat{H}_i$ involves utilizing $\frac{\partial}{\partial g(x)}\left\{\arctan\left(\frac{g(x)}{\sqrt{a^2-g^2(x)}}\right)-\mathrm{i}\ln\left[-\frac{g(x)+\mathrm{i}\sqrt{a^2-g^2(x)}}{a}\right]\right\}=0$ and applying integration by parts. Here, detailed expressions of displacement and stress components are omitted for brevity. Theoretical analysis reveals that both $\dot{\mathrm{T}}_{0zz}$ and $\dot{D}_{0z}$ exhibit a singularity of order $-\frac{1}{2}$ at the crack tip, which read

$$\lim_{z\to 0}\sigma_{zs}=P_s\left\{\frac{a^2-2\rho^2+2\rho\sqrt{\rho^2-a^2}}{2\sqrt{\rho^2-a^2}}\right\}.\quad (s=1,2;\rho>a) \tag{E.3}$$

Then, the incremental intensity factors are derived as

$$\begin{aligned}\dot{K}_{\mathrm{IT}}&=\lim_{\rho\to a}\left[\sqrt{2(\rho-a)}\dot{\mathrm{T}}_{0zz}|_{z=0}\right]=-\frac{1}{2}\left(\sqrt{a}\right)^3P_1,\\ \dot{K}_{\mathrm{ID}}&=\lim_{\rho\to a}\left[\sqrt{2(\rho-a)}\dot{D}_{0z}|_{z=0}\right]=-\frac{1}{2}\left(\sqrt{a}\right)^3P_2.\end{aligned} \tag{E.4}$$

E.2. Axisymmetric parabolic loading

Assuming that $P_j(\rho,\phi)\equiv P_j\rho^2$, the densities and the corresponding potential functions are derived as

$$\omega_i(\rho)=\frac{2\sum_{j=1}^{2}\eta_{ij}P_j}{9\pi^2}\sqrt{a^2-\rho^2}\left(a^2+2\rho^2\right) \tag{E.5}$$

and

$$\widehat{H}_i(\rho,z_k)=\frac{\sum_{j=1}^{2}\eta_{ij}P_j}{72\pi}\left\{3\left(8a^4-8z_k^4+24\rho^2z_k^2-3\rho^4\right)\arcsin\left[\frac{l_1(a)}{\rho}\right]+l_1(a)\left[6l_1^6(a)+24\rho^2z_k^4\right.\right.$$
$$\left.\left.+9\rho^6-72\rho^4z_k^2-3l_1^4(a)\left(\rho^2+8z_k^2\right)-4l_1^2(a)\left(3\rho^4-24\rho^2z_k^2+8z_k^4\right)\right]\Big/\left[\sqrt{\rho^2-l_1^2(a)}\right]^3\right\}, \tag{E.6}$$

respectively. Concerning

$$\lim_{z\to 0}\sigma_{zs}=P_s\left[\frac{2}{\pi}\rho^2\arcsin\left(\frac{a}{\rho}\right)-\frac{2}{3\pi}\frac{a(3\rho^2-a^2)}{\sqrt{\rho^2-a^2}}\right],\quad (s=1,2;\rho>a) \tag{E.7}$$

the incremental intensity factors are in the form of

$$\begin{aligned}\dot{K}_{\mathrm{IT}}&=\lim_{\rho\to a}\left[\sqrt{2(\rho-a)}\dot{\mathrm{T}}_{0zz}|_{z=0}\right]=-\frac{4}{3\pi}\left(\sqrt{a}\right)^5P_1,\\ \dot{K}_{\mathrm{ID}}&=\lim_{\rho\to a}\left[\sqrt{2(\rho-a)}\dot{D}_{0z}|_{z=0}\right]=-\frac{4}{3\pi}\left(\sqrt{a}\right)^5P_2.\end{aligned} \tag{E.8}$$

E.3. Loading under axisymmetric elementary functions

In this subsection, we focus exclusively on the solutions of the integro-differential equations and forgo a detailed treatment of the potential functions.

(1) Polynomial loading $P_j(\rho,\phi)\equiv P_j\rho^n,\quad (n\geq 0)$

$$\omega_i(\rho) = \frac{\sum_{j=1}^{2}\eta_{ij}P_j}{4\pi\sqrt{\pi}} \frac{\Gamma\left(\frac{n}{2}+1\right)}{\Gamma\left(\frac{n}{2}+\frac{3}{2}\right)} \left[\sqrt{\pi} \frac{\Gamma\left(-\frac{n}{2}-\frac{1}{2}\right)}{\Gamma\left(-\frac{n}{2}\right)} \rho^{n+1} + \frac{2a^{n+1}}{n+1} {}_2\widetilde{F}_1\left(\frac{1}{2}, -\frac{n}{2}-\frac{1}{2}; -\frac{n}{2}+\frac{1}{2}; \frac{\rho^2}{a^2}\right) \right]. \tag{E.9}$$

Here ${}_2\widetilde{F}_1(\#,\#;\#;\#)$ is the Gauss hypergeometric function, and $\Gamma(\#)$ is the gamma function. According to the Weierstrass approximation theorem, any continuous loading function defined on S can be approximated by polynomial functions. The approximation is essential for solving various engineering challenges.

(b) Trigonometric loading $P_j(\rho,\phi) \equiv P_j\sin(\rho/\rho_c)$ or $P_j(\rho,\phi) \equiv P_j\cos(\rho/\rho_c)$

$$\omega_i(\rho) = \frac{\sum_{j=1}^{2}\eta_{ij}P_j}{2\pi} \begin{cases} \displaystyle\int_\rho^a x\widetilde{J}_1\left(\frac{x}{\rho_c}\right) \Big/ \sqrt{x^2-\rho^2}\,\mathrm{d}x = \sum_{n=0}^{\infty} \frac{(-1)^n}{2\sqrt{\pi}(2n+1)!} \frac{\Gamma\left(n+\frac{3}{2}\right)}{\Gamma(n+2)} \left[\frac{\sqrt{\pi}\Gamma(-n-1)}{\Gamma\left(-n-\frac{1}{2}\right)} - \widetilde{B}\left(\frac{\rho^2}{a^2}; -n-1, \frac{1}{2}\right) \right] \frac{\rho^{2n+2}}{\rho_c^{2n+1}}, & \text{(sine)} \\ \displaystyle\int_\rho^a x\widetilde{H}_{-1}\left(\frac{x}{\rho_c}\right) \Big/ \sqrt{x^2-\rho^2}\,\mathrm{d}x = \sum_{n=0}^{\infty} \frac{(-1)^n}{2(2n)!} \frac{\Gamma(n+1)\Gamma\left(-n-\frac{1}{2}\right) + \sqrt{\pi}\widetilde{B}\left(\frac{\rho^2}{a^2}; -n-\frac{1}{2}, \frac{1}{2}\right)csc(n\pi)}{\Gamma\left(n+\frac{3}{2}\right)\Gamma(-n)} \frac{\rho^{2n+1}}{\rho_c^{2n}}. & \text{(cosine)} \end{cases} \tag{E.10}$$

Here $\widetilde{J}_v(\#)$ is the Bessel function of the first kind; $\widetilde{H}_v(\#)$ is the Struve function; $\widetilde{B}(\#;\#)$ is the incomplete beta function; and $\rho_c(>a>0)$ is a constant with the dimension of length introduced to render a dimensionless ρ/ρ_c quantity.

(c) Logarithmic loading $P_j(\rho,\phi) \equiv P_j\ln(\rho/\rho_c)$

$$\omega_i(\rho) = \frac{\sum_{j=1}^{2}\eta_{ij}P_j}{\pi^2} \left\{ \left[\ln\left(\frac{2a}{\rho_c}\right) - 2\right]\sqrt{a^2-\rho^2} - \rho\arctan\left(\frac{\rho}{\sqrt{a^2-\rho^2}}\right) + \frac{\pi}{2}\rho \right\}. \tag{E.11}$$

(d) Exponential loading $P_j(\rho,\phi) \equiv P_j\exp(\rho/\rho_c)$

$$\begin{aligned} \omega_i(\rho) &= \frac{\sum_{j=1}^{2}\eta_{ij}P_j}{2\pi} \int_\rho^a x\left[\widetilde{I}_1\left(\frac{x}{\rho_c}\right) + \widetilde{L}_{-1}\left(\frac{x}{\rho_c}\right)\right] \Big/ \sqrt{x^2-\rho^2}\,\mathrm{d}x \\ &= \frac{\sum_{j=1}^{2}\eta_{ij}P_j}{4\pi\sqrt{\pi}} \sum_{n=0}^{\infty} \frac{\rho_c^{-n}}{n!} \frac{\Gamma\left(\frac{n}{2}+1\right)}{\Gamma\left(\frac{n}{2}+\frac{3}{2}\right)} \left[\sqrt{\pi} \frac{\Gamma\left(-\frac{n}{2}-\frac{1}{2}\right)}{\Gamma\left(-\frac{n}{2}\right)} \rho^{n+1} + \frac{2a^{n+1}}{n+1} {}_2\widetilde{F}_1\left(\frac{1}{2}, -\frac{n}{2}-\frac{1}{2}; -\frac{n}{2}+\frac{1}{2}; \frac{\rho^2}{a^2}\right) \right]. \end{aligned} \tag{E.12}$$

Here $\widetilde{I}_v(\#)$ is the modified Bessel function of the first kind, and $\widetilde{L}_v(\#)$ is the modified Struve function.

(e)Inverse trigonometric loading $P_j(\rho,\phi) \equiv P_j\arcsin(\rho/\rho_c)$ or $P_j(\rho,\phi) \equiv P_j\arccos(\rho/\rho_c)$

$$\omega_i(\rho) = \frac{\sum_{j=1}^{2}\eta_{ij}P_j}{\pi^2\rho_c} \begin{cases} \displaystyle\int_\rho^a \left\{ \rho_c^2\left[\widetilde{K}\left(\frac{x^2}{\rho_c^2}\right) - \widetilde{E}\left(\frac{x^2}{\rho_c^2}\right)\right] - x^2\widetilde{K}\left(\frac{x^2}{\rho_c^2}\right) \right\} \Big/ \sqrt{x^2-\rho^2}\,\mathrm{d}x, & \text{(arcsine)} \\ \displaystyle\int_\rho^a \left\{ \rho_c^2\left[\widetilde{K}\left(\frac{x^2}{\rho_c^2}\right) - \widetilde{E}\left(\frac{x^2}{\rho_c^2}\right)\right] - x^2\widetilde{K}\left(\frac{x^2}{\rho_c^2}\right) + \rho_c\frac{\pi x}{2} \right\} \Big/ \sqrt{x^2-\rho^2}\,\mathrm{d}x, & \text{(arccosine)} \end{cases} \tag{E.13}$$

where $\widetilde{K}(\#)$ and $\widetilde{E}(\#)$ are the complete elliptic integral of the first and second kinds, respectively. It is noted that $\rho_c > a > x$ is adopted in Eq. (E.13) to ensure convergence of the following solutions:

$$\omega_i(\rho)=\frac{\sum_{j=1}^{2}\eta_{ij}P_j}{4\pi\sqrt{\pi}}\begin{cases}\displaystyle\sum_{n=0}^{\infty}\frac{(2n)!}{4^n(n!)^2(2n+1)}\frac{\Gamma\left(n+\frac{3}{2}\right)}{\Gamma(n+2)}\left[\frac{\sqrt{\pi}\Gamma(-n-1)}{\Gamma\left(-n-\frac{1}{2}\right)}-\widetilde{B}\left(\frac{\rho^2}{a^2};-n-1,\frac{1}{2}\right)\right]\frac{\rho^{2n+2}}{\rho_c^{2n+1}}, & \text{(arcsine)}\\ \displaystyle 2\sqrt{\pi(a^2-\rho^2)}-\sum_{n=0}^{\infty}\frac{(2n)!}{4^n(n!)^2(2n+1)}\frac{\Gamma\left(n+\frac{3}{2}\right)}{\Gamma(n+2)}\left[\frac{\sqrt{\pi}\Gamma(-n-1)}{\Gamma\left(-n-\frac{1}{2}\right)}-\widetilde{B}\left(\frac{\rho^2}{a^2};-n-1,\frac{1}{2}\right)\right]\frac{\rho^{2n+2}}{\rho_c^{2n+1}}. & \text{(arccosine)}\end{cases} \tag{E.14}$$

E.4. Non-axisymmetric loading

Take $P_j(\rho,\phi)\equiv P_j\rho\sin(\phi)$ or $P_j(\rho,\phi)\equiv P_j\rho\cos(\phi)$ for instance. According to the definition of $\mathscr{L}(k)$ in Appendix B, we have

$$\mathscr{L}(k)\sin(\phi)=k\sin(\phi),\quad \mathscr{L}(k)\cos(\phi)=k\cos(\phi), \tag{E.15}$$

leading to

$$\omega_i(\rho,\phi)=\frac{2\sum_{j=1}^{2}\eta_{ij}P_j}{3\pi^2}\rho\sqrt{a^2-\rho^2}\sin(\phi), \tag{E.16}$$

and the potential functions are derived as

$$\begin{aligned}\widehat{H}_i(\rho,\phi,z_k)=\frac{\sum_{j=1}^{2}\eta_{ij}P_j}{12\pi}\sin(\phi)\Bigg\{&\rho\left(4a^2+12z_k^2-3\rho^2\right)\arctan\left[\frac{l_1(a)}{\sqrt{\rho^2-l_1^2(a)}}\right]\\ &+l_1(a)\frac{3\rho^4-\rho^2\left[4a^2+12z_k^2+l_1^2(a)\right]-2l_1^2(a)\left[l_1^2(a)-2a^2-2z_k^2\right]}{\rho\sqrt{\rho^2-l_1^2(a)}}\Bigg\}.\end{aligned} \tag{E.17}$$

The analytical solution for the cosine case can be directly obtained simply by replacing the sine functions in Eqs. (E.16) and (E.17) with cosine functions.

Appendix F. Potential theory method for anti-crack problems

Without loss of generality, we may take the simplified formulation established in Appendix B, that is, the displacement and stress components are defined as the zeroth and first-order derivatives of potential functions $H_i(\rho,\phi,z)$, which are defined in Eq. (B.1). Concerning the incremental displacement boundary conditions shown in Eq. (56) and the property of the single layer potential, we have

$$\int_0^a\frac{\mathrm{d}x}{\sqrt{\rho^2-x^2}}\int_x^a\frac{\rho_0\mathrm{d}\rho_0}{\sqrt{\rho_0^2-x^2}}\mathscr{L}\left(\frac{x^2}{\rho\rho_0}\right)\sigma_{zi}^{\mathrm{I}}(\rho_0,\phi)+\int_\rho^\infty\frac{\mathrm{d}x}{\sqrt{x^2-\rho^2}}\int_a^x\frac{\rho_0\mathrm{d}\rho_0}{\sqrt{x^2-\rho_0^2}}\mathscr{L}\left(\frac{\rho\rho_0}{x^2}\right)\sigma_{zi}^{\mathrm{II}}(\rho_0,\phi)=0, \tag{F.1}$$

which leads to

$$\begin{aligned}\sigma_{zi}^{\mathrm{II}}(\rho,\phi)&=-\frac{1}{\pi^2}\frac{1}{\sqrt{\rho^2-a^2}}\int_0^{2\pi}\int_0^a\frac{\sqrt{a^2-\rho_0^2}\sigma_{zi}^{\mathrm{I}}(\rho_0,\phi_0)}{\rho^2+\rho_0^2-2\rho\rho_0\cos(\phi-\phi_0)}\rho_0\mathrm{d}\rho_0\mathrm{d}\phi_0\\ &=-\frac{2}{\pi\sqrt{\rho^2-a^2}}\int_0^a\frac{\sqrt{a^2-\rho_0^2}}{\rho^2-\rho_0^2}\mathscr{L}\left(\frac{\rho_0}{\rho}\right)\sigma_{zi}^{\mathrm{I}}(\rho_0,\phi)\rho_0\mathrm{d}\rho_0\end{aligned}\qquad(\rho\geq a) \tag{F.2}$$

according to Eqs. (B.34) to (B.37), where $\sigma_{zi}^{\mathrm{I}}(\rho,\phi)$ and $\sigma_{zi}^{\mathrm{II}}(\rho,\phi)$ are $\sigma_{zi}(\rho,\phi,0)$ defined on $S^{\mathrm{I}}=\{(\rho,\phi)|0\leq\rho<a;0\leq\phi\leq2\pi\}$ and $S^{\mathrm{II}}=\{(\rho,\phi)|\rho\geq a;0\leq\phi\leq2\pi\}$, respectively. Then, the potential function can be represented in terms of σ_{zi}^{I} as

$$H_i(\rho,\phi,z)=4\int_{l_2(0)}^{l_2(a)}\frac{\mathrm{d}x}{\sqrt{x^2-\rho^2}}\int_0^{g(x)}\frac{\rho_0\mathrm{d}\rho_0}{\sqrt{g^2(x)-\rho_0^2}}\mathscr{L}\left(\frac{\rho\rho_0}{x^2}\right)\sigma_{zi}^{\mathrm{I}}(\rho_0,\phi). \tag{F.3}$$

Substituting the incremental displacement boundary conditions on S^{I} into Eq. (F.3) yields

$$W_i(\rho,\phi)=4\int_\rho^a\frac{\mathrm{d}x}{\sqrt{x^2-\rho^2}}\int_0^x\frac{\rho_0\mathrm{d}\rho_0}{\sqrt{x^2-\rho_0^2}}\mathscr{L}\left(\frac{\rho\rho_0}{x^2}\right)\sigma_{zi}^{\mathrm{I}}(\rho_0,\phi), \tag{F.4}$$

leading to

$$\sigma_{zi}^{\mathrm{I}}(\rho,\phi) = -\frac{1}{\pi^2\rho}\mathscr{L}\left(\frac{1}{\rho}\right)\frac{\mathrm{d}}{\mathrm{d}\rho}\int_0^{\rho}\frac{x\mathrm{d}x}{\sqrt{\rho^2-x^2}}\mathscr{L}(x^2)\frac{\mathrm{d}}{\mathrm{d}x}\int_x^a\frac{\rho_0\mathrm{d}\rho_0}{\sqrt{\rho_0^2-x^2}}\mathscr{L}\left(\frac{1}{\rho_0}\right)W_i(\rho_0,\phi) \tag{F.5}$$

according to Eq. (B.45). Eventually, $\sigma_{zi}^{\mathrm{II}}$ are derived by substituting Eq. (F.5) into Eq. (F.2). Its form is nearly identical to that of Eq. (F.5), except that the upper limit of the first integral should be changed from ρ to a.

Through Eq. (C.11), $\sigma_{zi}^{\mathrm{II}}$ can be further simplified as

$$\begin{aligned}\sigma_{zi}^{\mathrm{II}} &= \frac{1}{\pi^2}\mathscr{L}\left(\frac{1}{\rho}\right)\int_0^a\frac{x\mathrm{d}x}{(\rho^2-x^2)^{3/2}}\mathscr{L}(x^2)\frac{\mathrm{d}}{\mathrm{d}x}\int_x^a\frac{\rho_0\mathrm{d}\rho_0}{\sqrt{\rho_0^2-x^2}}\mathscr{L}\left(\frac{1}{\rho_0}\right)W_i(\rho_0,\phi)\\ &= \frac{1}{\pi^2}\int_0^a\frac{\mathrm{d}x}{(\rho^2-x^2)^{3/2}}\int_x^a\frac{\rho_0\mathrm{d}\rho_0}{\sqrt{\rho_0^2-x^2}}\frac{\mathrm{d}}{\mathrm{d}\rho_0}\left[\rho_0\mathscr{L}\left(\frac{x^2}{\rho\rho_0}\right)W_i(\rho_0,\phi)\right],\end{aligned} \tag{F.6}$$

where $W_i(a,\phi)=0$ is used above. It is important to note that $\sigma_{zi}^{\mathrm{II}}$ in Eq. (F.6) are also solutions to the type-A integro-differential equations, i.e., they can be expressed as type-A integro-differential equations by interchanging of the order of integration.

Appendix G. Bifurcation equations in surface stability analysis

Here $\mathfrak{M}_x$ and $\mathfrak{M}_\rho$ in Eq. (67) and Eq. (77) are expressed in the forms

$$\mathfrak{M}_x = \begin{bmatrix} c_{88}\mathfrak{s}_1^2-c_{11} & 0 & 0 & -(c_{13}+c_{58})\mathfrak{s}_1 & 0 & 0 & -(e_{15}+e_{31})\mathfrak{s}_1 & 0 & 0 \\ 0 & c_{88}\mathfrak{s}_2^2-c_{11} & 0 & 0 & -(c_{13}+c_{58})\mathfrak{s}_2 & 0 & 0 & -(e_{15}+e_{31})\mathfrak{s}_2 & 0 \\ 0 & 0 & c_{88}\mathfrak{s}_3^2-c_{11} & 0 & 0 & -(c_{13}+c_{58})\mathfrak{s}_3 & 0 & 0 & -(e_{15}+e_{31})\mathfrak{s}_3 \\ (c_{13}+c_{58})\mathfrak{s}_1 & 0 & 0 & c_{33}\mathfrak{s}_1^2-c_{55} & 0 & 0 & e_{33}\mathfrak{s}_1^2-e_{15} & 0 & 0 \\ 0 & (c_{13}+c_{58})\mathfrak{s}_2 & 0 & 0 & c_{33}\mathfrak{s}_2^2-c_{55} & 0 & 0 & e_{33}\mathfrak{s}_2^2-e_{15} & 0 \\ 0 & 0 & (c_{13}+c_{58})\mathfrak{s}_3 & 0 & 0 & c_{33}\mathfrak{s}_3^2-c_{55} & 0 & 0 & e_{33}\mathfrak{s}_3^2-e_{15} \\ c_{13} & c_{13} & c_{13} & c_{33}\mathfrak{s}_1 & c_{33}\mathfrak{s}_2 & c_{33}\mathfrak{s}_3 & e_{33}\mathfrak{s}_1 & e_{33}\mathfrak{s}_2 & e_{33}\mathfrak{s}_3 \\ -c_{88}\mathfrak{s}_1 & -c_{88}\mathfrak{s}_2 & -c_{88}\mathfrak{s}_3 & c_{58} & c_{58} & c_{58} & e_{15} & e_{15} & e_{15} \\ e_{31} & e_{31} & e_{31} & e_{33}\mathfrak{s}_1 & e_{33}\mathfrak{s}_2 & e_{33}\mathfrak{s}_3 & -\varepsilon_{33}\mathfrak{s}_1 & -\varepsilon_{33}\mathfrak{s}_2 & -\varepsilon_{33}\mathfrak{s}_3 \end{bmatrix}, \tag{G.1}$$

$$\mathfrak{M}_\rho = \begin{bmatrix} c_{88}\mathfrak{s}_1^2-c_{11} & 0 & 0 & (c_{13}+c_{58})\mathfrak{s}_1 & 0 & 0 & (e_{15}+e_{31})\mathfrak{s}_1 & 0 & 0 \\ 0 & c_{88}\mathfrak{s}_2^2-c_{11} & 0 & 0 & (c_{13}+c_{58})\mathfrak{s}_2 & 0 & 0 & (e_{15}+e_{31})\mathfrak{s}_2 & 0 \\ 0 & 0 & c_{88}\mathfrak{s}_3^2-c_{11} & 0 & 0 & (c_{13}+c_{58})\mathfrak{s}_3 & 0 & 0 & (e_{15}+e_{31})\mathfrak{s}_3 \\ -(c_{13}+c_{58})\mathfrak{s}_1 & 0 & 0 & c_{33}\mathfrak{s}_1^2-c_{55} & 0 & 0 & e_{33}\mathfrak{s}_1^2-e_{15} & 0 & 0 \\ 0 & -(c_{13}+c_{58})\mathfrak{s}_2 & 0 & 0 & c_{33}\mathfrak{s}_2^2-c_{55} & 0 & 0 & e_{33}\mathfrak{s}_2^2-e_{15} & 0 \\ 0 & 0 & -(c_{13}+c_{58})\mathfrak{s}_3 & 0 & 0 & c_{33}\mathfrak{s}_3^2-c_{55} & 0 & 0 & e_{33}\mathfrak{s}_3^2-e_{15} \\ c_{13} & c_{13} & c_{13} & -c_{33}\mathfrak{s}_1 & -c_{33}\mathfrak{s}_2 & -c_{33}\mathfrak{s}_3 & -e_{33}\mathfrak{s}_1 & -e_{33}\mathfrak{s}_2 & -e_{33}\mathfrak{s}_3 \\ c_{88}\mathfrak{s}_1 & c_{88}\mathfrak{s}_2 & c_{88}\mathfrak{s}_3 & c_{58} & c_{58} & c_{58} & e_{15} & e_{15} & e_{15} \\ e_{31} & e_{31} & e_{31} & -e_{33}\mathfrak{s}_1 & -e_{33}\mathfrak{s}_2 & -e_{33}\mathfrak{s}_3 & \varepsilon_{33}\mathfrak{s}_1 & \varepsilon_{33}\mathfrak{s}_2 & \varepsilon_{33}\mathfrak{s}_3 \end{bmatrix}, \tag{G.2}$$

respectively. Besides, Eq. (64) enables simplification of the determinant from 9×9 to a compact 3×3 form, thereby facilitating its numerical computation.

Nomenclature

$(x,y,z);(\rho,\phi,z)$	Cartesian and cylindrical coordinate systems
$\overline{\mathbb{B}}_r,\overline{\mathbb{B}},\overline{\mathbb{B}}_c$	Reference, initial, and current configurations
$\mathbf{N},\mathbf{n},\widetilde{\mathbf{n}}$	Outward unit normal vectors of $\partial\overline{\mathbb{B}}_r$, $\partial\overline{\mathbb{B}}$, and $\partial\overline{\mathbb{B}}_c$
$\mathbf{X},\mathbf{x},\widetilde{\mathbf{x}}$	Material point position vectors in $\overline{\mathbb{B}}_r$, $\overline{\mathbb{B}}$, and $\overline{\mathbb{B}}_c$
$\{\boldsymbol{E}^r_\alpha\},\{\boldsymbol{e}_i\},\{\widetilde{\boldsymbol{e}}_a\}$	Bases in $\overline{\mathbb{B}}_r$, $\overline{\mathbb{B}}$, and $\overline{\mathbb{B}}_c$
$\chi:\mathbf{X}\mapsto\mathbf{x}$	Mapping of material point position vectors between $\overline{\mathbb{B}}_r$ and $\overline{\mathbb{B}}$
$\mathbf{F}=\partial\mathbf{x}/\partial\mathbf{X},\widetilde{\mathbf{F}}=\partial\widetilde{\mathbf{x}}/\partial\mathbf{X}$	Deformation gradients
$\mathbf{b}=\mathbf{F}\mathbf{F}^{\mathrm{T}},\mathbf{C}=\mathbf{F}^{\mathrm{T}}\mathbf{F}$	Left and right Cauchy-Green deformation tensors
$\mathrm{d}\widehat{\boldsymbol{A}},\mathrm{d}\widehat{\boldsymbol{a}}$	Surface elements in $\overline{\mathbb{B}}_r$ and $\overline{\mathbb{B}}$
$\mathrm{d}V,\mathrm{d}v$	Volume elements in $\overline{\mathbb{B}}_r$ and $\overline{\mathbb{B}}$
$J=\det\mathbf{F}$	Volume ratio
$a_r,a,\widetilde{a}_c$	Crack surface radius in $\overline{\mathbb{B}}_r$, $\overline{\mathbb{B}}$, and $\overline{\mathbb{B}}_c$
a_p	Radial crack propagation length in $\overline{\mathbb{B}}$
$\widetilde{f}(\{\lambda_i\})$	Ratio of crack surface radius
Grad,Div,Curl	Gradient, divergence, and curl operator in $\overline{\mathbb{B}}_r$
grad,div,curl	Gradient, divergence, and curl operator in $\overline{\mathbb{B}}$
$\mathbf{T},\boldsymbol{\tau}$	Nominal stress tensor and Cauchy stress tensor
$\mathscr{D},\mathbf{D}$	Lagrangian and Eulerian electric displacement vectors
$\mathscr{E},\mathbf{E}$	Lagrangian and Eulerian electric field vectors
$\mathbf{E}^*,\widetilde{\mathbf{E}}^*$	Exterior electric field vectors in $\mathbb{B}$ and $\mathbb{B}_c$
$\mathbf{t}_{\hat{A}},\mathbf{t}_{\hat{a}}$	Surface traction on $\partial\overline{\mathbb{B}}_r$ and $\partial\overline{\mathbb{B}}$
$q_{\hat{A}},q_{\hat{a}}$	Charge density per unit area on $\partial\overline{\mathbb{B}}_r$ and $\partial\overline{\mathbb{B}}$
$\Omega(\mathbf{F},\mathscr{D})$	Energy density function per reference volume
$\mathscr{I}_m$	Invariants ($m=1,\cdots,6$)
Ω_m,Ω_{mn}	Partial derivatives of Ω ($\partial\Omega/\partial\mathscr{I}_m$ and $\partial^2\Omega/(\partial\mathscr{I}_m\partial\mathscr{I}_n)$)
$\mathbf{I},\widetilde{\mathbb{I}}$	Unit tensors in $\overline{\mathbb{B}}_r$ and $\overline{\mathbb{B}}$
$\mathbf{I},I_{\circledast}$	Two-point unit tensors ($\mathbf{I}=\delta_{i\alpha}\boldsymbol{e}_i\otimes\boldsymbol{E}^r_\alpha$ and $I_{\circledast}=\delta_{ai}\widetilde{\boldsymbol{e}}_a\otimes\boldsymbol{e}_i$)
$\mathbf{u}(\mathbf{x})=\mathbf{u}(\chi(\mathbf{X}))=\dot{\mathbf{x}}(\mathbf{X})$	Incremental deformation
$\dot{\mathbf{F}}=\left(I^{\mathrm{T}}\widetilde{\mathbf{F}}-\mathbf{F}\right)$	Incremental deformation gradient
$\dot{\mathbf{T}},\dot{\mathbf{T}}_0$	Incremental nominal stress tensor and its push-forward version
$\dot{\mathscr{D}},\dot{\mathbf{D}}_0$	Incremental electric displacement vector and its push-forward version
$\dot{\mathscr{E}},\dot{\mathbf{E}}_0$	Incremental electric field vector and its push forward version
$\mathbf{L}=\dot{\mathbf{F}}\mathbf{F}^{-1}=\mathrm{grad}\mathbf{u}$	Displacement gradient tensor
$\mathbf{A}_0,\mathbf{M}_0,\mathbf{K}_0$	Instantaneous material tensors of the 4$^{\mathrm{th}}$-, 3$^{\mathrm{rd}}$-, and 2$^{\mathrm{nd}}$-order
$\dot{\mathbf{t}}_{\hat{A}},\dot{\mathbf{t}}_{\hat{a}}$	Incremental surface traction on $\partial\overline{\mathbb{B}}_r$ and $\partial\overline{\mathbb{B}}$
$\dot{q}_{\hat{A}},\dot{q}_{\hat{a}}$	Incremental charge density per unit area on $\partial\overline{\mathbb{B}}_r$ and $\partial\overline{\mathbb{B}}$
λ_i	Pre-stretches (diagonal element of $\mathbf{F}$; $i=1,2,3$)
D_i	External electric displacement vector components ($i=1,2,3$)
$\widetilde{\varphi}$	Electric potential
$c_{mn},e_{mn},\varepsilon_{mn}$	Equivalent constants [Appendix A]
Δ	Planar Laplacian
$\psi_0,\widetilde{\psi},\Phi_0,\widetilde{\Phi},\Psi$	Displacement functions
$\mathfrak{D},\mathfrak{D}^\dagger$	Operator matrix and its adjugate
$\mathfrak{F}_{ij}$	Cofactor of $\mathfrak{D}$ ($i,j=1,2,3$)
$\xi_k^{(i)},\psi_k$	Quasi-harmonic functions ($i,k=1,2,3$)
$\hbar_i$	Coefficients of the characteristic equation [Appendix A]
s_j^2	Roots of the characteristic equation [Appendix A]
$z_j=s_jz$	Equivalent axial coordinate component ($j=1,2,3$)
$a_i,b_i,d_j,\alpha_{mk},\gamma_{ik},\varpi_{ik}$	Coefficients for the combination of quasi-harmonic functions [Eq. (27)]
$w_i,\sigma_{zm},\sigma_{\rho m},\sigma_{\phi m},$ $\sigma_{\rho t},\sigma_{\phi t},\sigma_{zt}$	Equivalent mechanical and electrical variables [Eqs. (30) and (31)]
S_r,S	Crack surfaces in $\overline{\mathbb{B}}_r$ and $\overline{\mathbb{B}}$
P_1,P_2	Prescribed $\dot{\mathrm{T}}_{0zz}$ and $\dot{\mathrm{D}}_{0z}$ on S
W_1,W_2	Prescribed u_z and φ on S
$\widehat{H}_i,H_i$	Single layer potentials ($i=1,2$)
ω_i	Densities ($i=1,2$)
ς_{ki},η_{ij}	Coefficients for the combination of potentials [Eqs. (38) and (41)]

(continued on next page)

(*continued*)

δ_{ji}	Kronecker delta
$l_1(\#)$,$l_2(\#)$	Equivalent radical coordinate components
$g(\#)$	Inverse of $l_1(\#)$ or $l_2(\#)$
R_0,R	Distance between two points (3D and 2D)
$\mathscr{L}(\#)$	Poisson operator
$\mathscr{G}(\#,\#)$	Kernel in $\mathscr{L}(\#)$
$\dot{K}_{\mathrm{IT}}$,$\dot{K}_{\mathrm{ID}}$	Incremental intensity factors (mode I)
Λ,ζ_1,ζ_2	Dimensionless coefficients of a specific material [Eq. (52)]
μ,ν	Shear modulus and Poisson's ratio
$\varepsilon_0 = 8.854 \times 10^{-12}(\mathrm{F/m})$	Dielectric permittivity in vacuum
${}_2\widetilde{F}_1(\#,\#;\#;\#)$	Gauss hypergeometric function
$\Gamma(\#)$	Gamma function
$\widetilde{J}_v(\#)$,$\widetilde{I}_v(\#)$	Bessel and modified Bessel functions of the first kind
$\widetilde{H}_v(\#)$,$\widetilde{L}_v(\#)$	Struve and modified Struve functions
$\widetilde{B}(\#;\#)$	Incomplete beta function
$\widetilde{K}(\#)$,$\widetilde{E}(\#)$	Complete elliptic integral of the first and second kinds,
$\widehat{k}$	Wave number
$\vartheta_i(\#)$,$\mathfrak{A}_j$,$\mathfrak{B}_j$,$\mathfrak{C}_j$	Functions and coefficients for a non-trivial solution in stability analysis
$\mathfrak{s}_j$	Eigenvalues introduced in $\vartheta_i(\#)$ [Eqs. (62) and (63)]
$\mathfrak{M}_x$,$\mathfrak{M}_\rho$	Matrices in bifurcation equations of two instability cases
G,G_c,G^*	Energy release rates in $\overline{\mathbb{B}}$ and $\overline{\mathbb{B}}_c$ together with the critical value
$\dot{G} = G_c - G$	Incremental energy release rate
$\dot{\Pi}$,$\dot{\Pi}_c$, $\dot{\mathscr{U}}$, $\dot{\mathscr{U}}_c$, $\dot{\mathscr{W}}$	Incremental total potential energy in $\overline{\mathbb{B}}$ and $\overline{\mathbb{B}}_c$, incremental internal energy in $\overline{\mathbb{B}}$ and $\overline{\mathbb{B}}_c$, and incremental work
$\delta\dot{\Pi} = \delta(\Pi_c - \Pi) = 0$	The principle of incremental minimum potential energy
R_i	Stable or unstable regions ($i = 1, 2, 3, 4$)
$\mathrm{Re}(\#)$,$\mathrm{Im}(\#)$	Real and imaginary part of #
$\mathscr{C}_{n^+,n^-} = \mathscr{C}^+_{n^+} + \mathscr{C}^-_{n^-}$	Buckling topological number
$n^\natural$	Number of half-wavelengths in the buckling mode ($\natural = +, -$)
λ_c^p	Critical transition stretch
$\epsilon = \mathrm{sym}(\mathbf{L})$	Incremental strain
$\mathfrak{S}_x^\pm$,$\mathfrak{S}_\rho^\pm$	Upper and lower bounded half-spaces embedded with the crack in $\overline{\mathbb{B}}$ (Cartesian and cylindrical coordinates)
$\mathscr{O}(\#)$	Landau symbol
Υ_1,Υ_2	Constants introduced in the evaluation of $\dot{u}_{\mathfrak{S}_\rho^\pm}$
ρ_n	The n-th zero of $\widetilde{J}_0(\rho)$
$\overset{\star}{\mathbf{T}} = \dot{\mathbf{T}} - \mathbf{T}\mathbf{L}^{\mathrm{T}}$	Objective stress rate of the nominal stress tensor
$\mathring{\boldsymbol{\tau}} = \dot{\boldsymbol{\tau}} - \mathbf{L}\boldsymbol{\tau} - \boldsymbol{\tau}\mathbf{L}^{\mathrm{T}} + \mathrm{tr}(\mathbf{L})\boldsymbol{\tau}$	Truesdell rate of the Cauchy stress tensor
$\overset{\cdot n}{\mathbf{T}}_0$,$\overset{\cdot n}{\mathbf{E}}_0$	Push forward version of the generalized incremental nominal stress tensor and the incremental electric field vector
$\overset{\star n}{\mathbf{T}}_0$	Push forward version of the generalized objective stress rate of the nominal stress tensor
$\mho$	Equivalent coefficient in the roots
$\lambdabar$	Arbitrary power index of distant R_0 or R ($-1 < \lambdabar < 1$)
M_0,N_0,N	Distinct points in cylindrical coordinates
$\mathscr{F}(\#)$,$f(\#)$	Arbitrary kernels in Abel integral equations
$h(\#)$	Equivalent length [Eq. (B.21)]
$\mathscr{Z}$,$\overline{\mathscr{Z}}$	Ratio of two distinct points and their complex conjugate [Eq. (B.29)]
δ_L	Dirac delta
$\partial\Omega_{\mathrm{in}}$,$S^{\mathrm{I}}$	Inside the circular domain of radius a
$\partial\Omega_{\mathrm{out}}$,$S^{\mathrm{II}}$	Outside the circular domain of radius a
σ_{zi}^{I},$\sigma_{zi}^{\mathrm{II}}$	σ_{zi} defined on S^{I} and S^{II}
$\boldsymbol{\Xi}_1 : \boldsymbol{\Xi}_2$	$(\Xi_1)_{ij}(\Xi_2)_{ij}$
$\boldsymbol{\Xi}_1 \cdot\cdot \boldsymbol{\Xi}_2$,$\mathbf{A}\cdot\cdot\cdot\cdot\mathbf{B}$	$(\Xi_1)_{ij}(\Xi_2)_{ji}$ and $A_{ijkl}B_{ijkl}$
$\boldsymbol{\Xi}_1 \underset{2}{\circ} \boldsymbol{\Xi}_2$	$(\Xi_1)_{ij}(\Xi_2)_{ik}\boldsymbol{e}_k \otimes \boldsymbol{e}_j$
$\boldsymbol{\Xi}_1 \otimes \boldsymbol{\Xi}_2$	$(\Xi_1)_{ij}(\Xi_2)_{kl}\boldsymbol{e}_i \otimes \boldsymbol{e}_j \otimes \boldsymbol{e}_k \otimes \boldsymbol{e}_l$

Data availability

Data will be made available on request.

References

Ahmad, D., Sahu, S.K., Patra, K., 2019. Fracture toughness, hysteresis and stretchability of dielectric elastomers under equibiaxial and biaxial loading. Polym. Test. 79, 106038. https://doi.org/10.1016/j.polymertesting.2019.106038.

Bar-Cohen, Y., 2002. Electroactive polymers: current capabilities and challenges. Smart Structures and Materials 2002: Electroactive Polymer Actuators and Devices (EAPAD), pp. 1–7. https://doi.org/10.1117/12.475159.

Branz, F., Francesconi, A., 2017. Experimental evaluation of a Dielectric Elastomer robotic arm for space applications. Acta Astronaut. 133, 324–333. https://doi.org/10.1016/j.actaastro.2016.11.007.

Cao, C.J., Gao, X., Conn, A.T., 2019. Towards efficient elastic actuation in bio-inspired robotics using dielectric elastomer artificial muscles. Smart Mater. Struct. 28, 095015. https://doi.org/10.1088/1361-665X/ab326b.

Chen, C., Wang, Z.J., Suo, Z.G., 2017. Flaw sensitivity of highly stretchable materials. Extreme Mech. Lett. 50–57. https://doi.org/10.1016/j.eml.2016.10.002.

Chen, W.Q., 2000. On piezoelastic contact problem for a smooth punch. Int. J. Solids Struct. 37, 2331–2340. https://doi.org/10.1016/S0020-7683(98)00307-2.

Chen, W.Q., Ding, H.J., 2004. Potential theory method for 3D crack and contact problems of multi-field coupled media: a survey. J. Zhejiang Univ.-SCI. A 5, 1009–1021. https://doi.org/10.1631/jzus.2004.1009.

Chen, W.Q., 2015. Some recent advances in 3D crack and contact analysis of elastic solids with transverse isotropy and multifield coupling. Acta Mech. Sin. 31, 601–626. https://doi.org/10.1007/s10409-015-0509-3.

Chen, W.Q., Lee, K.Y., Ding, H.J., 2004. General solution for transversely isotropic magneto-electro-thermo-elasticity and the potential theory method. Int. J. Eng. Sci. 42, 1361–1379. https://doi.org/10.1016/j.ijengsci.2004.04.002.

Ding, H.J., Chen, B., Liang, J., 1996. General solutions for coupled equations for piezoelectric media. Int. J. Solids Struct. 33, 2283–2298. https://doi.org/10.1016/0020-7683(95)00152-2.

Dorfmann, A., Ogden, R.W., 2006. Nonlinear electroelastic deformations. J. Elast. 82, 99–127. https://doi.org/10.1007/s10659-005-9028-y.

Dorfmann, A., Ogden, R.W., 2010. Nonlinear electroelastostatics: incremental equations and stability. Int. J. Eng. Sci. 48, 1–14. https://doi.org/10.1016/j.ijengsci.2008.06.005.

Dorfmann, L., Ogden, R.W., 2014. Nonlinear Theory of Electroelastic and Magnetoelastic Interactions. Springer US, Boston, MA. https://doi.org/10.1007/978-1-4614-9596-3.

Fabrikant, V.I., 1989. Applications of Potential Theory in Mechanics: A Selection of New Results. Kluwer Academic Publishers, Dordrecht, Boston.

Fakhouri, S., Hutchens, S.B., Crosby, A.J., 2015. Puncture mechanics of soft solids. Soft. Matter. 11, 4723–4730. https://doi.org/10.1039/C5SM00230C.

Gent, A.N., Razzaghi-Kashani, M., Hamed, G.R., 2003. Why do cracks turn sideways? Rubber Chem. Technol. 76, 122–131. https://doi.org/10.5254/1.3547727.

Gu, G.Y., Zhu, J., Zhu, L.M., Zhu, X.Y., 2017. A survey on dielectric elastomer actuators for soft robots. Bioinspir. Biomim. 12, 011003. https://doi.org/10.1088/1748-3190/12/1/011003.

Hua, M.T., Wu, S.W., Ma, Y.F., Zhao, Y.S., Chen, Z.L., Frenkel, I., Strzalka, J., Zhou, H., Zhu, X.Y., He, X.M., 2021. Strong tough hydrogels via the synergy of freeze-casting and salting out. Nature 590, 594–599. https://doi.org/10.1038/s41586-021-03212-z.

Huang, D.Y., Ma, J.X., Han, Y.B., Xue, C., Zhang, M.Y., Wen, W.J., Sun, S., Wu, J.B., 2025. Artificial intelligence artificial muscle of dielectric elastomers. Mater. Des. 251, 113691. https://doi.org/10.1016/j.matdes.2025.113691.

Ji, X.B., Liu, X.C., Cacucciolo, V., Imboden, M., Civet, Y., El Haitami, A., Cantin, S., Perriard, Y., Shea, H., 2019. An autonomous untethered fast soft robotic insect driven by low-voltage dielectric elastomer actuators. Sci. Robot. 4, eaaz6451. https://doi.org/10.1126/scirobotics.aaz6451.

Jiang, Y.Z., Sun, P., Du, L., Wang, H.M., Xiao, R., 2025. Puncture of mechanochromic tough elastomeric membranes. Acta Mech. Solida Sin. https://doi.org/10.1007/s10338-025-00671-z.

Kaliske, M., Storm, J., Kanan, A., Klausler, W., 2022. The Ogden and the extended tube model as backbone in describing electroactive polymers: advancements in modelling nonlinear behaviour and fracture. Philos. Trans. R. Soc. A: Math. Phys. Eng. Sci. 380, 20210329. https://doi.org/10.1098/rsta.2021.0329.

Khatami, M., Bairwan, R.D., Khalil, H.P.S.A., Surya, I., Mawardi, I., Ahmad, A., Yahya, E.B., 2024. The role of natural fiber reinforcement in thermoplastic elastomers biocomposites. Fibers Polym. 25, 3061–3077. https://doi.org/10.1007/s12221-024-00621-5.

Kim, J.S., Zhang, G.G., Shi, M.X.Z., Suo, Z.G., 2021. Fracture, fatigue, and friction of polymers in which entanglements greatly outnumber cross-links. Science 374, 212–216. https://doi.org/10.1126/science.abg6320.

Koh, S.J.A., Keplinger, C., Li, T.F., Bauer, S., Suo, Z.G., 2011. Dielectric elastomer generators: how much energy can be converted? IEEE/ASME Trans. Mechatron. 16, 33–41. https://doi.org/10.1109/TMECH.2010.2089635.

Kornbluh, R.D., Pelrine, R., Joseph, J., Heydt, R., Pei, Q.B., Chiba, S., 1999. High-field electrostriction of elastomeric polymer dielectrics for actuation. Smart Structures and Materials 1999: Electroactive Polymer Actuators and Devices (EPAD), pp. 149–161. https://doi.org/10.1117/12.349672.

Kornbluh, R.D., Pelrine, R., Prahlad, H., Wong-Foy, A., McCoy, B., Kim, S., Eckerle, J., Low, T., 2012a. From boots to buoys: promises and challenges of dielectric elastomer energy harvesting. In: Rasmussen, L. (Ed.), Electroactivity in Polymeric Materials. Springer US, Boston, MA, pp. 67–93. https://doi.org/10.1007/978-1-4614-0878-9_3.

Kornbluh, R.D., Pelrine, R., Prahlad, H., Wong-Foy, A., McCoy, B., Kim, S., Eckerle, J., Low, T., 2012b. Dielectric elastomers: stretching the capabilities of energy harvesting. MRS Bull. 37, 246–253. https://doi.org/10.1557/mrs.2012.41.

Lee, S.H., Pharr, M., 2019. Sideways and stable crack propagation in a silicone elastomer. Proc. Natl. Acad. Sci. 116, 9251–9256. https://doi.org/10.1073/pnas.1820424116.

Leng, J.S., Liu, L., Liu, Y.J., Yu, K., Sun, S.H., 2009. Electromechanical stability of dielectric elastomer. Appl. Phys. Lett. 94, 211901. https://doi.org/10.1063/1.3138153.

Li, C.H., Yang, H., Suo, Z.G., Tang, J.D., 2020. Fatigue-resistant elastomers. J. Mech. Phys. Solids 134, 103751. https://doi.org/10.1016/j.jmps.2019.103751.

Liu, B.H., Yin, T.H., Zhu, J.Y., Zhao, D.H., Yu, H.H., Qu, S.X., Yang, W., 2023. Tough and fatigue-resistant polymer networks by crack tip softening. Proc. Natl. Acad. Sci. 120, e2217781120. https://doi.org/10.1073/pnas.2217781120.

Long, R., Hui, C.Y., 2016. Fracture toughness of hydrogels: measurement and interpretation. Soft. Matter. 12, 8069–8086. https://doi.org/10.1039/C6SM01694D.

Maas, J., Graf, C., 2012. Dielectric elastomers for hydro power harvesting. Smart Mater. Struct. 21, 064006. https://doi.org/10.1088/0964-1726/21/6/064006.

Manikkavel, A., Kumar, V., Lee, D.J., 2020. Simple fracture model for an electrode and interfacial crack in a dielectric elastomer under tensile loading. Theor. Appl. Fract. Mech. 108, 102626. https://doi.org/10.1016/j.tafmec.2020.102626.

Moreno-Mateos, M.A., Mehnert, M., Steinmann, P., 2024. Electro-mechanical actuation modulates fracture performance of soft dielectric elastomers. Int. J. Eng. Sci. 195, 104008. https://doi.org/10.1016/j.ijengsci.2023.104008.

O'Halloran, A., O'Malley, F., McHugh, P., 2008. A review on dielectric elastomer actuators, technology, applications, and challenges. J. Appl. Phys. 104, 071101. https://doi.org/10.1063/1.2981642.

Park, H.S., Nguyen, T.D., 2012. Viscoelastic effects on electromechanical instabilities in dielectric elastomers. Soft. Matter. 9, 1031–1042. https://doi.org/10.1039/C2SM27375F.

Pelrine, R., Kornbluh, R., Joseph, J., Heydt, R., Pei, Q.B., Chiba, S., 2000. High-field deformation of elastomeric dielectrics for actuators. Mater. Sci. Eng.: C 11, 89–100. https://doi.org/10.1016/S0928-4931(00)00128-4.

Pharr, M., Sun, J.Y., Suo, Z.G., 2012. Rupture of a highly stretchable acrylic dielectric elastomer. J. Appl. Phys. 111, 104114. https://doi.org/10.1063/1.4721777.

Sharma, A.K., Kosta, M., Shmuel, G., Amir, O., 2022. Gradient-based topology optimization of soft dielectrics as tunable phononic crystals. Compos. Struct. 280, 114846. https://doi.org/10.1016/j.compstruct.2021.114846.

Shian, S., Bertoldi, K., Clarke, D.R., 2015. Dielectric elastomer based "grippers" for soft robotics. Adv. Mater. 27, 6814–6819. https://doi.org/10.1002/adma.201503078.

Sun, Y.X., Ju, Y.W., Wen, H., Liu, R.Q., Cao, Q.L., Li, L., 2023. Hybrid-excited magneto-responsive soft actuators for grasping and manipulation of objects. Appl. Mater. Today 35, 101917. https://doi.org/10.1016/j.apmt.2023.101917.

Suo, Z.G., 2010. Theory of dielectric elastomers. Acta Mech. Solida Sin. 23, 549–578. https://doi.org/10.1016/S0894-9166(11)60004-9.

Wang, Z.J., Liu, J.J., Chen, P.J., Suo, Z.G., 2023. Osmotic instability in soft materials under well-controlled triaxial stress. J. Mech. Phys. Solids 172, 105195. https://doi.org/10.1016/j.jmps.2022.105195.

Yamada, M., Murakami, Y., Kawashima, T., Nagao, M., 2014. Electrical breakdown of dielectric elastomer and its lamination effect. In: 2014 IEEE Conference on Electrical Insulation and Dielectric Phenomena (CEIDP), pp. 126–129. https://doi.org/10.1109/CEIDP.2014.6995795.

Zhang, W.L., Qian, J., Chen, W.Q., 2012. Indentation of a compressible soft electroactive half-space: some theoretical aspects. Acta Mech. Sin. 28, 1133–1142. https://doi.org/10.1007/s10409-012-0134-3.

Zhao, X.H., Hong, W., Suo, Z.G., 2007. Electromechanical hysteresis and coexistent states in dielectric elastomers. Phys. Rev. B 76, 134113. https://doi.org/10.1103/PhysRevB.76.134113.

Zheng, Q.S., 1994. Theory of representations for tensor functions—a unified invariant approach to constitutive equations. Appl. Mech. Rev. 47, 545–587. https://doi.org/10.1115/1.3111066.

Zhou, J.Y., Jiang, L.Y., Cai, S.Q., 2020. Predicting the electrical breakdown strength of elastomers. Extreme Mech. Lett. 34, 100583. https://doi.org/10.1016/j.eml.2019.100583.

Zhou, Y.T., Xu, Y.L., Gong, H.R., Wang, C.Y., 2024. Prediction and regulation of delamination at flexible film/finite-thickness-substrate structure interfaces. Acta Mech. Solida Sin. 37, 238–251. https://doi.org/10.1007/s10338-023-00437-5.